JOURNAL OF PETROLOGY | VOLUME 47 | NUMBER 9 | PAGES 1705–1749 | 2006 | doi:10.1093/petrology/egl025

Combined Trace Element and Pb-Nd–Sr-O Isotope Evidence for Recycled Oceanic Crust (Upper and Lower) in the Iceland Mantle Plume

THOMAS FIND KOKFELT[1]*, KAJ HOERNLE[1], FOLKMAR HAUFF[1], JENS FIEBIG[2]†, REINHARD WERNER[3] AND DIETER GARBE-SCHÖNBERG[4]

[1]IFM-GEOMAR LEIBNIZ INSTITUTE FOR MARINE SCIENCES, WISCHHOFSTRAßE 1–3, 24148 KIEL, GERMANY

[2]LAUSANNE INSTITUT DE MINÉRALOGIE ET PÉTROGRAPHIE, UNIVERSITÉ DE LAUSANNE BFSH 2, 1015 LAUSANNE, SWITZERLAND

[3]TETHYS GEOCONSULTING, WISCHHOFSTRAßE 1–3, 24148 KIEL, GERMANY

[4]INSTITUTE FOR GEOSCIENCES, CHRISTIAN-ALBRECHT UNIVERSITÄT ZU KIEL, OLSHAUSENSTRAßE 40, 24118 KIEL, GERMANY

RECEIVED JUNE 23, 2003; ACCEPTED MARCH 28, 2006; ADVANCE ACCESS PUBLICATION MAY 2, 2006

We present the results of a comprehensive major element, trace element and Sr–Nd–Pb–O isotopic study of post-glacial volcanic rocks from the Neovolcanic zones on Iceland. The rocks studied range in composition from picrites and tholeiites, which dominate in the main rift systems, to transitional and alkalic basalts confined to the off-rift and propagating rift systems. There are good correlations of rock types with geochemical enrichment parameters, such as La/Sm and La/Yb ratios, and with long-term radiogenic tracers, such as Sr–Nd–Pb isotope ratios, indicating a long-lived enrichment/depletion history of the source region. $^{87}Sr/^{86}Sr$ vs $^{143}Nd/^{144}Nd$ defines a negative array. Pb isotopes define well-correlated positive arrays on both $^{206}Pb/^{204}Pb$ vs $^{207}Pb/^{204}Pb$ and $^{208}Pb/^{204}Pb$ diagrams, indicating mixing of at least two major components: an enriched component represented by the alkali basalts and a depleted component represented by the picrites. In combined Sr–Nd–Pb isotopic space the individual rift systems define coherent mixing arrays with slightly different compositions. The enriched component has radiogenic Pb ($^{206}Pb/^{204}Pb > 19{\cdot}3$) and very similar geochemistry to HIMU-type ocean island basalts (OIB). We ascribe this endmember to recycling of hydrothermally altered upper basaltic oceanic crust. The depleted component that is sampled by the picrites has unradiogenic Pb ($^{206}Pb/^{204}Pb < 17{\cdot}8$), but geochemical signatures distinct from that of normal mid-ocean ridge basalt (N-MORB). Highly depleted tholeiites and picrites have positive anomalies in mantle-normalized trace element diagrams for Ba, Sr, and Eu (and in some cases also for K, Ti and P), negative anomalies for Hf and Zr, and low $\delta^{18}O_{olivine}$ values (4·6–5·0‰) below the normal mantle range. All of these features are internally correlated, and we, therefore, interpret them to reflect source characteristics and attribute them to recycled lower gabbroic oceanic crust. Regional compositional differences exist for the depleted component. In SW Iceland it has distinctly higher Nb/U (~68) and more radiogenic $^{206}Pb/^{204}Pb$ ratios (18·28–18·88) compared with the NE rift (Nb/U ~47; $^{206}Pb/^{204}Pb = 18{\cdot}07$–$18{\cdot}47$). These geochemical differences suggest that different packages of recycled oceanic lithosphere exist beneath each rift. A third and minor component with relatively high $^{87}Sr/^{86}Sr$ and $^{207}Pb/^{204}Pb$ is found in a single volcano in SE Iceland (Öræfajökull volcano), indicating the involvement of recycled sediments in the source locally. The three plume components form an integral part of ancient recycled oceanic lithosphere. The slope in the uranogenic Pb diagram indicates a recycling age of about 1·5 Ga with time-integrated Th/U ratios of 3·01.

*Corresponding author. Telephone: +49 431 6002638. Fax: +49 431 6002924. E-mail: tkokfelt@ifm-geomar.de

†Present address: University of Frankfurt, Senkenberganlage 32–34, Postfach 11 19 32, D-60054 Frankfurt/M, Germany

Surprisingly, there is little evidence for the involvement of North Atlantic N-MORB source mantle, as would be expected from the interaction of the Iceland plume and the surrounding asthenosphere in form of plume–ridge interaction. The preferential sampling of the enriched and depleted components in the off-rift and main rift systems, respectively, can be explained by differences in the geometry of the melting regions. In the off-rift areas, melting columns are truncated deeper and thus are shorter, which leads to preferential melting of the enriched component, as this starts melting deeper than the depleted component. In contrast, melting proceeds to shallower depths beneath the main rifts. The longer melting columns also produce significant amounts of melt from the more refractory (lower crustal/lithospheric) component.

KEY WORDS: *basalts; trace element and Sr, Nd, Pb, O isotope geochemistry; Iceland plume; isotope ratios; oceanic crustal recycling; partial melting; plume–ridge interaction*

INTRODUCTION

The present-day setting of the Iceland plume impinging beneath the northern mid-Atlantic Ridge (MAR) makes Iceland an excellent target for studies of crustal accretion and plume–ridge interaction processes. The Iceland plume was probably one of the driving forces in the opening of the North Atlantic around 60 Myr ago (Schilling & Noe-Nygaard, 1974) and the continuous outflow of the Iceland plume appears to have influenced the chemistry of large parts of the North Atlantic Igneous Province (Taylor *et al.*, 1997). Although Foulger & Natland (2003) argued that an Iceland plume is not required, seismic tomographic studies show the presence of a cylindrical low-velocity anomaly beneath Iceland, consistent with the presence of a mantle plume (Wolfe *et al.*, 1997; Helmberger *et al.*, 1998; Shen *et al.*, 1998; Bijwaard & Spakman, 1999; Montelli *et al.*, 2004). Radial distribution of $(^{230}Th)/(^{238}U)$ ratios in post-glacial volcanic rocks provides further support for an upwelling cylindrical mantle feature with systematically decreasing upwelling rates outwards from the cylinder's centre (located beneath the Vatnajökull Glacier) to its margins (Kokfelt *et al.* 2003). Some tomographic (Helmberger *et al.*, 1998; Shen *et al.*, 1998; Bijwaard & Spakman, 1999), oxygen, and noble gas (Hattori & Muehlenbachs, 1982; Condomines *et al.*, 1983; Kurz *et al.*, 1985; Harrison *et al.*, 1999; Hilton *et al.*, 1999; Breddam *et al.*, 2000; Dixon *et al.*, 2000; Moreira *et al.*, 2001) studies are consistent with a lower mantle origin for some of the upwelling Iceland source material.

During the last decade, a number of detailed geochemical and geophysical studies have been undertaken in Iceland to solve some of the outstanding questions. Central to the debate is the nature and origin of the melt source components involved in magma generation beneath Iceland and their distribution in the mantle. The isotopic variability of the Icelandic lavas clearly indicates (a) heterogeneous source(s). The question we wish to discuss here is to what extent the heterogeneity reflects plume components from greater depths, asthenospheric components or lithospheric interaction. In particular, the origin of the depleted component in Iceland is enigmatic: it could be an intrinsic plume component or could represent entrained upper mantle (Mertz *et al.*, 1991; Hémond *et al.*, 1993; Kerr *et al.*, 1995; Fitton *et al.*, 1997; Hanan & Schilling, 1997; Mertz & Haase, 1997; Chauvel & Hémond, 2000; Hanan *et al.*, 2000; Kempton *et al.*, 2000; Skovgaard *et al.*, 2001; Breddam, 2002; Stracke *et al.*, 2003). The Icelandic picrites appear to play an important role in this debate, because they define a depleted compositional endmember among the Icelandic volcanism with relatively unradiogenic Sr and Pb and radiogenic Nd isotopic compositions. The geochemistry of the Icelandic picrites is distinct from that of normal mid-ocean ridge basalts (MORB): they show positive anomalies for Sr, Ba and Eu (Hémond *et al.*, 1993) in mantle-normalized trace element diagrams, and also appear to have distinctly lower Zr/Y at a given Nb/Y ratio (Fitton *et al.*, 1997; Chauvel & Hémond, 2000). The positive Ba, Sr and Eu anomalies have been variously attributed to exhaustive melting of plagioclase at relatively shallow depths in the mantle beneath Iceland (Gurenko & Chaussidon, 1995), recycling of oceanic gabbros into the Iceland plume (Chauvel & Hémond, 2000; Skovgaard *et al.*, 2001; Breddam, 2002), and contamination of mantle-derived magmas in the lower crust (Hémond *et al.*, 1993). An alternative model for the depleted component in Iceland, based on Pb isotope data, was proposed by Hanan & Schilling (1997). According to their three-component mixing model, the depleted endmember is the result of mixing of North Atlantic depleted upper mantle with a shallow enriched component of subcontinental lithospheric origin. More recently, Thirlwall *et al.* (2004) used double-spike Pb isotopic data on main rift tholeiites from the Neovolcanic zones of Iceland and MORB samples from the adjacent ridges to argue for the existence of seven distinct components beneath Iceland. Based on local binary mixing arrays, they proposed that the various components are geographically restricted, probably reflecting zonation of the Icelandic mantle plume.

We elaborate on this debate by presenting a comprehensive regional major element, trace element and Sr–Nd–Pb–O isotopic dataset for post-glacial Icelandic basalts. U-series data on the same sample set have been published by Kokfelt *et al.* (2003). The data provide evidence for the existence of two major types of intrinsic plume components—enriched and depleted type components. A minor enriched component resides locally beneath the Öræfajökull central volcano in SE Iceland (Prestvik *et al.*, 2001). The new Pb isotope data are

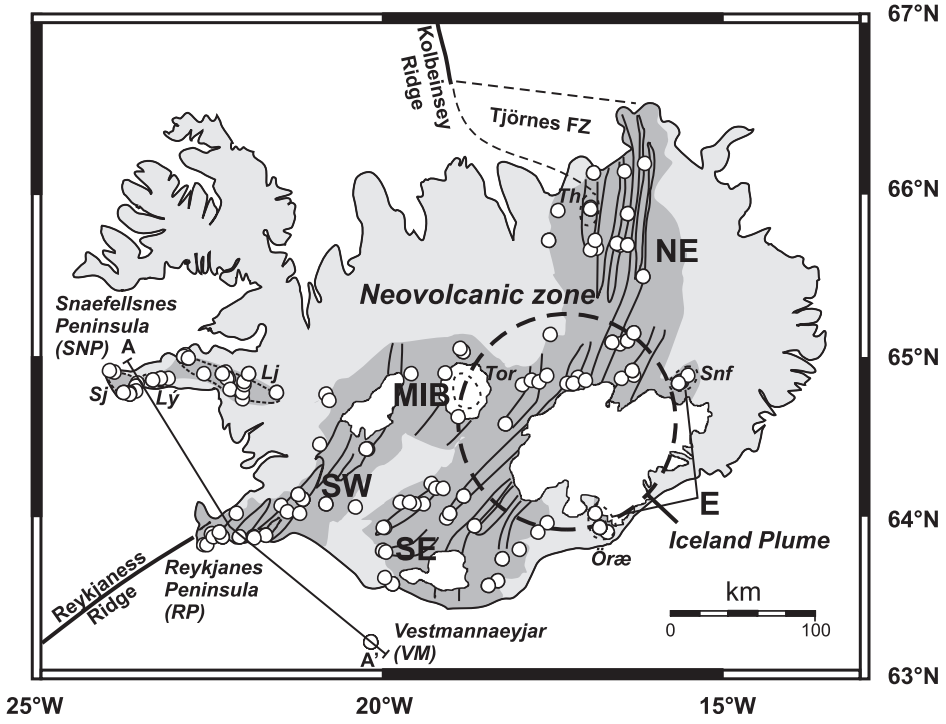

Fig. 1. Map showing the Neovolcanic zones of Iceland (dark shading) and sample locations of all 142 lavas (open circles) on which this study is based. The dashed circle represents the outline of the Iceland plume at ~200 km depth (Wolfe *et al.*, 1997). The rift zones are indicated as follows: SW, southwest; SE, southeast; MIB, Mid-Iceland Belt; NE, northeast; E, east rifts. RP, Reykjanes Peninsula; Lj, Ljósufjöll; Ly, Lýsuskarð; Sj, Snæfellsjökull; Th, Theistareykir; Öræ, Öræfajökull volcano; Tor, Torfajökull volcano; Snf, Snæfellsjökull volcano. Major glaciers are shown as white filled outlines. Profile section A–A' refers to model sketch in Fig. 13.

consistent with an average recycling age for the two major plume components of around ~1·5 Ga, and suggest intermediate recycling ages compared with those proposed for the source regions of St. Helena (~1·8 Ga; Chauvel *et al.*, 1992), Madeira and the Caribbean Large Igneous Province (<500–900 Ma; Geldmacher & Hoernle, 2000; Hauff *et al.*, 2000). Thus, it appears that subducted and recycled oceanic crust (±sediment) may be preserved over a broad range of time within the mantle, before being returned to the surface via mantle plumes (Thirlwall, 1997). This study also shows that the Iceland plume is heterogeneous on different scales. The different rift zones on Iceland are fed by different packages of recycled oceanic crust with distinct geochemical characteristics, whereas different parts of the recycled oceanic crust are preferentially sampled at different depths in the melting column. Finally, we present a model for the formation of picrites and tholeiites beneath the main rift systems, and alkali basalts and transitional tholeiites beneath the off-axis and propagating rift systems.

GEOLOGICAL SETTING AND SAMPLING

Iceland is the most prominent example of a mantle plume interacting with a mid-ocean ridge. The current expression of the lateral spread of the Iceland plume is the progressive decrease of the axial water depth along the Reykjanes Ridge towards Iceland and the propagating 'V'-shaped ridges pointing away from Iceland (White *et al.*, 1995; Abelson & Agnon, 2001; Ito, 2001). These morphological features are associated with geochemical gradients in the erupted MORB with more enriched 'plume'-like signatures towards Iceland, such as higher La/Sm, $^{3}He/^{4}He$ and $^{87}Sr/^{86}Sr$ isotopic ratios closer to Iceland (Hart *et al.*, 1973; Schilling, 1973; Sun *et al.*, 1975; Poreda *et al.*, 1986; Taylor *et al.*, 1997; Hilton *et al.*, 2000; Murton *et al.*, 2002). Seismic tomographic studies indicate that the Iceland plume conduit is situated beneath Vatnajökull glacier in SE Iceland (Fig. 1) (Wolfe *et al.*, 1997; Shen *et al.*, 1998) and may extend to the core–mantle boundary (Bijwaard & Spakman, 1999). A lower mantle origin is also suggested from primordial noble gas signatures in lavas erupted directly above the plume stem (Condomines *et al.*, 1983; Kurz *et al.*, 1985; Breddam *et al.*, 2000; Dixon *et al.*, 2000; Moreira *et al.*, 2001; Dixon, 2003). The significant thermal anomaly associated with the Iceland plume (ΔT ~200°C; White *et al.*, 1995) has led to enhanced melt production and crustal thickening; in central Iceland the crust reaches a thickness of up to ~40 km compared with ~16 km along the Reykjanes Peninsula (Darbyshire *et al.*, 2000; Weir *et al.*, 2001).

The Neovolcanic rift zones of Iceland represent the subaerial continuation of the Mid-Atlantic Ridge system as it connects the Reykjanes Ridge in the SW with the Kolbeinsey Ridge via the Tjörnes fracture zone in the NE (Fig. 1). The Neovolcanic rift zones consist of sub-rift systems arranged in an en-echelon fashion. Central volcanoes and associated fissure swarms occur within each sub-rift system. The overall oblique spreading symmetry and the continuous interference of the Iceland plume with the normal spreading ridge has resulted in several episodes of rift jumps through the geological past, and the repeated generation of dying rift arms such as recorded in NW Iceland (Hardarson *et al.*, 1997). It is likely in the future that the southward propagating SE rift will actually replace the SW (Reykjanes) rift, requiring the development of a transform fault south of Iceland linking the SE rift to the Reykjanes Ridge (Saemundsson, 1979; Furman *et al.*, 1991). Although the Mid-Atlantic Ridge is moving to the west in relation to the mantle, the estimated offsets of the NE and SE Iceland rifts suggest rift capture by the Iceland plume. The off-rift areas are characterized by less robust magma supply, a smaller heat flux, and probably smaller degrees of partial melting leading to more alkalic volcanism.

A total of 142 basaltic lavas were collected along the Neovolcanic zones of Iceland, almost exclusively post-glacial in age (Table 1). The sampling strategy allows us to investigate regionally related geochemical and isotopic differences along the rift zones and to evaluate the influence of plume–ridge interaction by establishing several profiles across the Iceland plume. In a companion paper, we presented U-series disequilibria data on a subset of these samples (Kokfelt *et al.*, 2003). We concentrate primarily on basaltic compositions erupted away from the central volcanoes to minimize the effects of differentiation and to avoid alteration features that are related to hydrothermal circulation systems (e.g. Gautason & Muehlenbachs, 1998). In addition to the majority of tholeiitic basalts from the main rifts, we also sampled the volumetrically smaller picrite flows, such as the Vatnsheidi and Lágafell flows (Reykjanes Peninsula), the so-called Thor's picrites at Mælifell (SW rift) and the picritic tholeiites at the Theistareykir area (NE rift). Off-rift regions included are the Snæfellsnes Peninsula (SNP) in the SW, the southern tip of the SE-propagating rift system (Vestmannaeyjar) and the E rift (Snæfell and Öræfajökull volcanoes). These lavas are tholeiitic to transitional basalts, ranging to alkali basalts. The tholeiitic lavas from the main rift zones are aphyric to moderately porphyritic ($\leq$10% crystals) with plagioclase and olivine being the main phenocryst phases. The picrites have abundant olivine and rarely contain plagioclase (except H86). The alkalic lavas from the SNP typically contain olivine, plagioclase and clinopyroxene (cpx) as pheno(xeno)-cryst phases, which may reach considerable sizes ($\leq$1 cm). Two samples from SNP (H102 and H106) are classified as alkali picrites, and contain mainly olivine (up to 20%) and very minor cpx and plagioclase (<1%).

We report major (X-ray fluorescence; XRF) and trace element (XRF and inductively coupled plasma mass spectrometry; ICP-MS) data for 83 (79 post-glacial and four glacial) of the least evolved lavas. Major elements were analysed at the IFM-GEOMAR Leibniz Institute for Marine Sciences, whereas trace element analyses were performed at the Christian-Albrecht University (CAU). In total 69 lavas were analysed for Sr–Nd–Pb isotope ratios at IFM-GEOMAR. Details of the analytical precision are given in the Appendix. Despite the young age of the samples, special caution was exercised in collecting the freshest samples and in preparing the rock powders. Chip-sized rock fragments were picked under a binocular microscope to remove pieces with surface alteration features, zeolite or other fillings in vesicles, and xenoliths or xenocrysts. Samples were ground using an agate swing-mill. Subsequently, geochemical criteria, such as unusually low large ion lithophile element to high field strength element (LILE/HFSE) ratios (e.g. $K_2O/P_2O_5 < 1$), and/or raised loss on ignition were used to identify rare altered samples that were not readily identified as altered on visual grounds. For the most depleted rocks, we performed Sr–Nd–Pb isotopic measurements on leached chips instead of the powder (see Table 2). This was done to avoid contamination (in particular for Pb) from the crushing procedure.

RESULTS

Major elements

Table 1 lists the major and trace element compositions of the 83 selected lavas. For the classification of the rocks we use the TAS diagram (Fig. 2a; showing the total dataset) and we define picrites as rocks with MgO >10 wt %. Our main rift zone lavas comprise primarily olivine and/or plagioclase-bearing tholeiitic basalts. We divide the main rift lavas into three groups (open plot symbols): (1) northeast (NE); (2) Mid-Iceland Belt (MIB); (3) southwest (SW) plus Reykjanes Peninsula (RP). Off-rift volcanism (filled symbols) is characterized by lavas from Snaefellsnes Peninsula (SNP), Vestmannaeyjar (VM), the SE-propagating rift system (SE), and the two central volcanoes in the eastern (E) rift, Snaefell and Öræfajökull volcanoes. Our samples from the off-rift and propagating rifts (henceforth referred to simply as 'off-rift systems') consist of tholeiitic, transitional tholeiitic to alkalic basalts, basaltic andesites and trachyandesites, which are, overall, more SiO_2-undersaturated than the on-rift lavas. The MgO contents of the lavas range widely (2·8–24·2 wt %), with the majority having between

Table 1: Major and trace element compositions of Icelandic post-glacial lavas

Sample:	H21	H26	H22	H131	H20	H18	H19	H23	H25	H16
Rift-zone:	NE	NE	NE	NE	NE	NE	NE	NE	NE	NE
Locality:	Dyngjufjöll	Sveinahraun	Askja	Krafla	Randarholar	Hwy 85 betw. 866/867	Gasavatn, E	Herðubreið-artögl, S	Sveinagjá, E	Hraungerði
Longitude:	16·628	16·399	16·508	16·399	16·395	16·434	16·146	16·404	16·173	17·433
Latitude:	65·053	65·656	65·052	65·656	65·842	66·105	66·152	65·068	65·466	65·867
Age:	h	h	ph	h	ph	pg-ph	ph	pg	ph	ph
Rock type:	q-th	q-th	q-th	q-th	q-th	q-th	q-th	q-th	ol-th	ol-th
*Major elements by XRF (wt %)**										
SiO_2	50·67	50·67	50·30	49·68	49·76	49·75	49·99	49·58	47·78	49·32
TiO_2	2·80	2·79	2·33	2·06	1·74	1·75	1·70	1·71	1·82	1·53
Al_2O_3	13·00	13·00	13·00	13·34	13·83	13·84	13·94	13·92	14·42	14·91
Fe_2O_3	17·54	17·56	16·99	16·26	14·31	14·16	14·00	13·53	13·30	12·48
MnO	0·24	0·24	0·24	0·24	0·21	0·21	0·21	0·20	0·20	0·19
MgO	4·65	4·74	5·27	5·86	6·85	6·87	6·96	7·05	7·06	7·51
CaO	9·17	9·19	9·82	10·35	11·70	11·71	11·80	11·89	11·21	12·73
Na_2O	2·77	2·75	2·53	2·01	2·22	2·26	2·28	2·26	2·20	2·08
K_2O	0·56	0·53	0·41	0·33	0·24	0·25	0·24	0·28	0·34	0·16
P_2O_5	0·32	0·31	0·23	0·21	0·17	0·16	0·16	0·17	0·20	0·15
H_2O	0·11	0·17	0·33	0·12	0·16	0·13	0·16	0·21	0·13	0·08
CO_2	0·01	0·02	0·05	0·01	0·02	0·02	0·02	0·01	0·07	0·01
Sum	101·72	101·78	101·12	100·34	101·03	100·96	101·28	100·59	98·53	101·06
*Trace elements XRF (ppm)**										
Co	69	70	76	60	64	62	61	63	60	54
Cr	52	46	36	122	77	81	76	171	213	125
Ni	33	32	35	61	63	60	56	72	84	70
V	496	499	445	442	369	369	363	352	354	318
Zn	139	137	131	123	101	100	98	96	94	89
ICP-MS (ppm)†										
Rb	11·8	12·2	7·8	6·7	4·6	4·7	4·2	5·0	7·7	3·0
Sr	183	184	170	161	152	154	147	166	199	154
Y	43·5	40·5	35·9	31·6	27·9	28·4	26·2	24·4	23·3	24·1
Zr	177·6	172	133	110	90·4	91·4	84·0	85·0	87·4	79·1
Nb	18·7	18·6	13·6	11·2	9·2	9·4	8·6	9·5	10·8	7·8
Cs	0·146	0·118	0·090	0·082	0·052	0·055	0·049	0·055	0·078	0·033
Ba	127	113	88·5	88·9	53·7	53·7	51·1	62·3	82·1	35·4
La	16·7	15·0	11·6	9·68	7·40	7·44	6·83	7·70	8·75	5·91
Ce	40·4	35·3	28·6	24·1	18·5	18·6	17·2	19·1	20·8	15·1
Pr	5·60	4·93	4·03	3·43	2·69	2·69	2·49	2·73	2·93	2·23
Nd	25·4	22·6	18·7	16·1	12·7	12·7	11·8	12·9	13·5	10·7
Sm	6·88	6·10	5·23	4·67	3·75	3·74	3·50	3·59	3·63	3·19
Eu	2·25	1·97	1·78	1·58	1·35	1·34	1·25	1·29	1·29	1·16
Gd	7·87	6·97	6·13	5·52	4·60	4·52	4·24	4·26	4·18	3·87
Tb	1·32	1·16	1·04	0·955	0·799	0·795	0·746	0·732	0·692	0·677
Dy	8·23	7·43	6·69	6·18	5·17	5·12	4·84	4·60	4·43	4·38
Ho	1·71	1·53	1·38	1·30	1·08	1·07	1·01	0·953	0·905	0·916
Er	4·77	4·25	3·87	3·75	3·03	3·03	2·85	2·63	2·53	2·55
Tm	0·702	0·612	0·566	0·535	0·447	0·440	0·416	0·382	0·366	0·370
Yb	4·57	3·99	3·71	3·62	2·90	2·89	2·71	2·47	2·37	2·39
Lu	0·666	0·589	0·547	0·531	0·432	0·419	0·396	0·362	0·350	0·352
Hf	5·21	4·09	4·01	3·20	2·74	2·67	2·55	2·57	2·33	2·36
Ta	1·28	1·05	0·908	0·743	0·597	0·592	0·561	0·609	0·608	0·506
Pb	1·37	1·14	1·06	0·802	0·643	0·631	0·587	0·699	0·713	0·508
Th	1·65	1·42	1·09	0·743	0·642	0·624	0·592	0·664	0·791	0·500
U	0·481	0·405	0·321	0·235	0·189	0·185	0·175	0·197	0·234	0·148
ID-MS (ppm)‡										
Th	1·46	1·40		0·720	0·584		0·535	0·647	0·754	0·488
U	0·442	0·424		0·228	0·180		0·171	0·199	0·236	0·153

Table 1: Continued

Sample:	H134	H15	H17	H124	H125	H24	H129	H127	Q10
Rift-zone:	NE	NE	NE	NE	NE	NE	NE	NE	MIB
Locality:	Krepputunga, S	Holtakot, SE	Flaeðar/Lón	Kviahraun	Þeistareykir, Ketilfjall	Herðubreið-artögl, E	Þeistareykir, Bóndhólshraun	Þeistareykir, Borgrahraun	Trolla-dyngja, S
Longitude:	16·324	17·571	16·905	17·540	16·934	16·315	16·973	17·002	17·303
Latitude:	64·880	65·686	66·099	65·106	65·889	65·113	65·765	65·852	64·806
Age:	pg	ph	ph	pg	pg-ph	ph	pg	pg	pg
Rock type:	q-th	ol-th	q-th	q-th	q-th	ol-th	ol-th	ol-th	ol-th
*Major elements by XRF (wt %)**									
SiO_2	49·51	49·00	49·95	49·32	49·90	47·13	49·20	48·81	50·07
TiO_2	1·35	0·92	0·98	1·41	0·94	1·74	0·72	0·71	2·08
Al_2O_3	15·16	16·34	14·94	14·40	15·29	14·78	15·18	14·72	13·48
Fe_2O_3	11·60	10·44	12·57	11·87	12·18	13·15	10·50	10·34	15·10
MnO	0·18	0·16	0·20	0·19	0·20	0·19	0·17	0·17	0·23
MgO	7·73	7·87	8·03	8·15	8·45	8·55	10·31	10·93	6·26
CaO	13·17	13·94	12·04	13·10	11·96	10·96	12·62	13·03	10·83
Na_2O	1·74	1·74	1·95	1·73	1·66	2·14	1·41	1·20	2·61
K_2O	0·14	0·07	0·14	0·13	0·13	0·37	0·08	0·06	0·28
P_2O_5	0·12	0·07	0·10	0·13	0·09	0·18	0·06	0·05	0·23
H_2O	0·13	0·18	0·14	0·09	0·12	0·19	0·09	0·16	0·12
CO_2	—	0·04	0·01	0·01	—	0·02	—	0·01	—
Sum	100·70	100·55	100·90	100·43	100·80	99·19	100·25	100·02	101·17
*Trace elements XRF (ppm)**									
Co	49	49	56	51	55	60	52	53	57
Cr	206	274	86	233	85	369	345	576	33
Ni	75	93	84	83	79	142	162	208	27
V	292	255	297	311	286	316	247	244	409
Zn	80	68	89	81	80	90	63	65	113
ICP-MS (ppm)†									
Rb	2·3	1·4	3·1	2·2	2·3	7·1	1·5	0·9	5·7
Sr	143	124	138	148	127	257	125	102	171
Y	16·2	17·0	18·8	17·7	14·1	18·6	14·5	15·5	35·7
Zr	55·7	40·3	43·1	60·0	36·4	89·6	31·8	30·0	139
Nb	6·2	2·9	3·8	6·3	3·4	11·5	2·2	1·6	12·0
Cs	0·026	0·012	0·034	0·022	0·030	0·078	0·022	0·013	0·059
Ba	31·7	15·3	40·8	31·6	40·0	102	22·7	15·7	58·0
La	5·13	2·61	3·56	5·01	3·39	9·77	2·15	1·66	9·43
Ce	13·5	6·92	8·79	13·5	8·82	23·9	5·54	4·54	23·4
Pr	1·97	1·09	1·32	2·01	1·30	3·25	0·856	0·746	3·41
Nd	9·33	5·59	6·48	9·86	6·35	15·0	4·29	3·91	16·1
Sm	2·79	1·90	2·04	3·01	2·02	3·94	1·47	1·45	4·70
Eu	1·05	0·743	0·814	1·11	0·786	1·32	0·605	0·598	1·61
Gd	3·22	2·51	2·70	3·47	2·44	4·03	2·02	2·06	5·49
Tb	0·554	0·451	0·492	0·597	0·440	0·648	0·370	0·392	0·988
Dy	3·59	3·03	3·31	3·89	2·97	4·13	2·52	2·70	6·35
Ho	0·744	0·647	0·714	0·808	0·642	0·842	0·544	0·586	1·32
Er	2·08	1·84	2·06	2·27	1·86	2·33	1·58	1·69	3·67
Tm	0·298	0·266	0·306	0·314	0·264	0·295	0·233	0·255	0·530
Yb	2·00	1·77	2·05	2·10	1·83	2·01	1·58	1·72	3·51
Lu	0·278	0·265	0·305	0·296	0·263	0·293	0·234	0·257	0·519
Hf	1·78	1·18	1·24	1·90	1·21	2·61	0·925	0·916	3·54
Ta	0·449	0·172	0·209	0·451	0·300	0·826	0·134	0·104	0·765
Pb	0·404	0·255	0·345	0·529	0·354	0·747	0·220	0·245	0·754
Th	0·406	0·204	0·264	0·368	0·242	0·796	0·140	0·096	0·850
U	0·135	0·060	0·077	0·123	0·081	0·276	0·044	0·031	0·259
ID-MS (ppm)‡									
Th	0·405	0·192	0·243		0·242	0·791	0·134		
U	0·127	0·0600	0·0772		0·0752	0·239	0·0433		

Sample:	H31	Q9	H6	CIS46	Q4	Q6	CIS47	Q5	503
Rift-zone:	MIB	MIB	MIB	MIB	MIB	MIB	MIB	MIB	MIB
Locality:	Tungnafells-jökull, NW	Trolladyngja	Hágöngur	Illahraun	Hofsjökull, N	Hofsjökull, NW	Kerlingarfjöll–Setluhraun	Lambahraun	Hallamundarhraun
Longitude:	17·959	17·602	18·199	19·109	18·834	18·873	18·959	18·825	20·825
Latitude:	64·797	64·859	64·561	64·623	65·009	65·022	64·585	65·007	64·738
Age:	g	pg	pg	pg	pg	pg	pg	pg	pg
Rock type:	ol-th	ol-th	ol-th	ol-th	ol-th	ol-th	ol-th	ol-th	ol-th
*Major elements by XRF (wt %)**									
SiO_2	49·26	49·58	49·45	49·05	48·83	48·84	49·15	48·99	47·90
TiO_2	1·44	1·42	1·23	1·09	1·08	1·07	1·01	1·04	1·04
Al_2O_3	15·38	14·24	14·81	14·75	15·01	15·49	14·70	15·07	16·00
Fe_2O_3	12·31	12·38	11·64	12·05	11·82	11·69	11·87	11·70	11·11
MnO	0·19	0·19	0·18	0·19	0·18	0·18	0·18	0·18	0·17
MgO	7·64	8·01	8·05	8·48	8·67	8·74	8·74	8·78	9·01
CaO	12·31	12·87	13·32	13·05	13·03	13·06	13·18	13·14	11·97
Na_2O	1·82	2·01	1·95	1·81	1·98	1·98	1·86	1·97	2·00
K_2O	0·15	0·14	0·11	0·09	0·08	0·07	0·08	0·07	0·11
P_2O_5	0·13	0·14	0·11	0·10	0·09	0·09	0·09	0·10	0·12
H_2O	0·14	0·17	0·11	0·15	0·15	0·13	0·11	0·14	0·21
CO_2	—	—	0·01	—	—	0·01	—	0·01	0·13
Sum	100·63	100·98	100·85	100·66	100·77	101·21	100·86	101·04	99·43
Trace elements									
*XRF (ppm)**									
Co	52	53	51	54	54	53	54	52	53
Cr	244	177	232	311	314	330	311	312	148
Ni	91	78	76	96	105	108	104	104	154
V	324	320	296	302	307	294	298	300	265
Zn	93	83	80	80	84	80	78	77	72
ICP-MS (ppm)†									
Rb	2·8	2·7	2·3	0·66	0·98	0·95	0·49	0·96	1·2
Sr	129	150	132	70	132	131	61	133	75
Y	19·7	24·4	20·1	10·8	19·5	18·8	9·2	19·3	11·6
Zr	65·0	74·3	53·4	23·7	40·9	39·7	19·2	40·1	29·7
Nb	6·0	6·7	4·9	1·6	2·5	2·5	1·2	2·4	2·7
Cs	0·030	0·029	0·019	0·008	0·012	0·012	0·006	0·013	0·015
Ba	33·5	31·5	23·5	10·8	17·9	17·5	8·5	17·4	17·0
La	5·10	5·16	4·01	1·40	2·28	2·24	1·10	2·22	2·14
Ce	13·4	13·2	10·3	3·76	6·27	6·13	2·98	6·13	5·38
Pr	1·96	1·99	1·55	0·605	1·03	1·01	0·487	1·01	0·816
Nd	9·25	9·74	7·68	3·14	5·46	5·34	2·57	5·36	4·02
Sm	2·84	3·02	2·42	1·10	1·95	1·90	0·910	1·91	1·29
Eu	1·09	1·11	0·900	0·439	0·794	0·772	0·369	0·786	0·490
Gd	3·50	3·66	3·07	1·45	2·59	2·51	1·22	2·57	1·62
Tb	0·607	0·665	0·543	0·274	0·494	0·479	0·232	0·490	0·302
Dy	3·96	4·36	3·61	1·86	3·35	3·25	1·58	3·32	2·02
Ho	0·827	0·906	0·760	0·398	0·718	0·695	0·338	0·717	0·426
Er	2·31	2·52	2·14	1·13	2·05	1·97	0·960	2·04	1·21
Tm	0·349	0·368	0·311	0·166	0·302	0·290	0·143	0·300	0·177
Yb	2·33	2·40	2·03	1·10	2·01	1·92	0·943	1·98	1·18
Lu	0·332	0·356	0·301	0·165	0·303	0·289	0·141	0·300	0·177
Hf	1·94	2·09	1·55	0·711	1·24	1·22	0·585	1·24	0·860
Ta	0·409	0·435	0·294	0·104	0·161	0·162	0·075	0·158	0·169
Pb	0·567	0·434	0·336	0·192	0·288	0·253	0·138	0·263	0·192
Th	0·449	0·407	0·320	0·095	0·137	0·134	0·072	0·132	0·164
U	0·141	0·123	0·095	0·030	0·043	0·042	0·022	0·041	0·051
ID-MS (ppm)‡									
Th			0·311				0·149	0·130	
U			0·0983				0·0471	0·0414	

Table 1: Continued

Sample:	Q12	501	502	Q7	CIS57	502b	H67	H61	H4
Rift-zone:	MIB	MIB	MIB	MIB	MIB	MIB	SE	SE	SE
Locality:	Hrimalda, SE	Kjolur	Langjökull, W	Tunguhraun	Tindafell	Langjökull, W	Hekla	Skálmarbæjar-hraun, Eldja	Skálmarbæjarhraun, Eldja
Longitude:	17·035	19·592	20·808	17·818	19·668	20·791	19·606	18·451	18·648
Latitude:	64·825	64·859	64·708	64·834	64·786	64·704	64·078	63·569	63·937
Age:	pg	pg	pg	pg	pg	pg	1970	AD 933	AD 934
Rock type:	ol-th	ol-th	ol-th	ol-th	ol-th	ol-th	ba	tb	tb
*Major elements by XRF (wt %)**									
SiO_2	47·30	47·33	47·03	47·59	47·98	46·98	54·29	47·19	47·43
TiO_2	1·75	1·30	1·67	1·31	0·62	1·66	2·03	4·49	4·49
Al_2O_3	15·43	15·93	14·61	15·19	16·85	14·65	14·80	13·20	13·17
Fe_2O_3	12·48	11·78	13·44	11·82	10·54	13·36	13·17	16·70	16·98
MnO	0·18	0·17	0·20	0·17	0·17	0·19	0·27	0·22	0·21
MgO	9·31	9·51	9·69	9·74	9·87	9·91	2·78	4·85	5·06
CaO	11·84	12·13	11·39	11·60	12·54	11·34	6·87	9·86	9·94
Na_2O	2·02	1·95	1·96	2·07	1·66	2·00	3·58	2·74	2·85
K_2O	0·20	0·08	0·15	0·10	0·03	0·14	1·24	0·77	0·74
P_2O_5	0·19	0·11	0·15	0·14	0·06	0·14	1·02	0·56	0·51
H_2O	0·11	0·17	0·16	0·16	0·12	0·20	0·09	0·22	0·20
CO_2	0·01	0·01	0·01	—	—	0·01	0·01	0·02	0·03
Sum	100·70	100·29	100·29	99·73	100·32	100·37	100·05	100·58	101·38
Trace elements									
*XRF (ppm)**									
Co	53	56	63	54	53	63	36	49	51
Cr	412	336	418	544	151	466	<18	18	39
Ni	177	189	201	215	168	207	<2	25	22
V	298	282	338	276	226	333	87	468	471
Zn	87	80	95	82	66	96	182	143	145
ICP-MS (ppm)†									
Rb	1·9	0·50	1·2	1·2	0·21	1·1	24·2	16·4	14·1
Sr	121	120	97	145	60	95	342	392	393
Y	14·4	11·6	13·1	22·3	9·1	12·4	65·0	37·7	35·3
Zr	57·4	30·5	41·1	70·0	13·3	36·8	401	252	220
Nb	5·8	2·5	4·0	5·3	0·41	3·8	58·1	36·7	31·5
Cs	0·021	0·006	0·014	0·014	0·003	0·013	0·292	0·196	0·185
Ba	30·5	13·1	23·4	25·6	3·7	22·3	327	204	181
La	3·91	1·95	2·92	4·04	0·511	2·78	51·0	29·0	25·9
Ce	10·1	5·34	7·48	10·9	1·56	7·11	117	68·7	61·6
Pr	1·52	0·866	1·14	1·71	0·287	1·09	15·4	9·24	8·32
Nd	7·37	4·43	5·59	8·57	1·69	5·29	65·6	40·6	37·1
Sm	2·15	1·46	1·69	2·73	0·715	1·59	15·3	9·86	8·87
Eu	0·786	0·578	0·648	1·04	0·317	0·618	4·69	3·19	2·96
Gd	2·43	1·77	2·01	3·37	1·07	1·90	15·4	9·77	8·96
Tb	0·423	0·322	0·361	0·611	0·214	0·342	2·37	1·49	1·35
Dy	2·66	2·09	2·34	3·99	1·52	2·22	13·7	8·39	7·64
Ho	0·537	0·434	0·488	0·827	0·334	0·460	2·66	1·55	1·43
Er	1·47	1·20	1·36	2·29	0·966	1·29	7·11	3·98	3·64
Tm	0·208	0·174	0·199	0·334	0·145	0·187	0·980	0·520	0·480
Yb	1·35	1·14	1·31	2·16	0·974	1·23	6·36	3·21	2·94
Lu	0·200	0·169	0·196	0·320	0·148	0·185	0·912	0·447	0·404
Hf	1·47	0·921	1·10	1·94	0·442	1·04	11·2	6·82	6·22
Ta	0·354	0·159	0·251	0·330	0·028	0·238	3·66	2·44	2·12
Pb	0·314	0·172	0·274	0·337	0·109	0·236	3·21	1·90	1·81
Th	0·237	0·076	0·163	0·170	0·029	0·151	4·51	2·69	2·49
U	0·073	0·025	0·051	0·059	0·009	0·048	1·36	0·801	0·761
ID-MS (ppm)‡									
Th	0·399	0·121		0·169		0·273		2·42	2·33
U	0·122	0·0404		0·0594		0·0873		0·766	0·731

Sample:	H2	H5	H66	H3	H8	Q1	H7	H122	H120	H119	OR58
Rift-zone:	SE	SE	SE	SE	SE	SE	SE	VM	VM	VM	E
Locality:	Raudabergs-hraun	Landmanna-lauga	Hekla	Eldhraun	Hraune-yjalon	Þhrihyrn-ingur, N	Veiðivötn	Heimey	Heimey	Heimey, S	Öræfajökull
Longitude:	17·594	19·026	19·538	18·239	19·294	20·015	18·826	20·180	20·180	20·180	16·801
Latitude:	63·952	64·008	64·071	63·734	64·193	63·788	64·113	63·220	63·220	63·220	63·924
Age:	AD 1783	pg-ph	1878	h	pg-ph	pg	h	1973	pg	pg	ph
Rock type:	q-th	ba	tb	q-th	q-th	q-th	q-th	haw	ab	tb	ol-th
*Major elements by XRF (wt %)**											
SiO_2	49·72	53·98	46·29	49·89	50·81	46·03	49·63	46·92	46·65	46·10	48·80
TiO_2	2·83	1·47	4·40	2·82	1·84	3·04	1·64	3·13	2·51	1·62	2·68
Al_2O_3	14·28	14·23	13·74	13·57	15·27	14·49	14·78	16·37	16·63	14·45	13·75
Fe_2O_3	14·78	11·55	17·13	15·19	11·84	15·37	13·00	15·08	13·93	12·18	15·33
MnO	0·21	0·19	0·25	0·22	0·18	0·21	0·20	0·23	0·20	0·18	0·21
MgO	5·30	5·37	5·39	5·64	5·93	6·76	6·89	4·40	6·12	11·10	5·15
CaO	10·21	9·48	9·68	10·41	10·86	10·70	12·26	8·46	9·97	11·55	9·75
Na_2O	2·77	3·01	2·62	2·59	2·74	2·53	2·19	4·05	3·39	1·94	3·22
K_2O	0·51	1·07	0·62	0·42	0·73	0·47	0·19	0·99	0·68	0·29	0·46
P_2O_5	0·28	0·15	0·56	0·30	0·23	0·40	0·15	0·51	0·33	0·17	0·30
H_2O	0·24	0·16	0·21	0·10	0·23	0·17	0·15	0·06	0·18	0·16	0·59
CO_2	0·02	0·01	0·02	0·01	0·03	0·01	0·02	—	0·01	0·01	
Sum	100·89	100·50	100·68	101·05	100·43	100·00	100·93	100·14	100·41	99·58	100·24
Trace elements											
*XRF (ppm)**											
Co	52	47	51	54	45	53	55	48	52	58	
Cr	96	63	<18	80	100	37	97	<18	103	611	50
Ni	39	49	18	39	53	93	60	42	68	266	35
V	403	277	414	411	269	390	332	273	308	286	365
Zn	119	103	146	126	96	119	92	126	101	75	141
ICP-MS (ppm)†											
Rb	9·5	23·7	12·0	7·3	14·0	8·6	3·7	20·9	15·6	5·9	10·6
Sr	234	149	332	206	209	337	159	349	384	276	287
Y	33·1	30·2	40·6	35·0	27·3	33·7	27·0	43·8	32·0	23·5	29·3
Zr	159	205	244	161	150	201	86·2	261	172	104	154
Nb	17·1	31·1	38·9	16·9	21·3	27·1	8·1	32·2	20·1	10·6	19·1
Cs	0·107	0·252	0·140	0·077	0·167	0·099	0·038	0·248	0·172	0·068	0·140
Ba	113	149	188	83·9	116	138	40·2	241	172	82·8	179
La	14·6	25·0	27·4	13·4	19·2	18·9	6·61	25·6	16·1	8·78	17·9
Ce	35·0	54·1	64·6	33·4	41·9	45·4	16·8	60·3	37·8	21·6	43·1
Pr	4·83	6·37	8·67	4·75	5·27	6·24	2·45	8·08	5·19	3·09	5·77
Nd	22·1	24·6	38·2	22·0	21·8	27·7	11·8	35·0	23·2	14·3	25·8
Sm	5·86	5·77	9·27	6·13	5·26	6·91	3·58	8·62	5·94	3·96	6·79
Eu	2·06	1·55	3·06	2·04	1·57	2·31	1·25	2·74	2·00	1·39	2·36
Gd	6·57	6·06	9·45	6·79	5·49	6·99	4·22	9·04	6·32	4·48	7·20
Tb	1·08	0·985	1·48	1·13	0·894	1·14	0·749	1·43	0·998	0·734	1·13
Dy	6·56	6·14	8·62	6·92	5·37	6·60	4·82	8·61	6·07	4·50	6·87
Ho	1·30	1·24	1·67	1·39	1·08	1·27	1·01	1·70	1·19	0·902	1·36
Er	3·50	3·46	4·44	3·75	2·94	3·34	2·79	4·63	3·24	2·45	3·66
Tm	0·492	0·508	0·605	0·534	0·420	0·457	0·403	0·645	0·450	0·338	0·514
Yb	3·15	3·39	3·85	3·37	2·72	2·89	2·66	4·22	2·87	2·18	3·30
Lu	0·449	0·474	0·549	0·483	0·387	0·416	0·386	0·611	0·417	0·313	0·454
Hf	4·55	5·74	6·69	4·70	4·71	4·87	2·55	6·39	3·85	2·76	4·66
Ta	1·14	2·10	2·58	1·14	1·59	1·65	0·529	1·93	1·10	0·637	1·50
Pb	1·15	2·36	1·60	0·973	1·61	1·22	0·516	2·08	1·91	0·707	1·57
Th	1·47	3·90	2·12	1·17	2·70	1·38	0·584	2·08	1·40	0·659	1·69
U	0·426	1·19	0·652	0·349	0·785	0·442	0·171	0·664	0·428	0·206	0·532
ID-MS (ppm)‡											
Th	1·41	3·82		1·13		1·39	0·578	2·10	1·29	0·638	1·60
U	0·427	1·14		0·354		0·447	0·177	0·705	0·422	0·207	0·492

Table 1: Continued

Sample:	H137	H136	H12	H11	H13	H88	H34	H32	H10	H84
Rift-zone:	E	E	SW	SW	SW	SW	SW	SW	SW	RP
Locality:	Snæfäll	Snæfäll	12 km N of F338	Þingvalla-vatn, SW	Lambahraun, E	Lambafell, E	Skaldbreiðar-hraun	Gráhraun	Seyðisholar	Eldvarpahraun
Longitude:	15·603	15·633	20·241	21·248	20·253	21·407	20·943	20·841	20·846	22·512
Latitude:	64·821	64·807	64·403	64·121	64·406	64·018	64·437	64·739	64·063	63·869
Age:	g	g	g	ph	ph	h	pg-ph	h	ph	pg
Rock type:	mug	tb	ol-th	ol-th	ol-th	q-th	ol-th	ol-th	ol-th	q-th
*Major elements by XRF (wt %)**										
SiO_2	53·74	47·62	48·29	48·65	47·87	48·80	48·71	48·75	47·47	48·94
TiO_2	2·53	1·79	1·98	1·63	1·90	1·59	1·44	1·04	1·71	2·10
Al_2O_3	15·03	15·00	15·18	14·40	14·78	14·52	14·88	16·27	14·76	13·64
Fe_2O_3	11·89	11·38	14·28	13·54	13·68	13·34	12·24	10·91	11·95	15·33
MnO	0·24	0·17	0·21	0·20	0·20	0·20	0·19	0·17	0·17	0·23
MgO	3·21	10·11	6·95	7·60	7·67	7·79	8·28	9·29	9·31	6·38
CaO	6·96	10·88	11·23	12·23	12·02	12·24	12·76	12·17	12·80	11·07
Na_2O	3·87	1·94	2·26	2·21	2·08	1·85	1·75	1·80	1·93	2·03
K_2O	1·58	0·66	0·26	0·20	0·17	0·19	0·12	0·11	0·29	0·23
P_2O_5	0·59	0·25	0·20	0·15	0·20	0·15	0·16	0·11	0·18	0·21
H_2O	0·18	0·47	0·22	0·19	0·14	0·20	0·12	0·07	0·14	0·19
CO_2	0·19	0·02	0·02	0·03	0·02	0·03	—	—	0·02	0·04
Sum	99·64	99·80	100·84	100·81	100·57	100·67	100·53	100·62	100·57	100·16
*Trace elements XRF (ppm)**										
Co	31	50	63	62	64	57	53	53	54	60
Cr	<18	835	128	132	289	128	369	138	217	110
Ni	16	198	76	77	98	85	98	132	145	93
V	180	269	385	353	341	354	320	257	283	438
Zn	139	75	108	95	101	90	89	75	80	117
ICP-MS (ppm)†										
Rb	35·9	15·6	4·7	3·5	2·5	3·7	1·4	1·8	5·0	4·7
Sr	368	384	186	185	196	205	154	124	276	158
Y	50·8	18·7	28·2	23·5	24·0	22·7	19·3	15·0	15·2	31·6
Zr	402	128	102	75·1	88·0	78·9	69·4	42·0	89·8	94·8
Nb	48·5	19·6	14·5	9·3	12·3	9·4	7·9	4·7	13·1	12·1
Cs	0·269	0·176	0·060	0·041	0·029	0·042	0·014	0·023	0·057	0·044
Ba	400	177	78·6	54·3	52·6	58·0	33·9	30·5	83·6	63·2
La	39·7	16·6	10·0	6·83	8·20	7·25	5·89	3·67	10·1	8·84
Ce	90·6	36·5	23·9	16·9	20·9	17·8	15·8	9·57	25·3	21·3
Pr	11·3	4·64	3·36	2·44	3·01	2·55	2·32	1·41	3·43	3·11
Nd	48·0	19·3	15·3	11·4	14·0	12·0	11·0	6·75	15·1	14·7
Sm	11·1	4·44	4·15	3·24	3·88	3·37	3·22	2·09	3·80	4·21
Eu	3·36	1·47	1·43	1·18	1·44	1·22	1·19	0·848	1·31	1·47
Gd	11·0	4·48	4·77	3·76	4·47	3·96	3·73	2·62	3·82	5·08
Tb	1·66	0·669	0·806	0·659	0·743	0·673	0·632	0·463	0·583	0·869
Dy	9·77	3·82	5·11	4·21	4·66	4·34	4·06	3·05	3·45	5·69
Ho	1·90	0·726	1·05	0·876	0·951	0·897	0·841	0·638	0·659	1·19
Er	5·03	1·91	2·90	2·48	2·61	2·50	2·35	1·80	1·71	3·38
Tm	0·698	0·260	0·419	0·358	0·382	0·362	0·341	0·272	0·226	0·490
Yb	4·42	1·67	2·80	2·35	2·50	2·37	2·28	1·83	1·46	3·23
Lu	0·642	0·234	0·406	0·342	0·360	0·346	0·320	0·257	0·198	0·479
Hf	8·52	3·14	2·92	2·20	2·52	2·23	2·02	1·32	2·56	2·60
Ta	2·56	1·14	0·897	0·577	0·777	0·578	0·511	0·301	0·875	0·673
Pb	1·97	1·36	0·737	0·583	0·644	0·564	0·564	0·316	0·700	0·879
Th	3·93	1·58	0·792	0·477	0·400	0·464	0·225	0·274	0·810	0·591
U	1·17	0·458	0·233	0·149	0·127	0·144	0·081	0·087	0·272	0·179
ID-MS (ppm)‡										
Th	3·84	1·53		0·460	0·385	0·460	0·220	0·287	0·803	
U	1·23	0·468		0·148	0·128	0·148	0·0773	0·0892	0·259	

Sample:	H36	H79	H37	H1	H80	H86	H82	H83	H97
Rift-zone:	RP	RP	RP	RP	RP	RP	RP	RP	SNP/Sj
Locality:	Blue lagoon	Mælifell	Hliðarvatn, N	Herdísar-víkurhraun	Háleyabunga	Þorbjarnar fell, E	Lágafell	Lágafell	Háahraun
Longitude:	22·422	22·115	21·744	21·909	22·656	22·378	22·534	22·534	23·743
Latitude:	63·893	63·863	63·876	63·864	63·819	63·867	63·880	63·880	64·742
Age:	h	h	h	pg	pg	pg	pg	pg	pg
Rock type:	q-th	q-th	ol-th	ol-th	ol-th	ol-th	pc	pc	haw
*Major elements by XRF (wt %)**									
SiO_2	48·99	49·40	48·21	48·42	48·39	47·52	46·03	45·55	48·01
TiO_2	2·00	1·49	1·79	1·42	0·46	0·45	0·37	0·34	3·51
Al_2O_3	13·91	14·25	15·31	15·32	15·15	14·96	11·14	10·20	14·94
Fe_2O_3	14·40	13·33	13·21	12·19	9·18	8·96	9·49	9·61	13·69
MnO	0·22	0·21	0·20	0·19	0·15	0·15	0·15	0·15	0·25
MgO	6·75	7·73	7·72	8·33	12·35	14·21	21·85	24·22	4·13
CaO	11·38	12·38	12·02	12·47	13·26	12·64	9·99	9·16	8·86
Na_2O	1·93	1·77	1·86	2·00	1·10	1·08	0·74	0·68	3·59
K_2O	0·22	0·18	0·23	0·15	0·01	0·02	0·01	0·01	1·56
P_2O_5	0·20	0·14	0·19	0·14	0·03	0·03	0·03	0·02	1·32
H_2O	0·16	0·10	0·13	0·10	0·14	0·26	0·14	0·13	0·32
CO_2	0·02	0·02	—	0·02	—	0·02	—	—	0·01
Sum	100·00	100·88	100·74	100·63	100·08	100·02	99·80	99·94	99·86
Trace elements									
*XRF (ppm)**									
Co	56	55	54	55	50	54	69	74	38
Cr	159	117	258	294	696	891	2235	2576	<18
Ni	65	71	103	110	234	333	700	839	21
V	410	353	350	314	203	184	157	149	305
Zn	109	90	96	86	56	51	53	55	130
ICP-MS (ppm)†									
Rb	3·7	3·3	3·6	2·6	0·15	0·3	0·2	0·12	30·0
Sr	161	167	183	159	65	80	39	35	536
Y	25·5	22·9	18·5	20·3	12·5	11·9	10·6	9·6	39·7
Zr	90·7	70·9	73·8	62·8	15·6	15·5	12·6	11·4	283
Nb	12·0	8·5	11·6	7·9	0·40	0·82	0·47	0·39	78·5
Cs	0·043	0·037	0·043	0·030	0·003	0·005	0·003	0·003	0·363
Ba	64·6	52·4	68·3	42·4	3·6	6·9	3·5	2·9	726
La	8·73	6·37	8·32	5·66	0·535	0·807	0·489	0·411	59·2
Ce	22·3	15·8	20·7	14·0	1·75	2·27	1·45	1·25	129·8
Pr	3·16	2·30	2·87	2·02	0·345	0·392	0·269	0·238	16·2
Nd	14·9	10·8	12·8	9·59	2·14	2·21	1·62	1·43	66·7
Sm	4·24	3·16	3·45	2·81	0·958	0·934	0·771	0·673	13·3
Eu	1·47	1·15	1·29	1·02	0·428	0·423	0·326	0·295	4·31
Gd	4·83	3·76	3·86	3·31	1·50	1·46	1·23	1·11	11·9
Tb	0·818	0·667	0·627	0·580	0·304	0·291	0·252	0·226	1·64
Dy	5·35	4·38	3·93	3·73	2·18	2·06	1·83	1·63	9·21
Ho	1·12	0·915	0·793	0·779	0·487	0·458	0·407	0·369	1·77
Er	3·15	2·60	2·18	2·16	1·42	1·33	1·20	1·08	4·73
Tm	0·440	0·373	0·326	0·316	0·212	0·197	0·181	0·161	0·623
Yb	2·95	2·48	2·16	2·07	1·42	1·34	1·21	1·07	4·09
Lu	0·429	0·368	0·301	0·303	0·218	0·201	0·181	0·163	0·588
Hf	2·75	2·07	2·18	1·86	0·580	0·545	0·452	0·400	7·19
Ta	0·826	0·539	0·751	0·489	0·029	0·052	0·038	0·027	5·30
Pb	0·663	0·518	0·636	0·470	0·095	0·188	0·083	0·081	2·42
Th	0·532	0·424	0·539	0·372	0·022	0·044	0·031	0·023	3·90
U	0·183	0·129	0·171	0·114	0·007	0·013	0·010	0·009	1·27
ID-MS (ppm)‡									
Th	0·537	0·399	0·548	0·364		0·0409			3·76
U	0·174	0·130	0·177	0·117		0·0134			1·15

Table 1: Continued

Sample:	H100	H98	H99	H90	H91	H118	H117	H123
Rift-zone:	SNP/Sj	SNP/Sj	SNP/Sj	SNP/Ly	SNP/Ly	SNP/Lj	SNP/Lj	SNP/Lj
Locality:	Neshraun, Öndverðarnes	Drangahraun	Neshraun, Gufuskálamóða	Bláfeldarhraun	Búðahraun	Hólmshraun	Raudheilihraun	Gbroharhraun
Longitude:	24·042	23·826	23·971	23·282	23·394	21·978	22·052	21·569
Latitude:	64·881	64·752	64·876	64·839	64·825	64·866	64·822	64·746
Age:	pg	pg	pg	pg	pg	pg	pg	ph
Rock type:	ab	haw	ab	ab	ab	tb	tb	tb
*Major elements by XRF (wt %)**								
SiO_2	46·38	46·23	45·98	45·44	46·06	47·50	47·54	47·59
TiO_2	3·95	3·77	3·72	3·37	2·59	1·53	1·24	1·60
Al_2O_3	14·85	15·12	15·09	15·66	14·30	16·89	17·37	15·50
Fe_2O_3	15·36	15·04	14·91	15·21	12·61	11·83	10·59	11·88
MnO	0·24	0·23	0·22	0·21	0·19	0·18	0·17	0·19
MgO	4·97	5·02	5·23	6·40	9·76	8·22	9·02	9·07
CaO	9·49	9·96	10·26	10·20	11·50	11·65	12·43	11·69
Na_2O	3·21	2·98	2·80	2·61	2·05	1·99	1·81	1·97
K_2O	1·24	1·16	1·10	0·89	0·78	0·47	0·32	0·51
P_2O_5	0·87	0·81	0·77	0·45	0·44	0·19	0·13	0·19
H_2O	0·19	0·13	0·27	0·19	0·17	0·15	0·22	0·17
CO_2	0·03	0·01	0·03	0·05	0·02	—	—	0·01
Sum	100·56	100·32	100·08	100·44	100·28	100·45	100·62	100·19
Trace elements								
*XRF (ppm)**								
Co	45	46	46	53	51	52	50	52
Cr	<18	36	62	108	590	57	56	275
Ni	14	61	58	69	199	91	110	108
V	456	478	476	471	365	293	263	320
Zn	123	116	114	107	85	78	68	79
ICP-MS (ppm)†								
Rb	25·7	19·7	23·7	18·1	18·1	9·1	6·6	9·7
Sr	528	493	524	466	443	289	270	275
Y	38·8	28·4	36·0	24·7	23·0	16·8	19·7	16·3
Zr	275	201	244	168	160	85·3	80·0	84·8
Nb	67·5	55·5	59·0	40·2	40·2	16·7	11·1	18·1
Cs	0·254	0·142	0·279	0·194	0·177	0·113	0·082	0·123
Ba	560	540	502	404	342	135	93·2	143
La	43·4	40·3	38·0	28·8	27·4	13·4	8·98	14·3
Ce	94·2	89·3	83·6	62·1	59·3	31·7	21·0	33·6
Pr	11·8	11·1	10·6	7·83	7·44	4·11	2·88	4·29
Nd	48·5	45·5	43·9	32·5	30·4	17·6	12·8	18·2
Sm	9·91	9·26	9·01	6·80	6·26	4·08	3·21	4·15
Eu	3·35	3·21	3·10	2·37	2·10	1·33	1·13	1·36
Gd	8·95	8·45	8·21	6·35	5·94	3·94	3·41	3·97
Tb	1·35	1·17	1·25	0·914	0·850	0·608	0·581	0·609
Dy	7·53	6·64	6·94	5·14	4·77	3·74	3·60	3·70
Ho	1·43	1·27	1·34	0·988	0·912	0·754	0·733	0·739
Er	3·83	3·38	3·56	2·65	2·44	2·10	2·01	2·03
Tm	0·527	0·459	0·487	0·359	0·330	0·275	0·288	0·273
Yb	3·39	3·01	3·15	2·36	2·14	1·85	1·87	1·81
Lu	0·505	0·425	0·467	0·338	0·308	0·265	0·278	0·257
Hf	5·88	5·20	5·27	4·09	3·81	2·46	2·12	2·51
Ta	3·67	3·67	3·20	2·36	2·33	1·17	0·676	1·25
Pb	1·92	1·84	1·69	1·28	1·24	0·901	1·023	1·67
Th	3·00	2·74	2·68	1·94	1·98	1·19	0·812	1·31
U	0·882	0·854	0·812	0·568	0·574	0·416	0·255	0·449
ID-MS (ppm)‡								
Th	2·96	2·71	2·58	1·87	1·87	1·21		1·29
U	0·874	0·819	0·781	0·565	0·568	0·381		0·410

Sample:	H113	H110	H114	H109	H101	H104	H102	H106
Rift-zone:	SNP/Lj	SNP/Lj	SNP/Lj	SNP/Lj	SNP/Lj	SNP/Lj	SNP/Lj	SNP/Lj
Locality:	Barnaborga-hraun	Rauhalshraun	Hraudalshraun	Nyhurhraun	Berserkja-hraun, W	Berserkjahraun, N	Berserkjahraun, W	Berserkjahraun, E
Longitude:	22·251	22·286	22·074	22·366	22·931	22·940	22·940	22·884
Latitude:	64·765	64·834	64·716	64·864	64·977	64·970	64·970	64·965
Age:	pg	1000	pg	pg	pg	pg	pg	pg
Rock type:	tb	tb	tb	tb	ab	ab	tb	tb
*Major elements by XRF (wt %)**								
SiO_2	47·78	48·07	47·58	46·66	47·74	48·08	46·82	46·86
TiO_2	1·42	1·61	1·45	2·12	1·98	1·88	1·67	1·66
Al_2O_3	15·84	14·98	15·84	14·59	14·72	14·66	12·81	12·75
Fe_2O_3	11·64	11·90	11·44	11·00	10·87	10·33	11·12	11·06
MnO	0·18	0·19	0·18	0·18	0·17	0·17	0·18	0·18
MgO	9·30	9·44	9·52	9·78	9·89	9·85	13·77	13·77
CaO	12·14	11·72	11·95	11·95	11·37	11·35	11·08	11·13
Na_2O	1·93	1·99	1·88	2·04	2·00	2·04	1·67	1·60
K_2O	0·33	0·57	0·37	0·50	0·96	0·96	0·64	0·64
P_2O_5	0·14	0·22	0·16	0·45	0·38	0·34	0·25	0·25
H_2O	0·14	0·17	0·12	0·18	0·09	0·14	0·12	0·12
CO_2	—	0·01	0·01	0·01	0·01	0·02	0·02	—
Sum	100·70	100·69	100·37	99·27	100·08	99·66	100·01	99·90
Trace elements								
*XRF (ppm)**								
Co	55	51	52	49	45	44	54	54
Cr	262	451	329	665	751	775	1532	1548
Ni	147	166	131	178	216	195	390	341
V	284	291	276	323	292	281	280	274
Zn	80	81	75	79	76	77	76	72
ICP-MS (ppm)†								
Rb	6·7	13·2	7·8	11·5	21·9	19·3	16·4	15·7
Sr	219	266	253	363	452	396	349	339
Y	22·5	22·2	22·2	27·2	19·7	17·7	18·6	18·1
Zr	85·7	120	95·2	132	155	143	120	117
Nb	11·3	22·1	13·2	27·8	43·2	40·3	29·7	29·0
Cs	0·082	0·163	0·096	0·125	0·246	0·125	0·174	0·161
Ba	90·0	163	107	203	341	323	228	219
La	8·92	16·1	10·3	21·3	32·6	29·5	20·4	19·6
Ce	21·1	35·5	24·2	48·3	71·9	64·2	43·7	42·0
Pr	2·95	4·62	3·34	6·31	8·54	7·57	5·43	5·26
Nd	13·2	19·2	14·8	27·1	34·5	29·5	21·9	21·2
Sm	3·45	4·29	3·74	6·14	6·86	5·83	4·62	4·43
Eu	1·21	1·39	1·29	2·00	1·96	1·84	1·45	1·39
Gd	3·77	4·21	3·91	6·13	5·89	5·21	4·48	4·30
Tb	0·649	0·685	0·664	0·926	0·821	0·722	0·651	0·625
Dy	4·04	4·11	4·09	5·41	4·76	4·05	3·73	3·60
Ho	0·825	0·817	0·824	1·06	0·914	0·769	0·723	0·699
Er	2·28	2·25	2·26	2·84	2·45	2·06	1·94	1·90
Tm	0·327	0·319	0·322	0·396	0·294	0·285	0·268	0·260
Yb	2·15	2·09	2·11	2·51	1·98	1·85	1·74	1·69
Lu	0·319	0·312	0·311	0·364	0·282	0·257	0·252	0·246
Hf	2·24	2·87	2·40	3·40	4·20	3·76	2·96	2·87
Ta	0·683	1·32	0·794	1·65	3·08	2·58	1·74	1·68
Pb	0·749	1·11	0·907	1·03	1·32	1·45	1·07	1·01
Th	0·797	1·57	0·932	1·65	3·06	3·03	1·91	1·83
U	0·250	0·489	0·290	0·485	1·09	0·953	0·563	0·540
ID-MS (ppm)‡								
Th				1·48	2·99	2·99		1·85
U				0·466	0·924	0·921		0·569

*Fe_2O_3 is given as total Fe (= Fe_2O_3 + FeO/0·8998); see Appendix for analytical procedures.
†See Appendix for analytical procedures.
‡U and Th concentrations measured by isotope dilution mass spectrometry at IFM-GEOMAR as reported by Kokfelt *et al.* (2003). Major element composition of OR58 is from Prestvik (1985).
NE, Northeast rift; MIB, Mid-Iceland Belt; SE, SE rift; VM, Vestmannaeyjar; E, East rift; SW, Southwest rift; RP, Reykjanes Peninsula; SNP, Snaefellsnes Peninsula; Sj, Snæfellsjökull; Ly, Lýsuskarð; Lj, Ljósufjöll; q-th, quartz tholeiite; ol-th, olivine tholeiite; pc, picrite; tb, transitional basalt; ab, alkali basalt; haw, hawaiite; mug, mugearite; h, historic; pg, post-glacial; g, glacial.

5 and 10 wt % MgO. With decreasing MgO, CaO/Al_2O_3 in both the tholeiitic and alkalic groups decreases. Compared with the tholeiitic rocks, the majority of alkalic rocks have lower CaO/Al_2O_3 contents at a given MgO (Fig. 2b). The difference in CaO/Al_2O_3 could result from early olivine and plagioclase fractionation (the main observed phenocryst phases) in the parental tholeiites, whereas early olivine and clinopyroxene fractionation (the main observed phenocryst phases) dominates in the most primitive alkali basalts. The picritic lavas from the main rifts have high contents of MgO (10–24 wt %), Ni (162–839 ppm) and Cr (345–2576 ppm), very low alkali contents ($\leq$1 wt %; Fig. 2a) and high CaO/Al_2O_3 ratios (0·9–1·1; Fig. 2b). Accumulation of up to 36% olivine + Cr-spinel may explain the high MgO, Ni and Cr contents, if it is assumed that the mantle-derived melts had ~11% MgO (see Skovgaard *et al.*, 2001, fig. 2b). However, the high CaO/Al_2O_3 ratios in the picrites cannot reflect olivine accumulation.

The potential source rock material and pressure range for melt generation may be roughly estimated for the different rift zone magmas from the FeO* vs SiO_2 relationship by comparing the least evolved lavas (MgO >8 wt %) with experimental data (Fig. 2c). Picrites are corrected for the effects of olivine accumulation by normalizing to a fixed MgO content of 11% (see above), whereas all other lavas are plotted uncorrected. The corrected picrite data from Reykjanes Peninsula and Mælifell have relatively low FeO* contents (lowest in the former), which would indicate derivation from a depleted source, such as KLB-1 (mg-number = 89), or KG1 and KG2, at shallow pressures (~1·5–2·0 GPa). Assuming a fertile mantle rock (HK-66 with mg-number = 85), the equivalent pressure range of partial melting for tholeiites from the main rifts is ~1·5–2·5 GPa. Overall, the Iceland samples define a broad negative correlation on the SiO_2 vs FeO* diagram with the picrites having the highest SiO_2 and lowest FeO*. Comparison of the basalt data with experimental data suggests that the melts formed at the shallowest depths (picrites) come from the most depleted source material, whereas the melts formed at the greatest depths come from more fertile source material. Alternatively, the variability in FeO* could reflect the melting column morphology, which is strongly dictated by proximity to the plume and crustal thickness.

Trace elements

The incompatible trace element contents are shown for each rift system in Fig. 3. The trace element characteristics of the three major rock types (alkalic basalts, tholeiites and picrites) are summarized in Fig. 4. The off-rift alkalic basalts have the highest relative enrichments of highly and moderately incompatible trace elements, the main rift tholeiites intermediate contents and the picrites have the lowest concentrations. The alkali basalts also have relatively fractionated rare earth element (REE) patterns [$(La/Yb)_N$ = 4·9–11·2; subscript N denotes chondrite normalization], compared with tholeiites [$(La/Yb)_N$ = 0·9–4·7] and picrites [$(La/Yb)_N$ = 0·3–0·9]. The different REE patterns (i.e. slopes and normalized concentrations) cannot be produced by differentiation (note that only lavas with MgO >6 wt % are plotted in Figs 3 and 4), but must reflect variations in the source and to a lesser extent in the degree of partial melting. The fractionated REE patterns of the alkali basalts are consistent with derivation through relatively low degrees of partial melting in the presence of residual garnet (e.g. Shimizu & Kushiro, 1975; Wood, 1979). In contrast, the flatter REE pattern in the tholeiites indicates higher degrees of melting with little or no residual garnet in the source region. The strong light REE (LREE) depletion of the picrites indicates derivation from a depleted source, and the flat normalized heavy REE (HREE) patterns indicate the absence of residual garnet.

The alkali basalts show distinct positive anomalies for Ba, Nb (and Ta), La and Ce, and negative anomalies for Th, U, K and Pb (Fig. 4), resulting in high ratios of Ce/Pb (20–55), Nb/U (46–77), and low K/Nb (150–280), relative to primitive mantle (McDonough & Sun, 1995). These geochemical characteristics are very similar to those of St. Helena basalts, such as SH68 (Fig. 4). Picrites are strongly depleted in the most incompatible elements (Rb, Th, U, K) and show distinct positive anomalies at Sr, Ba and (less so) Eu, giving rise to relatively high ratios of Sr/Nd, Ba/(Rb, Th, U, Nb) and Eu/(Hf, Ti). Notably, these positive Sr, Ba and Eu anomalies do not reflect accumulation of plagioclase, because plagioclase is only rarely present modally (except in H86) and would have reduced the CaO/Al_2O_3 ratio. Picrites also show less distinct negative Pb anomalies, and hence lower Ce/Pb ratio (18 $\pm$ 5), as well as slight depletions in Zr and Hf relative to Sm, which has a comparable incompatibility. These geochemical characteristics are consistent with those reported previously for the Icelandic picrites (Hémond *et al.*, 1993; Chauvel & Hémond, 2000; Skovgaard *et al.*, 2001) and were also described in primitive glasses from Kistufell in central Iceland (Breddam, 2002).

In addition, several of the high-MgO olivine tholeiites from the MIB (but not all) show distinct positive anomalies for K, P and Ti (Figs 3b and 4), a feature that to our knowledge has not been reported for high-MgO basalts in Iceland before. For these rocks, the size of the Ba, Sr, Eu, K, P and Ti anomalies are internally correlated, and inversely correlated with the degree of elemental depletion, meaning that the highest Sr/Nd, Eu/Eu*, K/Nb, P/Sm and Ti/Tb ratios, and lowest Zr/Y and Hf/Sm ratios are found in the most depleted MIB tholeiites

Table 2: Sr–Nd–Pb isotope compositions of lavas from the neovolcanic rift zones of Iceland

Sample	$^{206}Pb/^{204}Pb$	±2σ	$^{207}Pb/^{204}Pb$	±2σ	$^{208}Pb/^{204}Pb$	±2σ	$^{87}Sr/^{86}Sr$	±2σ	$^{143}Nd/^{144}Nd$	±2σ
NE Rift										
H15	18·327	4	15·448	3	37·974	8			0·513084	6
H15	18·323	4	15·445	3	37·964	8	0·703033	5	0·513091	2
H15*	18·325	6	15·447	4	37·969	15			0·513088	7
H16	18·419	3	15·450	2	38·079	5	0·703128	8	0·513055	4
H17	18·075	5	15·428	4	37·754	9	0·703147	8	0·513034	5
H17	18·072	3	15·422	2	37·743	6	0·703157	5	0·513029	8
H17							0·703151	8	0·513025	5
H17									0·513030	6
H17*	18·074	4	15·425	8	37·748	15	0·703152	8	0·513030	6
H19	18·454	4	15·473	2	38·168	6	0·703207	7	0·513045	8
H20	18·446	2	15·461	2	38·129	4	0·703211	8	0·513032	5
H21	18·444	2	15·466	2	38·138	5	0·703257	8	0·513016	8
H23	18·424	1	15·459	1	38·105	2	0·703245	9	0·513027	6
H24	18·346	1	15·461	1	38·069	2	0·703297	8	0·513009	6
H24	18·350	1	15·467	1	38·090	3	0·703317	8	0·513008	6
H24*	18·348	6	15·464	9	38·079	29	0·703307	20	0·513009	1
H25	18·390	1	15·468	1	38·103	3	0·703309	7	0·513017	6
H26	18·473	2	15·469	2	38·173	5				
H26	18·474	1	15·470	1	38·179	2			0·513023	7
H26	18·464	1	15·466	1	38·159	1	0·703236	5	0·513023	3
H26*	18·470	11	15·468	4	38·170	20			0·513023	0
H125	18·093	6	15·447	5	37·797	12	0·703121	7	0·513033	9
H125	18·081	3	15·440	2	37·778	6	0·703138	5	0·513043	7
H125*	18·087	16	15·443	10	37·787	27	0·703130	17	0·513038	10
H127†	18·072	5	15·427	5	37·732	11	0·703054	5	0·513080	4
H129	18·084	2	15·437	2	37·748	4	0·703094	8	0·513062	7
H131	18·253	1	15·448	1	37·925	3	0·703224	8	0·513033	5
H131							0·703228	6	0·513025	6
H131*							0·703226	4	0·513029	8
H134	18·368	2	15·453	1	38·012	4	0·703109	6	0·513068	8
Mid Iceland Belt (MIB)										
H6	18·353	3	15·446	3	38·005	7	0·703080	9	0·513078	7
H6	18·350	3	15·443	2	38·002	5	0·703085	6	0·513069	6
H6							0·703081	10	0·513072	7
H6*	18·352	4	15·444	5	38·003	4	0·703082	4	0·513073	7
501†	18·584	5	15·476	5	38·192	11	0·703192	6	0·513048	3
501†	18·578	4	15·475	4	38·190	9				
501*†	18·581	8	15·475	2	38·191	2				
502†	18·667	3	15·480	2	38·247	6	0·703118	8	0·513049	3
502B†	18·670	5	15·489	4	38·276	11	0·703114	6	0·513044	2
503†	18·622	6	15·475	4	38·202	11	0·703064	7	0·513053	8
CIS46†	18·445	4	15·450	4	38·053	9	0·703068	7	0·513078	3
CIS47†	18·423	5	15·452	4	38·046	10	0·703052	7	0·513080	3
CIS57†	18·137	6	15·433	5	37·875	12	0·703063	5	0·513117	2
CIS57†	18·139	2	15·437	2	37·887	6			0·513111	4
CIS57*†	18·138	3	15·435	7	37·881	17			0·513114	6

Table 2: Continued

Sample	$^{206}Pb/^{204}Pb$	±2σ	$^{207}Pb/^{204}Pb$	±2σ	$^{208}Pb/^{204}Pb$	±2σ	$^{87}Sr/^{86}Sr$	±2σ	$^{143}Nd/^{144}Nd$	±2σ
Q4†	18·421	5	15·454	4	38·048	10	0·703066	6	0·513080	4
Q5†	18·414	4	15·452	4	38·038	9	0·703057	6	0·513085	7
Q6†	18·437	6	15·454	5	38·058	13	0·703058	4	0·513077	3
Q7†	18·384	3	15·442	3	38·031	7	0·703062	5	0·513053	2
Q9†	18·421	3	15·450	2	38·075	6	0·703108	5	0·513070	3
Q10†	18·434	2	15·451	1	38·092	3	0·703129	4	0·513056	2
Q12†	18·448	3	15·469	2	38·189	5	0·703245	4	0·513021	3
Q12†	18·450	3	15·471	2	38·195	6				
Q12*†	18·449	3	15·470	4	38·192	9				
SE Rift										
H2	18·503	1	15·482	1	38·287	2	0·703336	8	0·513000	5
H2							0·703364	9	0·513005	6
H2*							0·703350	28	0·513003	5
H3	18·466	3	15·468	3	38·181	7	0·703251	7	0·513020	8
H4	19·243	1	15·546	1	38·917	2	0·703331	7	0·512955	6
H4	19·242	1	15·546	1	38·918	10	0·703310	8	0·512967	6
H4*	19·242	2	15·546	1	38·918	1	0·703321	21	0·512961	12
H5	19·126	1	15·525	1	38·723	1	0·703201	11	0·513002	6
H5							0·703187	7	0·513008	7
H5*							0·703194	14	0·513005	6
H7	18·411	3	15·450	3	38·063	7			0·513058	5
H7	18·408	2	15·451	1	38·072	4	0·703112	5	0·513058	3
H7*	18·409	4	15·451	1	38·067	13			0·513058	0
H61	19·232	1	15·557	1	38·933	2	0·703314	8	0·512962	4
Q1	19·015	2	15·514	2	38·531	4	0·703161	4	0·513007	3
Q1	19·019	3	15·516	2	38·536	6				
Q1*	19·017	6	15·515	3	38·533	7				
Vestmannaeyjar (VM)										
H119	18·980	1	15·529	1	38·566	3	0·703171	9	0·513011	7
H120	18·934	1	15·528	1	38·492	2	0·703149	5	0·513013	2
H122	19·014	8	15·530	1	38·569	2	0·703119	7	0·513006	5
E Rift										
H136	18·562	1	15·478	1	38·209	2	0·703179	9	0·512994	6
H137	18·437	1	15·465	1	38·107	1	0·703341	9	0·513001	6
Örafajokull										
OR58	18·479	2	15·523	1	38·381	3	0·703700	7	0·512943	9
OR58	18·478	1	15·521	1	38·376	2				
OR58	18·478	1	15·522	1	38·380	1	0·703694	5	0·512945	5
OR58*	18·478	2	15·522	2	38·379	6	0·703697	6	0·512944	2
SW Rift										
H10	18·882	3	15·500	2	38·372	6	0·703014	5	0·513035	5
H10	18·885	2	15·506	2	38·388	5	0·703010	5	0·513034	3
H10*	18·883	3	15·503	8	38·380	23	0·703012	5	0·513035	1
H11	18·740	4	15·498	3	38·324	7	0·703121	6	0·513024	3
H11	18·745	5	15·503	4	38·342	10	0·703130	7		

Table 2: Continued

Sample	$^{206}Pb/^{204}Pb$	±2σ	$^{207}Pb/^{204}Pb$	±2σ	$^{208}Pb/^{204}Pb$	±2σ	$^{87}Sr/^{86}Sr$	±2σ	$^{143}Nd/^{144}Nd$	±2σ
H11*	18·742	7	15·501	8	38·333	26	0·703125	9		
H13	18·694	2	15·506	3	38·323	7	0·703160	8	0·513026	6
H32	18·576	3	15·473	3	38·142	7	0·703047	6	0·513064	8
H34†	18·532	2	15·470	2	38·179	4	0·703105	5	0·513041	4
H88	18·717	2	15·491	2	38·284	5	0·703123	8	0·513023	6
Reykjanes Peninsula (RP)										
H1	18·779	3	15·508	3	38·374	6	0·703145	7	0·513028	7
H36	18·624	1	15·499	1	38·207	3	0·703146	5	0·513029	2
H37	18·737	2	15·499	2	38·277	4	0·703157	5	0·513020	2
H79	18·701	5	15·510	4	38·320	10	0·703133	7	0·513037	8
H80†	18·280	3	15·463	2	38·003	6	0·703025	7	0·513137	5
H80†							0·703028	4	0·513140	8
H80*†							0·703026	3	0·513138	3
H83†	18·499	4	15·469	3	38·131	9	0·702902	5	0·513140	5
H83†	18·491	6	15·461	5	38·104	13			0·513144	5
H83*†	18·495	12	15·465	10	38·118	37			0·513142	4
H84†	18·762	2	15·488	2	38·330	5	0·703121	5	0·513034	4
H86†	18·527	9	15·488	7	38·207	17	0·703152	5	0·513060	4
Snaefellsness Peninsula (SNP)										
H90	18·968	1	15·499	1	38·550	2	0·703405	4	0·512933	5
H90	18·971	1	15·504	1	38·565	2	0·703401	9	0·512939	8
H90*	18·970	4	15·502	6	38·557	22	0·703403	3	0·512936	6
H91	18·957	1	15·504	7	38·544	2	0·703362	10	0·512960	4
H97	18·864	2	15·508	1	38·454	3	0·703346	8	0·512958	5
H98	18·810	1	15·497	1	38·380	2	0·703359	8	0·512956	5
H99	18·947	1	15·501	1	38·528	3	0·703347	5	0·512954	2
H100	18·947	1	15·495	1	38·514	2	0·703347	4	0·512959	2
H100	18·951	2	15·500	1	38·529	3				
H100*	18·949	6	15·498	6	38·521	21				
H101	19·241	1	15·538	1	38·836	2	0·703429	7	0·512893	7
H101							0·703431	10	0·512892	7
H101*							0·703430	2	0·512893	1
H104	19·226	2	15·539	1	38·818	4	0·703427	6	0·512895	5
H106	19·113	1	15·528	1	38·712	1	0·703348	8	0·512929	5
H109	19·035	1	15·517	5	38·613	2	0·703352	9	0·512940	8
H118	18·783	2	15·494	1	38·335	3	0·703265	6	0·512942	8
H123†	18·874	2	15·499	2	38·422	4	0·703294	5	0·512933	4

*Average of replicate analyses with corresponding 2σ external precision. All other errors are 2σ internal precision at the last significant digit.
†Chips of 1–2 mm size were analysed; otherwise unleached powders were analysed.

(such as CIS057) (Fig. 3b). Most of these geochemical features (except P) are also found in oceanic gabbros drilled from the lower part of the oceanic crust (e.g. Hart *et al.*, 1999; Fig. 4), where these anomalies reflect the presence of cumulus plagioclase (±alkali feldspar) and Fe–Ti oxides (ilmenite ± magnetite).

Sr–Nd–Pb isotopes

The new isotope data are consistent with existing Iceland data ($^{87}Sr/^{86}Sr$ = 0·7030–0·7037; $^{143}Nd/^{144}Nd$ = 0·51289–0·51308; $^{206}Pb/^{204}Pb$ = 18·01–19·24; $^{207}Pb/^{204}Pb$ = 15·42–15·54; $^{208}Pb/^{204}Pb$ = 37·67–38·91; (O'Nions & Pankhurst, 1973; Sun & Jahn, 1975;

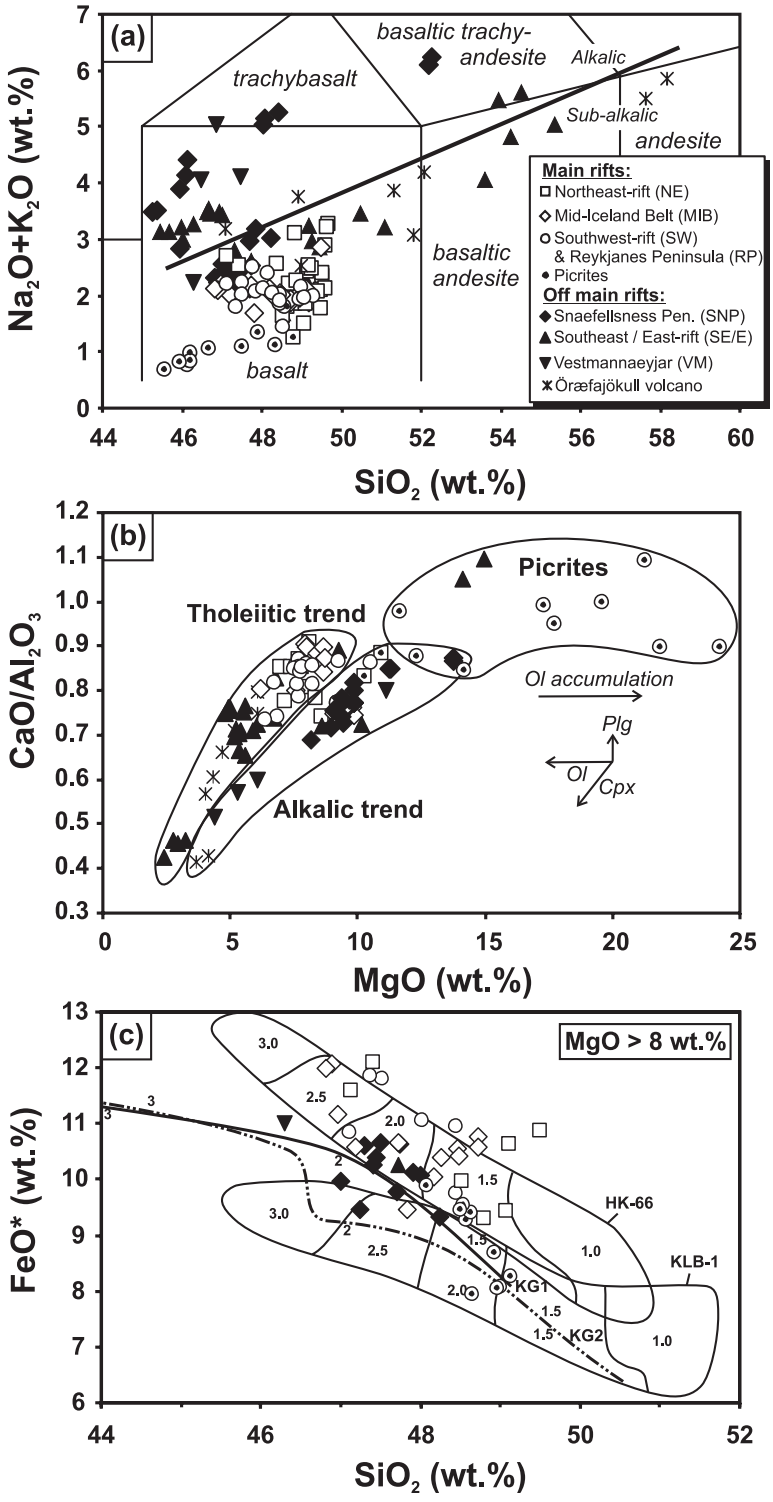

Fig. 2. Major element variations. (a) Total alkali–silica diagram for classification after Le Bas *et al.* (1986). (b) CaO/Al_2O_3 vs MgO (wt %). Arrows indicate the effect of fractional crystallization of plagioclase (plg), olivine (ol) and clinopyroxene (cpx). (c) FeO* vs SiO_2 (wt %) for the least evolved lavas (MgO >8 wt %) compared with experimental high-pressure partial melts of lherzolite (KLB-1 is refractory with mg-number = 89, whereas HK-66 is fertile with mg-number = 85; Hirose & Kushiro, 1993). Melt compositions for mixtures of depleted lherzolite and average MORB in proportions of 1:1 (KG1, continuous line) and 2:1 (KG2, dot–dashed line), respectively (Kogiso *et al.*, 1998). Picrites are corrected for olivine accumulation (up to 36% in sample H83) by subtracting, or adding magnesium-rich olivine until a MgO content of 11 wt % is reached in the melt. All other data are plotted uncorrected. Numbers in fields are pressure in GPa.

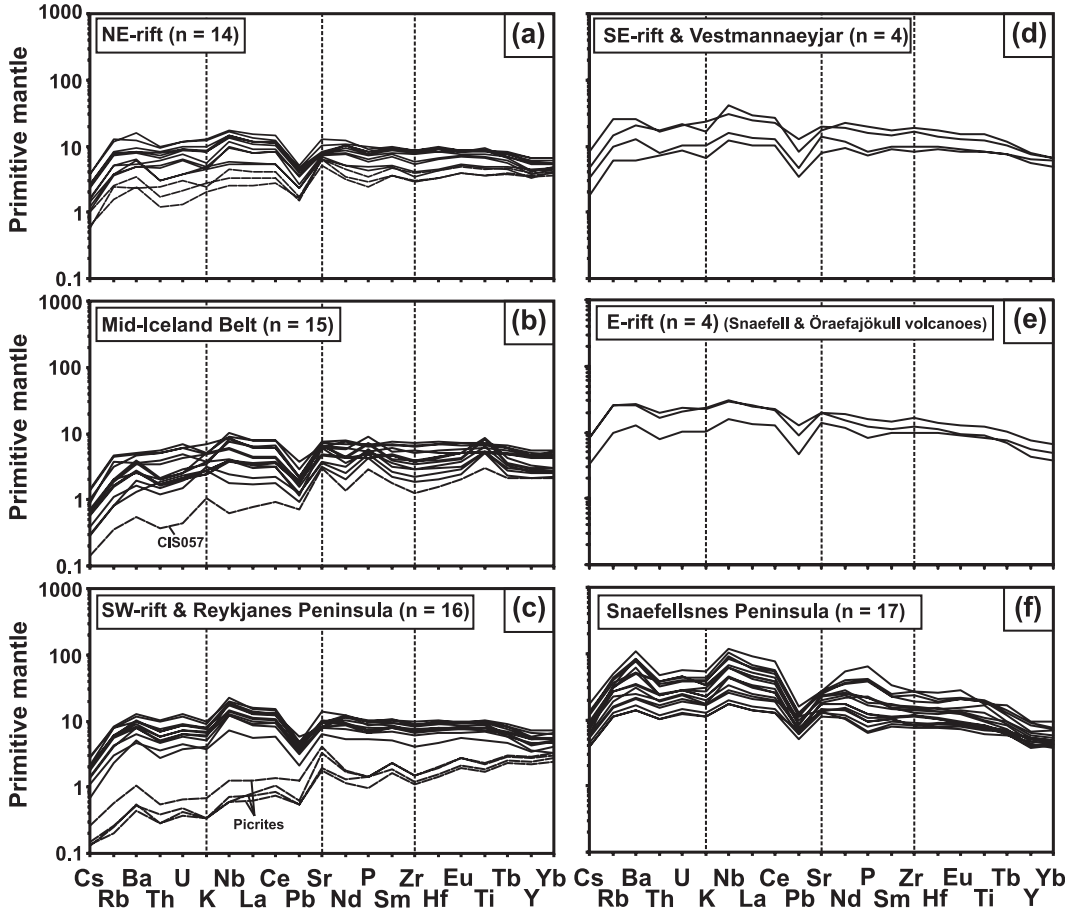

Fig. 3. Primitive mantle-normalized incompatible trace element diagrams for individual rift zones (MgO > 6%, except for Snæfellsjökull and Öræfajökull volcanoes). The main rift tholeiites (a–c) have intermediate normalized trace element patterns, compared with the more extreme patterns of off-rift enriched alkalic basalts (d–f) and main rift depleted picrites (c). Several tholeiites from MIB (such as CIS057) have positive anomalies for K, Ti and P in addition to Ba, Sr, and Eu. For the MIB tholeiites, the size of the Sr and Eu anomalies is inversely proportional to the degree of trace element depletion. Primitive mantle values are after McDonough & Sun (1995).

O'Nions *et al.*, 1976, 1977; Wood, 1978; Wood *et al.*, 1979; Zindler *et al.*, 1979; Condomines *et al.*, 1983; Hémond *et al.*, 1988, 1993; Elliott *et al.*, 1991; Furman *et al.*, 1991; Sigmarsson, 1991; Sigmarsson *et al.*, 1992*a*, 1992*b*; Gee *et al.*, 1998; Stecher *et al.*, 1999; Chauvel & Hémond, 2000; Kempton *et al.*, 2000; Prestvik *et al.*, 2001; Skovgaard *et al.*, 2001; Stracke *et al.*, 2003; Thirlwall *et al.*, 2004), but form comparatively tighter arrays in Sr–Nd–Pb isotope space (Figs 5 and 6), similar to those reported by Thirlwall *et al.* (2004). In Sr–Nd isotopic space (Fig. 5), our data generally lie at lower $^{87}Sr/^{86}Sr$ isotopic ratios than previously published data, consistent with our sample set being virtually unaffected by alteration and crustal interaction with hydrothermally altered material. In the Sr–Nd isotope diagram (Fig. 5) our data fall on a broad binary mixing array ($R^2 = 0{\cdot}90$, excluding the Örafæjökull volcanic rocks), with the enriched endmember represented by alkali basalts from SNP (Ljósufjöll system; Fig. 1), and the depleted endmember by picrites from the Reykjanes Peninsula (H83). A third possible endmember is represented by the Öræfajökull volcanics that have relatively high $^{87}Sr/^{86}Sr$ isotopic ratios and plot to the right of the array formed by the rest of the data. The NE rift tholeiites have relatively high $^{87}Sr/^{86}Sr$ isotopic ratios (for their $^{143}Nd/^{144}Nd$), compared with tholeiites from SW Iceland, suggesting some degree of isotopic heterogeneity in the source regions of the different rift zones. Lavas from the RP and SW rift have a relatively restricted Sr–Nd isotopic range. The SE rift lavas overlap the fields for the NE and SW Iceland volcanic rocks (Fig. 5). The lavas from Vestmannaeyjar (Heimaey) and Snaefell volcano (E rift) fall along a mixing trajectory pointing towards SNP. In the plot of 1/Sr vs $^{87}Sr/^{86}Sr$ (Fig. 5b), there are good linear correlations for each rift system, which suggest that mixing has occurred between melts,

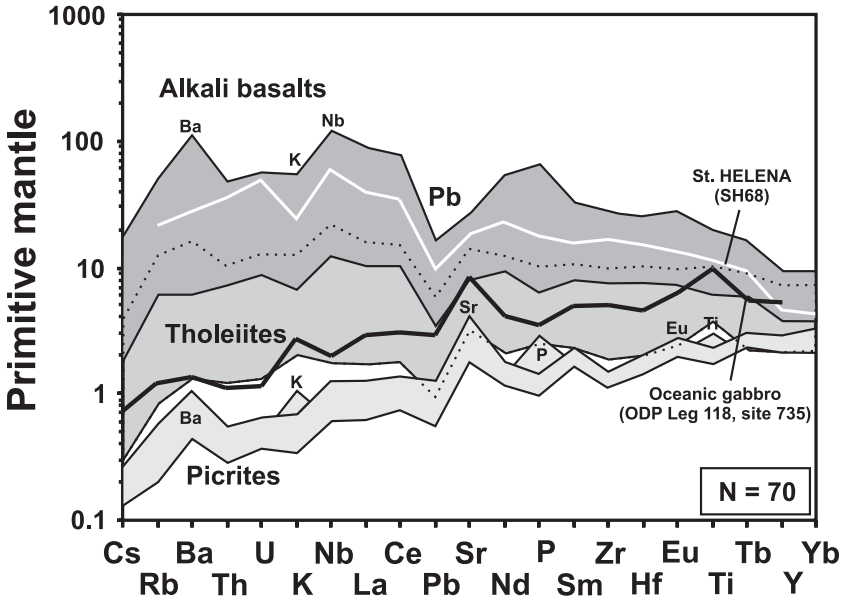

Fig. 4. Composite primitive mantle-normalized trace element diagram, comparing the alkalic basalts with typical HIMU-basalt from St. Helena (SH68; Chaffey *et al.*, 1989; Thirlwall, 1997) and the Icelandic picrites with average oceanic gabbros drilled from Ocean Drilling Program Leg 118 (Hart *et al.*, 1999). Primitive mantle values are after McDonough & Sun (1995).

rather than between solids on an intra-rift scale, because source mixing would generate more scatter on this diagram. Recently, it has been shown that mixing along the Galápagos or Cocos–Nazca spreading centre also occurs between melts rather than solids (Kokfelt *et al.*, 2005).

In Pb–Pb isotopic space, our data form excellent positive correlations ($^{207}Pb/^{204}Pb$ vs $^{206}Pb/^{204}Pb$; $R^2 = 0{\cdot}92$ and $^{208}Pb/^{204}Pb$ vs $^{206}Pb/^{204}Pb$; $R^2 = 0{\cdot}97$; excluding the Örafæjökull lavas) (Fig. 6), agreeing well with double-spike Pb isotope data presented by Thirlwall *et al.* (2004). In both uranogenic and thorogenic Pb diagrams, the new data define linear arrays with a shallower slope than that of the Northern Hemisphere Reference Line (NHRL; Hart, 1984). The linear arrays are consistent with mixing of depleted (picritic) and enriched (alkali basaltic) endmembers. Although the Iceland array overlaps the Atlantic MORB field (Reykjanes and Kolbeinsey Ridges) on the uranogenic diagram (Fig. 6b), it lies slightly above the Atlantic MORB field on the thorogenic diagram (Fig. 6a). The Örafæjökull lavas plot above the general arrays and consequently have higher $\Delta 7/4$ and $\Delta 8/4$ values, consistent with previous findings (Prestvik *et al.*, 2001).

On plots of $^{206}Pb/^{204}Pb$ vs $^{87}Sr/^{86}Sr$ (Fig. 6c) and $^{143}Nd/^{144}Nd$ (Fig. 6d), the lavas from the three rift systems (NE, SE/E and SW) and Snaefellsnes define relatively distinct fields, indicating derivation from different combinations of source components. The MIB lavas, located in central Iceland, overlap the fields for all three rift systems.

Oxygen isotope composition of olivine

Olivine separates from five alkali basalts and five (tholeiitic) picrites were analysed for their oxygen isotope composition (Table 2). The analytical procedures have been given by Sharp (1990). Reproducibility was monitored by repeated runs of UWG-2 garnet, which gave a value of 5·83 (±0·07‰; $n = 2$) relative to SMOW (Standard Mean Ocean Water), in accordance with the cited value of 5·87‰ (Valley *et al.*, 1995). Therefore, no corrections were applied to the data. Multiple analyses were performed to check for sample homogeneity. In three cases discrepancies were found between several analyses of the same separate (H129, H80, H119; see Table 2), indicating some degree of isotopic heterogeneity. The most plausible explanation for this isotopic heterogeneity is that some of the olivines are xenocrysts rather than phenocrysts, which at least for some of the most MgO-rich picrites, would suggest that they are the products of olivine accumulation. The remaining (seven) samples gave consistent values, within error.

Overall, $\delta^{18}O$ varies from 4·45‰ to 5·36‰, with consistently higher values in the alkali basalts ($\delta^{18}O$ = 4·78–5·36‰, average 5·14‰) than in the picrites ($\delta^{18}O$ = 4·45–5·07‰, average 4·84‰) (Table 2 and Fig. 7). Assuming a fractionation factor between olivine and basaltic melt at 1250°C of 0·4‰ (Kyser *et al.*, 1982), this would indicate that the oxygen isotopic range in the equilibrium melts would have $\delta^{18}O$ values of 4·8–5·5‰ for the picrites and 5·2–5·8‰ for the alkali basalts. These $\delta^{18}O$ values overlap and extend to significantly lower

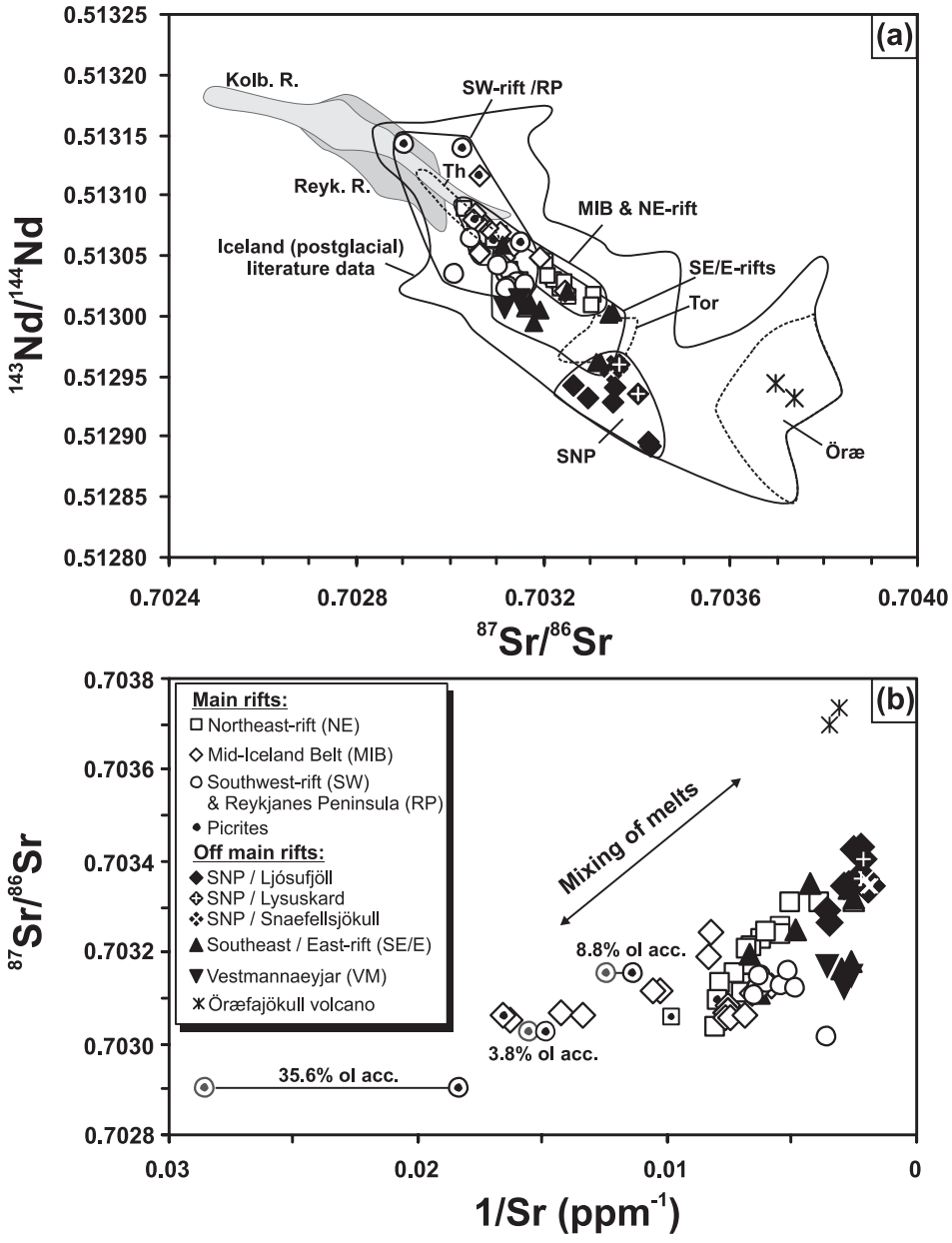

Fig. 5. (a) $^{87}Sr/^{86}Sr$ vs $^{143}Nd/^{144}Nd$ for Icelandic basalts. Fields for lavas typically referred to as isotopic endmember compositions in Iceland are shown: Theistareykir (Th), Torfajökull (Tor) and Öræfajökull (Öræ). Also shown are the fields for the neighbouring Mid-Atlantic Ridge, the Reykjanes Ridge and Kolbeinsey Ridge. (b) 1/Sr vs $^{87}Sr/^{86}Sr$ show good correlations for each rift system, indicating that mixing occurs between melts rather than solids on an intra-rift scale. Data sources for the Iceland post-glacial volcanics are given in the PetRidge web-database at http://www.ldeo.columbia.edu/datarep/index.html. Data sources for the Reykjanes and Kolbeinsey ridges are from Thirlwall *et al.* (2004).

values than the range in MORB (5·75 ± 0·2‰; Mattey *et al.*, 1994; Harmon & Hoefs, 1995; Eiler *et al.*, 2000). Compared with the range of previous oxygen isotope data for Icelandic picrites (3·68–5·75‰) (Muehlenbachs *et al.*, 1974; Condomines *et al.*, 1983; Hémond *et al.*, 1988; Gee *et al.*, 1998; Eiler *et al.*, 2000), our data are confined to a narrower interval at the upper end of the published range. Our oxygen isotope dataset for picrites and alkalic basalts forms very broad trends when plotted against source parameters, such as $^{143}Nd/^{144}Nd$ and $^{206}Pb/^{204}Pb$ (Fig. 7a and b), but also against ratios, such as Eu/Eu* and Ba/Th (Fig. 7c and d). We note that some Icelandic picrites from the literature have relatively high $\delta^{18}O$, forming a flat positive array in $\delta^{18}O$ vs $^{143}Nd/^{144}Nd$, trending opposite to our suggested picrite–alkalic basalt array.

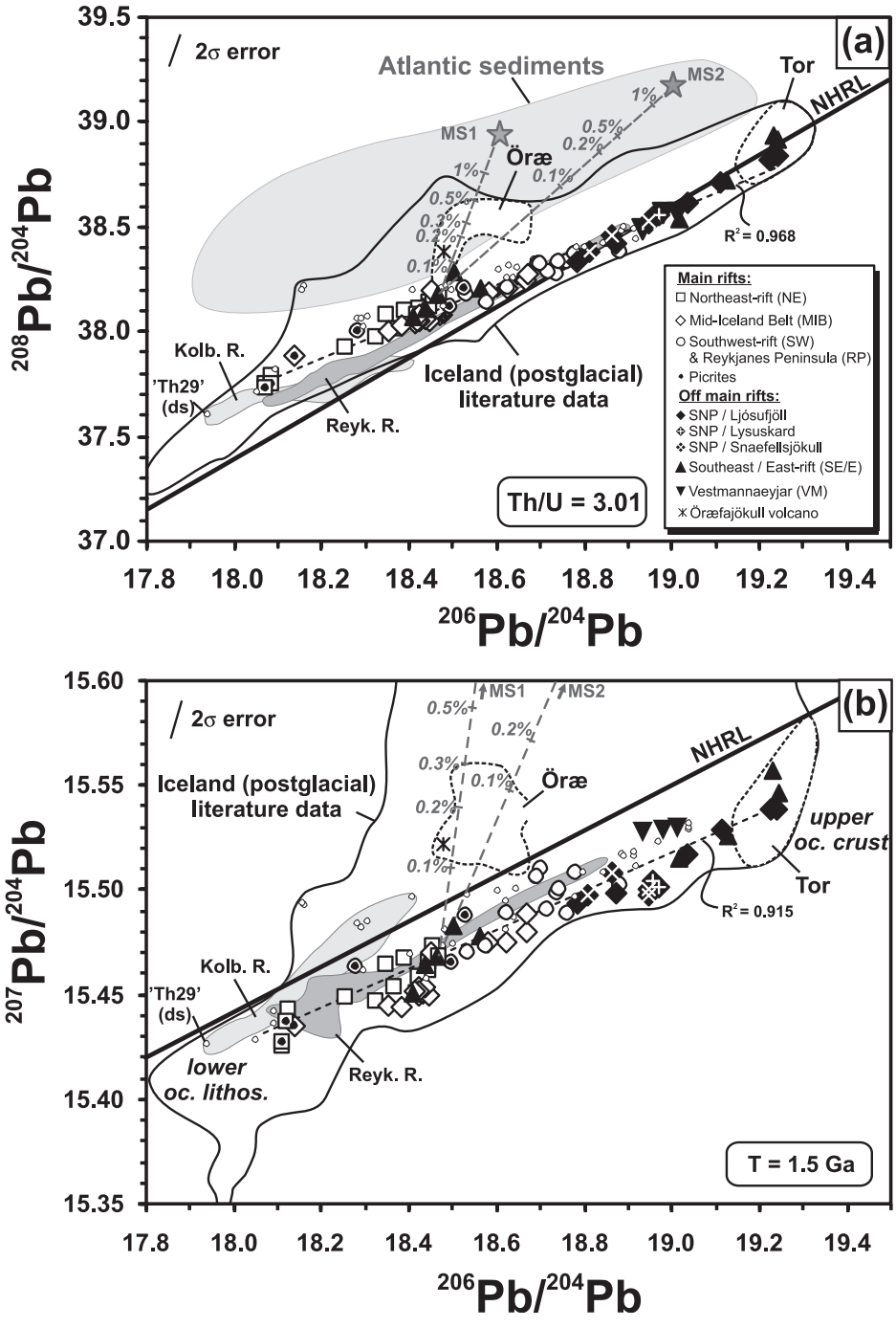

Fig. 6. Variations of $^{206}Pb/^{204}Pb$ vs $^{208}Pb/^{204}Pb$ (a) and $^{207}Pb/^{204}Pb$ (b) for samples from this study compared with data from the literature (R^2 = 0·97 and 0·92 respectively, excluding the Öræfajökull basalts). The Öræfajökull basalts are explained as the result of mixing between marine sediments of variable compositions ('MS1': $^{206}Pb/^{204}Pb$ = 18·604, $^{207}Pb/^{204}Pb$ = 15·685, $^{208}Pb/^{204}Pb$ = 38·947, Pb = 6 ppm; 'MS2': $^{206}Pb/^{204}Pb$ = 19·008, $^{207}Pb/^{204}Pb$ = 15·744, $^{208}Pb/^{204}Pb$ = 39·187, Pb = 25 ppm) and a mantle source with intermediate Pb isotopic composition ($^{206}Pb/^{204}Pb$ = 18·47, $^{207}Pb/^{204}Pb$ = 15·47, $^{208}Pb/^{204}Pb$ = 38·1, Pb = 0·15 ppm). The mixing model is further tested in Fig. 11. The data sources for the Iceland volcanics and Atlantic MORB are the same as given in the caption to Fig. 5. Individual data points are shown for the double-spike Pb dataset of Thirlwall *et al.* (2004) (small open circles). The field for Atlantic sediments is from Sun (1980), Ben Othman *et al.* (1989), Hoernle (1998) and Hoernle *et al.* (1991), and the Northern Hemisphere Reference Line (NHRL) is from Hart (1984). The fields for the adjacent North Atlantic ridges (Reykjanes and Kolbeinsey Ridges) are from Thirlwall *et al.* (2004). $^{206}Pb/^{204}Pb$ vs $^{87}Sr/^{86}Sr$ (c), $^{143}Nd/^{144}Nd$ (d) and Nb/U (e). In (c) and (d), mixing lines are between distinct depleted mantle plume components (DIP1, DIP2) and enriched (EIP, Öræ) mantle sources are indicated (stippled lines). The fields for the adjacent MAR ridges, the Kolbeinsey and the Reykjanes Ridges are shown. In (e), the 'normal' mantle Nb/U range of 47 ± 10 (Hofmann *et al.*, 1986) is indicated. Data sources as in Fig. 5.

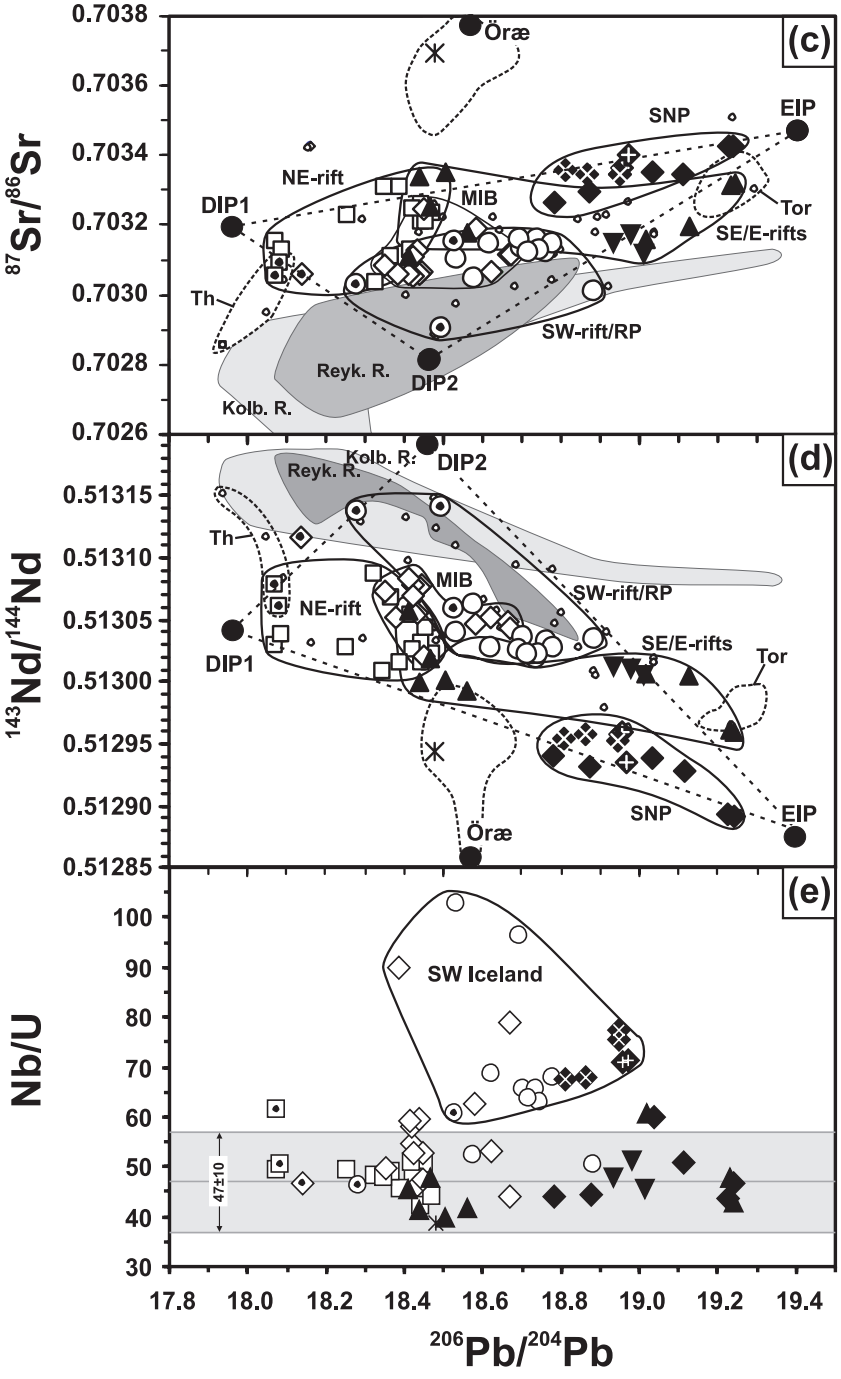

Fig. 6. Continued.

DISCUSSION

Excluding the Öræfajökull volcanic rocks, our Sr–Nd–Pb isotope data for the Iceland Neovolcanic zones (Figs 5 and 6) define well-correlated trends on the Nd–Sr ($R^2 = 0{\cdot}90$), uranogenic Pb ($R^2 = 0{\cdot}92$) and the thorogenic Pb ($R^2 = 0{\cdot}97$) isotope diagrams. Good correlations also are formed between major (e.g. K_2O; Fig. 8) and trace element ratios (Fig. 9) and Nd–Sr–Pb isotope ratios, suggesting that the recent Icelandic volcanism can be largely accounted for by two dominant endmembers, a geochemically and isotopically depleted and an enriched endmember. The enriched endmember, characterized by the alkali basalts, has high incompatible trace element

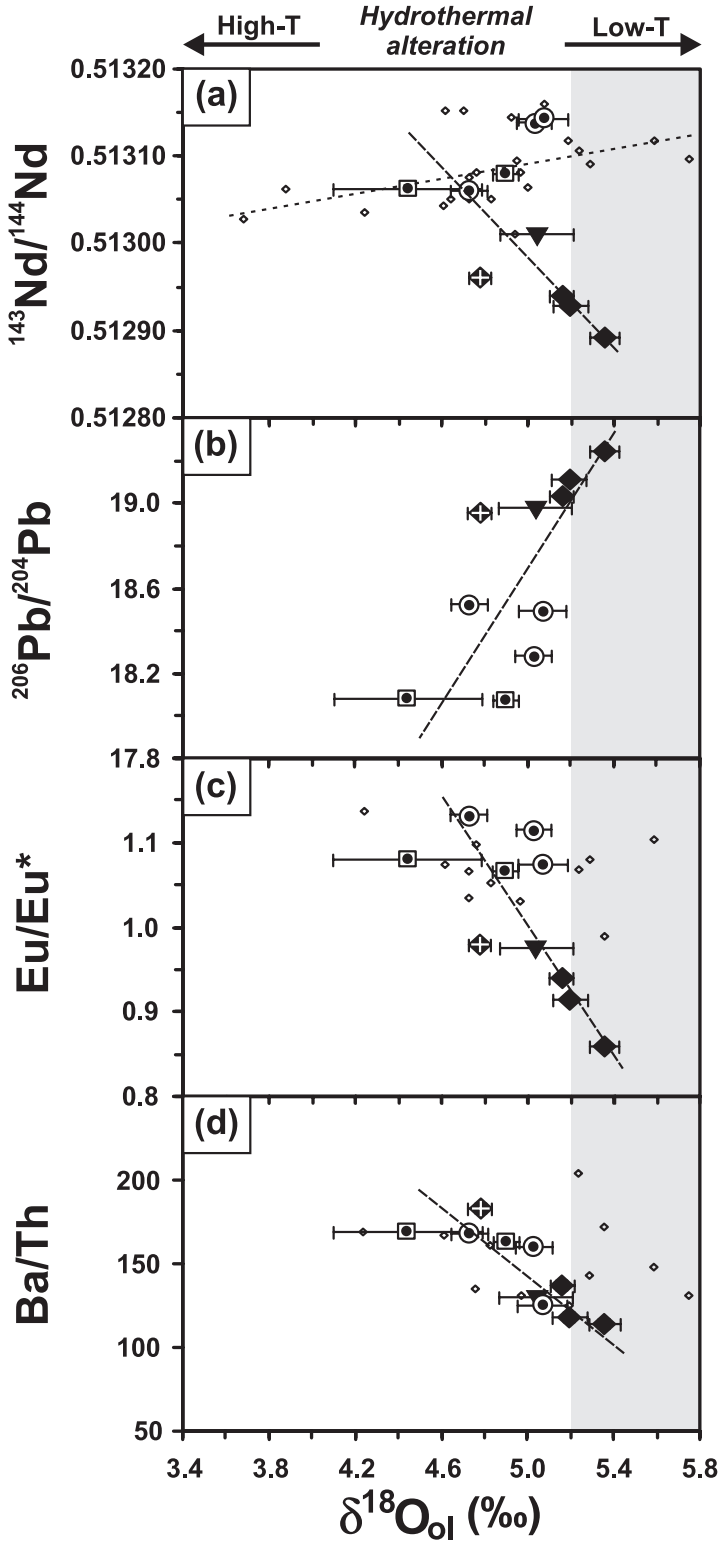

Fig. 7. $\delta^{18}O_{olivine}$ vs $^{143}Nd/^{144}Nd$ (a), $^{206}Pb/^{204}Pb$ (b), Eu/Eu* (c) and Ba/Th (d). Range of $\delta^{18}O$ in MORB uninfluenced by plumes is indicated by vertical grey band (Mattey *et al.*, 1994; Harmon & Hoefs, 1995). All values represent means of multiple runs and error bars indicate standard deviation (1σ) for the measured values (see Table 3). In all diagrams our new data form rough binary arrays (bold dashed lines). In (a), some of the published Icelandic picrites have relatively high $\delta^{18}O$, forming a depleted endmember in a positively trending array (fine dashed line). In (c), $Eu/Eu^* = (Eu)_N/[2/3(Sm)_N + 1/3(Gd)_N]$, where subscript N denotes chondrite normalization.

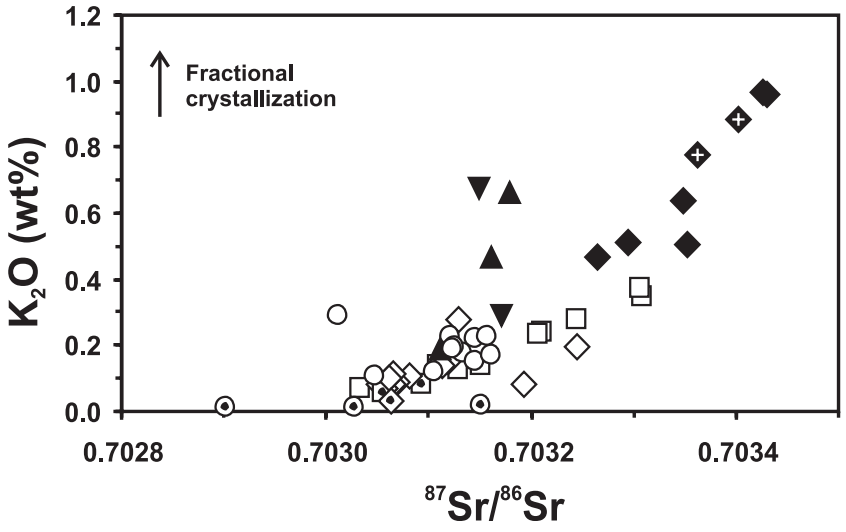

Fig. 8. $^{87}Sr/^{86}Sr$ vs K_2O (wt %) for basalts with MgO >6 wt %. The Iceland Neovolcanic rocks form a positive array. The effect of fractional crystallization is indicated by the vertical arrow.

concentrations, high La/Sm, Tb/Yb and Ce/Pb ratios, but low Sm/Nd, Eu/Eu* and Sr/Nd ratios. This component also has radiogenic Pb ($^{206}Pb/^{204}Pb \geq 19{\cdot}3$) and Sr ($^{87}Sr/^{86}Sr \geq 0{\cdot}70330$) and unradiogenic Nd ($^{143}Nd/^{144}Nd \leq 0{\cdot}51280$). In contrast, the depleted endmember, characterized by the picritic lavas, has low incompatible element concentrations, low La/Sm, La/Yb, Tb/Yb and Ce/Pb, and high Sm/Nd, Eu/Eu* and Sr/Nd. This endmember has unradiogenic Pb ($^{206}Pb/^{204}Pb \leq 18{\cdot}0$) and Sr ($^{87}Sr/^{86}Sr \leq 0{\cdot}70305$) and radiogenic Nd ($^{143}Nd/^{144}Nd \geq 0{\cdot}51310$). Tholeiites have intermediate trace element contents and isotopic compositions between the picrites and the alkali basalts and could be explained as mixtures of picritic and alkali basaltic melts (e.g. O'Nions & Pankhurst, 1973; Wood, 1979; Zindler *et al.*, 1979; Hémond *et al.*, 1988). Such mixing probably occurred at deep levels in the magma source region, rather than in shallow crustal magma chambers (see below). A third endmember, occurring at Öræfajökull, is characterized by intermediate incompatible element concentrations, intermediate La/Yb, high Tb/Yb, but low Ce/Pb, and by high $^{87}Sr/^{86}Sr$ and $\Delta 7/4Pb$. As discussed below, the different types of endmember summarized above have distinct geochemical characteristics for each ridge segment and, therefore, the actual number of endmembers is considerably higher than three. Below we briefly discuss the possible influence of crustal interaction on our dataset, before evaluating the possible nature of the inferred endmembers for the post-glacial volcanism in Iceland.

The role of crustal contamination?

Numerous studies have reported on the effects of crustal interaction on the Icelandic magmas, as typically shown by co-variations of O–Sr–Th isotopic ratios with the degree of differentiation (e.g. Muehlenbachs *et al.*, 1974; Hémond *et al.*, 1988; Nicholson *et al.*, 1991; Sigmarsson *et al.*, 1992*a*, 1992*b*; Eiler *et al.*, 2000). The widespread occurrence of Icelandic basalts with $\delta^{18}O$ of up to 1–2‰ lower than the normally accepted mantle range (Fig. 7) can have two possible origins: (1) it can result from reaction/interaction of ascending melts with hydrothermally altered Icelandic crust (e.g. Gee *et al.*, 1998; Eiler *et al.*, 2000), which in some places has $\delta^{18}O$ values down to −12‰ (Hattori & Muehlenbachs, 1982); or (2) it can be a primary signature of some Icelandic magmas, derived from the melting of low $\delta^{18}O$ material in the mantle source (Gautason & Muehlenbachs, 1998). In accordance with the first model, direct partial melting of the altered lower (amphibolitic) Icelandic crust could also generate low $\delta^{18}O$ melts (Óskarsson *et al.*, 1982). Because low $\delta^{18}O$ values in magmas can be generated within the mantle and/or the crust, a critical distinction between models based on oxygen isotope data alone will not always be successful. Correlations of $\delta^{18}O$ with trace elements and long-lived isotopic tracers, however, can help to distinguish the origin of the low $\delta^{18}O$ in Icelandic lavas (e.g. Nicholson *et al.*, 1991; Gee *et al.*, 1998). Interaction of melts with the upper crust is the easiest to identify, because of the larger range in O isotope ratios prevailing there, compared with the lower crust and mantle (Gautason & Muehlenbachs, 1998). The young age of the Iceland crust (<15 Ma) imposes rather tight restrictions on the possible range of radiogenic isotope ratios that can develop in the upper hydrothermally altered crust as a result of changes in parent/daughter ratios. Detectable differences in $^{87}Sr/^{86}Sr$, however, should exist as a result of

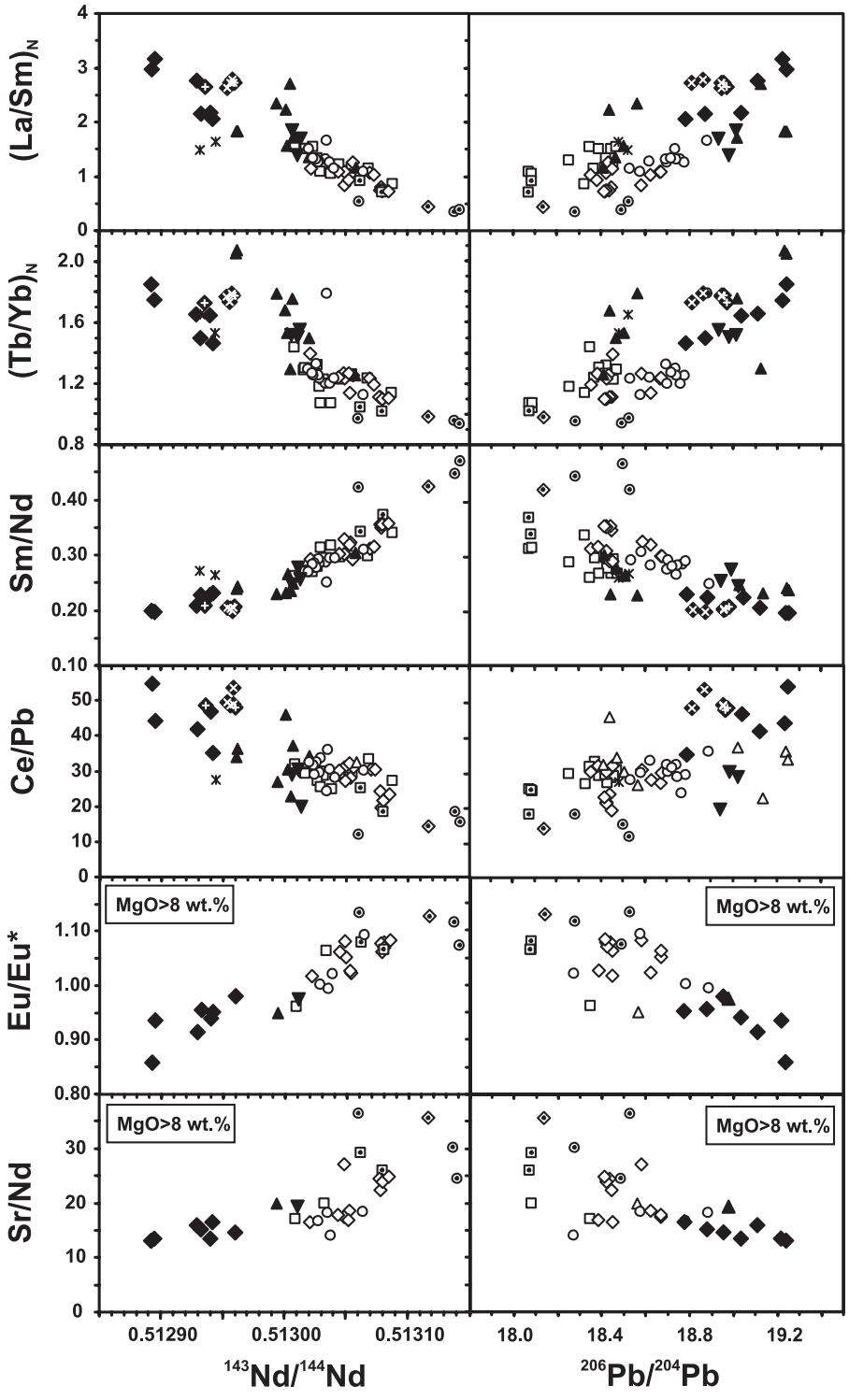

Fig. 9. $^{143}Nd/^{144}Nd$ and $^{206}Pb/^{204}Pb$ vs $(La/Sm)_N$, $(Tb/Yb)_N$, Sm/Nd, Ce/Pb, Eu/Eu* and Sr/Nd.

the high Sr concentration and $^{87}Sr/^{86}Sr$ isotope ratio of seawater and the permeability of the oceanic crust near the ridge (e.g. Gee *et al.*, 1998; Krolikowska-Ciaglo *et al.*, 2005). Another possibility is interaction with hydrothermal brines containing seawater Sr (Hémond *et al.*, 1988).

In the present dataset, there is limited evidence for crustal contamination. First, contribution from seawater

Table 3: Oxygen isotope composition of olivines

Sample	No. 1	No. 2	No. 3	No. 4	No. 5	Average	±1σ
Picrites							
H129	4·14*	4·18	4·72	4·68	4·52	4·45	0·27
H127	4·93	4·83	4·94			4·90	0·06
H80	4·97	5·09	4·53	5·25		5·03	0·08
H86	4·79	4·67				4·73	0·08
H83	5·15	4·99				5·07	0·11
Alkali basalts–transitional basalts							
H91	4·82	4·80	4·72			4·78	0·05
H109	5·21	5·1	5·17			5·16	0·06
H101 (1)	5·44	5·32	5·32			5·36	0·07
H101 (2)	5·3	5·26	5·33	5·22	5·09	5·28	0·05
H106	5·11	5·27	5·21			5·20	0·08
H119	5·16	4·92	4·65			5·04	0·17

Numbers 1–5 indicate individual measurements. For sample H101 two size fractions of olivine were measured: (1) 1–2 mm; (2) 2–4 mm.
*All $\delta^{18}O$ values are reported in ‰ relative to SMOW (Standard Mean Ocean Water) calculated as $10^3 \times [(^{18}O/^{16}O_{sample} - ^{18}O/^{16}O_{SMOW})/(^{18}O/^{16}O_{SMOW})]$.

should have created greater scatter on the $^{143}Nd/^{144}Nd$ vs $^{87}Sr/^{86}Sr$ (Fig. 5) and $^{87}Sr/^{86}Sr$ vs K_2O (Fig. 8) diagrams, with a tendency towards higher $^{87}Sr/^{86}Sr$ ratios and unsystematically variable K_2O contents. Second, there are good correlations of mobile vs immobile elements, such as K_2O (or Rb or U) vs Nb ($R^2 = 0{\cdot}92$). Chauvel & Hémond (2000) used the constancy of Cs/Rb ratios in their Icelandic dataset to reject any influence from crustal fluids. In our dataset the Cs/Rb ratio also shows little variation ($0{\cdot}0115 \pm 11$) and lies close to the primitive mantle value of 0·0112 (McDonough & Sun, 1995), indicating limited mobility of these highly mobile elements and limited interaction with altered crust.

The measured oxygen isotope ratios in olivines from the alkali basalts and picrites span the normal range for oceanic basalts (Fig. 7). Some of the low $\delta^{18}O$ values reported for the picrites, which we also find in one sample (H129), may indeed reflect interaction with altered crustal material (Gee *et al.*, 1998; Eiler *et al.*, 2000). On the other hand, it has for some time been proposed that the mantle beneath Iceland is characterized by moderately low $\delta^{18}O$ values (≥4·8‰, Thirlwall *et al.*, 1999; $5{\cdot}2 \pm 0{\cdot}3$‰, Gautason & Muehlenbachs, 1998), which many workers have interpreted to reflect an intrinsic characteristic of the plume (see below). Sample H129 has a heterogeneous oxygen isotope composition for its olivine ($\delta^{18}O = 4{\cdot}14$–$4{\cdot}72$‰; Table 3), which could suggest that its parent magma interacted with hydrothermally altered crust, or assimilated xenocrystic olivines that may have already undergone hydrothermal alteration in the crust. Such an explanation would seem to fit with the proposition of Skovgaard *et al.* (2001) that crustal interaction is more likely to have played a role in the larger ($>0{\cdot}8\,km^3$) picrite flows (because of a higher heat capacity), whereas the smaller ($<0{\cdot}01\,km^3$) flows should largely have avoided this process. On the other hand, there is no other geochemical evidence in H129 to support crustal interaction, such as anomalous Cs/Rb, K/Rb, Ba/Th or $^{87}Sr/^{86}Sr$ ratios. Because of the lack of evidence for crustal contamination, we propose that this was not significant in the petrogenesis of the Icelandic lavas. The homogeneous oxygen isotopic composition of the remaining picrite samples that we analysed (Table 3) indicates that these lavas did not undergo significant crustal contamination processes.

In relation to our preferred interpretation of a deep mantle origin for the anomalously low $\delta^{18}O$ values in primitive Icelandic lavas, we note that the voluminous 1783 Laki lava flow ($20\,km^3$), which is characterized by very homogeneous, low $\delta^{18}O$ values of ~3·1‰ (Sigmarsson, 1991), could represent tapping of a low $^{18}O/^{16}O$ mantle domain within the Iceland plume. The relatively low MgO contents (4–5 wt %) in the Laki lavas, however, could also be explained by assimilation of low $\delta^{18}O$ crust during fractional crystallization (AFC) or by differentiation without appreciable crustal assimilation.

Nature of the enriched Iceland source (alkali basalts)

The geochemistry of the Iceland alkalic basalts is very similar to that of HIMU-type ocean island basalts (OIB). The mantle-normalized multi-element patterns (Figs 3 and 4) are very similar to those from St. Helena, the HIMU type locality in the Atlantic Ocean. High Ce/Pb and low K/Nb ratios are also characteristic of HIMU basalts (Fig. 4; Chaffey *et al.*, 1989; Chauvel *et al.*, 1992). The Iceland alkali basalts contain more radiogenic Pb compared with MORB, but have less radiogenic Pb isotope ratios ($^{206}Pb/^{204}Pb \leq 19{\cdot}4$) than basalts from St. Helena ($^{206}Pb/^{204}Pb \geq 20{\cdot}5$; Chaffey *et al.*,1989). On the uranogenic Pb isotope diagram (Fig. 6b), the Iceland data fall below the NHRL (Hart, 1984), which is a common characteristic of young (<1·8 Ga) HIMU mantle (Thirlwall, 1997). On the thorogenic isotope diagram (Fig. 6a), the radiogenic end of the Iceland data array extends beneath the NHRL, also a characteristic of HIMU-type basalts (e.g. Zindler & Hart, 1986; Hofmann, 1997).

The source regions of HIMU basalts are commonly ascribed to recycled hydrothermally altered oceanic crust (Hofmann & White, 1982; Chauvel *et al.*, 1992; Kogiso *et al.*, 1997, 2003; Moreira & Kurz, 2002), although

alternative explanations have recently been proposed (Niu & O'Hara, 2003; Elliott *et al.*, 2004; Hieronymus & Baker, 2004). None the less, it is widely accepted that the enriched component giving rise to the alkalic volcanism in Iceland is contained in the Iceland plume as a recycled component. The tendency towards lower $\delta^{18}O$ in the alkalic lavas than generally found in MORB and upper mantle peridotites is consistent with a hydrothermally altered basaltic source. Alternative models of crustal interaction fail to explain the long-lived enriched isotopic signature, as discussed above. Because of the young age of the Icelandic crust, it should have had a Pb isotopic composition similar to North Atlantic N-MORB, which is clearly not the case (Fig. 6a and b). The less radiogenic $^{207}Pb/^{204}Pb$ relative to the NHRL in the Icelandic HIMU-type basalts may simply indicate shorter mantle recycling times, lower integrated (U, Th)/Pb ratios in the recycled source material, or both (e.g. Thirlwall, 1997). Kogiso *et al.* (1998) showed that it is possible to produce silica-undersaturated basalts with high Fe and Ti (very similar to that of shield-building lavas on ocean islands) through melting of homogeneous peridotite–basalt mixtures (KG-1 and KG-2). As illustrated on the SiO_2 vs FeO* diagram (Fig. 2c), the alkali basalts plot close to the experimental melting curves for KG-1 and KG-2. Alteration of upper basaltic oceanic crust is commonly associated with U addition of up to 15% (Staudigel *et al.*, 1981); hydrothermal alteration can also cause Pb loss and increased U concentrations (Hofmann & White, 1982; Vidal, 1992; Kogiso *et al.*, 1997; Hoernle, 1998). As a result of dehydration during subduction, both U and Pb are lost differentially from the subducting ocean crust. As a result of a combination of these processes, subducted upper oceanic crust can acquire high Ce/Pb, U/Pb and Th/Pb (Chauvel *et al.*, 1992; Vidal, 1992; Hoernle, 1998).

The most extreme representative of the enriched component in Iceland is found in the SNP, which consists of three volcanic systems (Snæfellsjökull, Lýsuskarð, Ljósufjöll). Westwards along the SNP, lava compositions become increasingly alkalic and at the same time several parameters, such as Th/U, Ba/Th and Zr/Hf, increase progressively (Sigmarsson *et al.*, 1992*b*; Kokfelt *et al.*, 2003). Such a gradual shift in geochemistry may best be attributed to variations in the composition of the source region, coupled with changing degrees of partial melting along the SNP (Sigmarsson *et al.*, 1992*b*; Kokfelt *et al.*, 2003). One possibility is melting of a locally heterogeneous mantle consisting of enriched mantle material with a relatively low solidus temperature, embedded in a more refractory matrix (Fitton *et al.*, 2003). The lower temperature in the mantle and deeper depth of truncation of the melting column towards the west along the SNP (where the mantle is colder and lithosphere is thicker) ensures that such enriched mantle material will dominate the bulk melt, compared with melts erupted closer to the main rift systems. Thus, the geochemical variation observed in the SNP lavas may provide an important clue to the distribution of mantle sources beneath the peninsula, which may possibly be extrapolated to the rest of Iceland.

The depleted Iceland source (picrites)

The picrites appear to be good representatives of the isotopic composition of the depleted endmember in the Iceland post-glacial volcanism (Figs 5 and 6). In comparison with immediately surrounding North Atlantic MORB from the Reykjanes and Kolbeinsey Ridges, the picrites appear to have relatively unradiogenic $^{143}Nd/^{144}Nd$ (0·51305–0·50315; Fig. 5), as well as a relatively light oxygen isotopic composition compared with MORB (Fig. 7). The picrites are strongly depleted in incompatible trace elements but have high ratios of CaO/Al_2O_3 (0·83–1·09), Sr/Nd (24–36), Eu/Eu* (1·05–1·13) and Ba/Th (113–169) and low Zr/Y (Figs 2, 4, 9 and 10). Arguably, the picrites may also be distinguished in the thorogenic Pb isotope diagram (Fig. 6a) by having higher $^{208}Pb/^{204}Pb$ for a given $^{206}Pb/^{204}Pb$ ratio than the immediately surrounding North Atlantic MORB. They also have relatively low Zr/Y for a given Nb/Y ratio. In a plot of Zr/Y vs Nb/Y (Fig. 10a), the Iceland Neovolcanic rocks form a linear array, which is distinct from those formed by the adjacent Mid-Atlantic Ridge, and the Kolbeinsey and Reykjanes Ridges. For the more MgO-rich Icelandic Neovolcanic zone basalts, Zr/Y also correlates with Eu/Eu* and U/Pb (Fig. 10b and c), suggesting a relationship between type of source material (Eu/Eu*) on the one hand and source depletion and degree of partial melting (Zr/Y and U/Pb) on the other.

Below we evaluate the various possibilities for the origin of picrites and their geochemical characteristics.

(1) In the field, the Icelandic picrites sometimes contain xenoliths of coarse-grained, unstrained gabbros, interpreted to represent magmatic cumulates (Gee *et al.*, 1998). Assimilation of such gabbro xenoliths could possibly explain their high ratios of Sr/Nd, Ba/Th and Eu/Eu*. Our oxygen isotope data for olivine in the picrites ($\delta^{18}O = 4{\cdot}45$–$5{\cdot}07‰$; Table 3) are consistently higher than those previously reported by Gee *et al.* (1998) and Eiler *et al.* (2000), but still lower than the normal range for olivine from mantle peridotite of $5{\cdot}3 \pm 0{\cdot}2‰$ (Mattey *et al.*, 1994). As discussed above, low $\delta^{18}O$ values could either reflect *in situ* contamination with Icelandic crust or represent an inherent source feature. Eiler *et al.* (2000) argued for crustal contamination in the petrogenesis of the MgO-rich Theistareykir lavas, based on a broad correlation of $\delta^{18}O$ with MgO. A similar conclusion was preferred by Gee *et al.* (1998) for primitive Reykjanes Peninsula lavas, whereas Skovgaard *et al.*

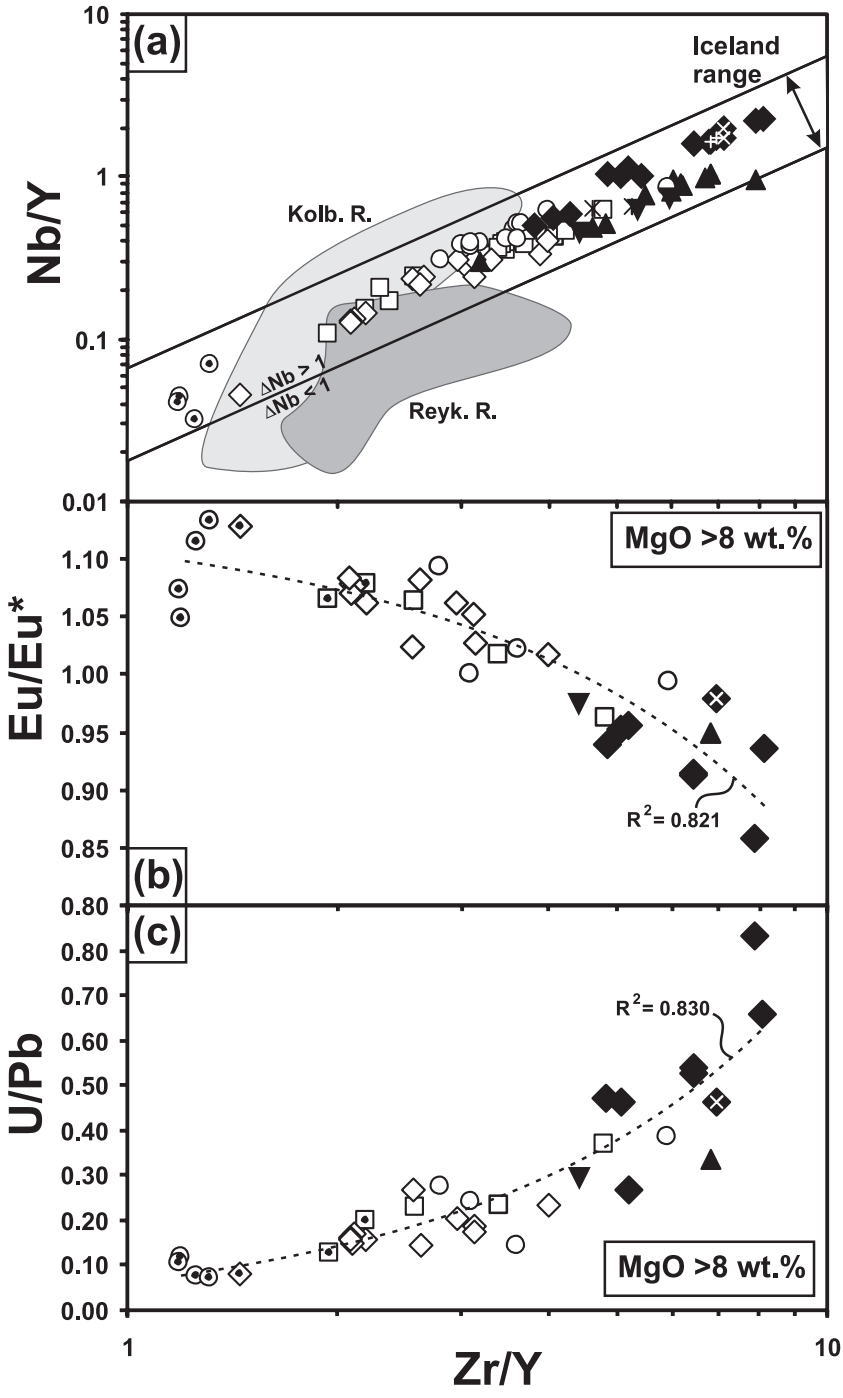

Fig. 10. Zr/Y vs Nb/Y (a), Eu/Eu* (b), and U/Pb (c). (a) is a double-log plot first used by Fitton *et al.* (1997) to discriminate between normal North Atlantic MORB and rocks influenced by the Iceland plume. In (b) and (c), it should be noted that both are semi-log plots for primitive rocks with MgO >8 wt %. In (b), Eu/Eu* = $(Eu)_N/[2/3(Sm)_N + 1/3(Gd)_N]$, where subscript N denotes chondrite normalization. Data sources for the Reykjanes and Kolbeinsey ridges are from the PetRidge web-database at http://www.ldeo.columbia.edu/datarep/index.html. Symbols are as in Fig. 2.

(2001) argued that only the large picrite flows of the Theistareykir area have been crustally contaminated. Assuming that parental picrite melts have $\delta^{18}O_{olivine}$ of 5·3‰ (within the normal mantle range), mass balance calculations would require high degrees of contamination to explain the observed range of $\delta^{18}O$ values. For example, a lowering in $\delta^{18}O$ from 5·3‰ to 4·5‰ would require 60% combined assimilation and fractionation

(AFC), with a contaminant with $\delta^{18}O$ of 3‰ and a *r* value of three (Allègre & Minster, 1978). Such large amounts of AFC would seem rather unlikely considering the high MgO contents in the picrites (groundmass), unless the high MgO was acquired subsequent to contamination, through the addition of cumulate olivines in the ascending magma. Even in the most beneficial case of selective contamination (and complete dissolution) of cumulate plagioclase, which could explain the positive trace element anomalies for Sr, Ba and Eu, this process would lead to a significant increase in Al_2O_3 resulting in a lowering of the CaO/Al_2O_3 ratio in the picrites compared with the tholeiites, rather than higher CaO/Al_2O_3 as is observed in the picrites. An additional argument against crustal contamination in our dataset comes from the correlated nature of oxygen isotopes with radiogenic isotope data. There are crude correlations of $\delta^{18}O$ with $^{206}Pb/^{204}Pb$ (positive) and with $^{143}Nd/^{144}Nd$ (negative), and fairly good correlations with Eu/Eu* and Ba/Th ratios (Fig. 7). Despite the likelihood that at least some olivines in some of the picrites are of xenocrystic origin, the correlated variation of $\delta^{18}O$ with radiogenic isotopes suggests that the $\delta^{18}O$ represents a source feature. Therefore, it is unlikely that contamination within the Icelandic crust can explain more than a minor part of the data range we report for the picrites. Moreover, selective contamination processes involving plagioclase cumulates should only affect those elements entering this mineral (Sr, Ba, Eu, CaO, Al_2O_3) and thus would not provide a comprehensive explanation for other distinctive geochemical features [e.g. low (Zr, Hf)/Sm], nor explain why the combined Sr–Nd–Pb isotopic compositions are different from North Atlantic MORB (Fig. 6 and below).

(2) In addition to unusually high CaO/Al_2O_3 ratios in the picrites, ultra-calcic melt inclusions (UCMI) have been reported in tholeiites and picrites, such as the Hengill lavas from the Reykjanes Peninsula (Gurenko & Chaussidon, 1995). The high CaO/Al_2O_3 ratios and the positive Sr anomalies in the UCMI have been variously attributed to crustal interaction processes and to an intrinsic feature of the Icelandic source. Partial melting at high temperatures (~1350°C) of a pyroxene-rich source lithology (Kamenetsky *et al.*, 1998; Kogiso & Hirschmann, 2001) or of highly depleted peridotite, such as KLB-1 (Kogiso & Hirschmann, 2001), have been proposed to generate UCMI. The involvement of a refractory mantle peridotite could explain the depleted major element characteristics of the Icelandic picrites (high CaO/Al_2O_3, low FeO*) and also provide an explanation for their strong depletion in incompatible trace elements [see paragraph (5) below]. Nevertheless, none of these models provide a coherent explanation for the associated Ba and Eu spikes (Figs 3 and 4), as well as the correlated variation of these features with isotopic compositions (Figs 7 and 9).

(3) Melting of plagioclase lherzolite with complete exhaustion of plagioclase could lead to melts with high Al_2O_3/TiO_2 ratios and presumably also with high Sr contents (Rampone *et al.*, 1993). As pointed out by Breddam (2002), however, the melting column in central Iceland, where some of the positive Sr anomalies are found, is truncated below the stability field of plagioclase peridotite, excluding this possibility as a general explanation.

(4) Blundy & Green (2000) ascribed positive Sr anomalies in mantle-derived melts to an increase in the partitioning of Sr in cpx with increasing pressure. Such a model is, however, unlikely also to account for the positive Ba and Eu anomalies and the correlations of these with radiogenic isotopic compositions.

(5) There is a very good match in bulk-rock geochemistry between gabbros from the present-day ocean floor (Hoernle, 1998; Schmincke *et al.*, 1998; Hart *et al.*, 1999) and the Icelandic picrites (Fig. 4), suggesting that the gabbros could represent a potential source for the picrites (assuming that the geochemical characteristics are preserved through the recycling process and that such gabbros would melt to a high extent).

In model (5), several points need mentioning. The first is that the presumed protolith—oceanic gabbros—appears to be similar in incompatible element composition to the Icelandic picrites (Fig. 4). Because partial melting, by definition, always causes the concentration level of incompatible elements (e.g. Wood, 1979) to increase in the melt over the source, this would either require 100% fusion of the source or that the gabbros alone cannot form the bulk source material (unless 1·5 Ga ancient oceanic gabbros were more depleted than today). One obvious possibility is that the source of the picrites also includes ultramafic cumulates of the lower oceanic crust and/or harzburgitic lithospheric mantle (Chauvel & Hémond, 2000; Geldmacher & Hoernle, 2000; Hauff *et al.*, 2000; Skovgaard *et al.*, 2001; Breddam, 2002), which are significantly more depleted than the gabbro section. A mixed source for the picrites, consisting of heterogeneous lower oceanic crust and mantle, would dilute the multi-element patterns of the gabbros without changing the characteristics of the patterns appreciably. With regard to the major element compositions of the derived melts, the restitic lithospheric mantle section should significantly contribute elements such as MgO, Ni, Co and Cr (Chauvel & Hémond, 2000; Skovgaard *et al.*, 2001; Breddam, 2002). The high CaO/Al_2O_3 ratios in the picrites is not expected to result from partial melting of plagioclase-dominated source materials (gabbros) alone, because oceanic gabbros generally, but not always (e.g. Schmincke *et al.*, 1998), have low CaO/Al_2O_3 (~0·77; Hart *et al.*, 1999). In this context, the high CaO/Al_2O_3 ratios observed in the picrites would also require a major melt contribution from a restitic source

component, such as the mantle part of the oceanic lithosphere. We note that Skovgaard *et al.* (2001) proposed that some of the Icelandic picrites with high $\delta^{18}O$ values and high $^{187}Os/^{188}Os$ could contain recycled upper oceanic crust (sheeted dikes and pillow lavas) in their mantle source region.

Lastly, if melts from recycled gabbroic lower crust/mantle lithosphere (picrites) mix with melts from recycled upper basaltic crust (alkali basalts), then the mixing array should essentially represent a two-point isochron in the Pb–Pb diagram (Fig. 6b), which has age significance (Geldmacher & Hoernle, 2000). The age determined from the slope of the Pb isotope array for Iceland is ~1·5 Ga (Fig. 6b), representing an average age of the recycling process. This age, together with the slope of the array in the thorogenic Pb diagram, would indicate an average Th/U ratio in the recycled crustal package of 3·01 (Fig. 6b).

The Öræfajökull component

The youngest basalts of the Öræfajökull central volcano have anomalously high $^{87}Sr/^{86}Sr$ (for their $^{143}Nd/^{144}Nd$), high Δ8/4Pb and Δ7/4Pb at intermediate $^{206}Pb/^{204}Pb$ ratios and only weak negative Pb anomalies in their multi-element patterns (Fig. 3e; Prestvik *et al.*, 2001, fig. 5), giving rise to relatively low Ce/Pb and U/Pb ratios. The trace element and isotopic ratios are consistent with the presence of an Atlantic pelagic sediment component in the source of the Öræfajökull magmas (Prestvik *et al.*, 2001). An alternative model of *in situ* crustal contamination was proposed by Hémond *et al.* (1988), but this fails to account for the (for Iceland) high $\delta^{18}O$ values (5·0–5·6‰; Prestvik *et al.*, 2001), as well as the relatively restricted range of variation in $^{87}Sr/^{86}Sr$ and $^{206}Pb/^{204}Pb$ isotope ratios in these rocks. The model of marine sediment addition is best tested from the Pb isotopic systematics. In both Pb isotope diagrams (Fig. 6a and b), the Öræfajökull volcanics define a cloud lying above the general Iceland array. The high Δ8/4Pb in the Öræfajökull volcanics could conceivably be explained as a mixture between a depleted 'picritic' mantle component (as represented by sample 'TH29') and a radiogenic pelagic sediment composition (Fig. 6a). However, despite the large compositional span for Atlantic marine sediments, it is not readily possible to fit a mixing line connecting a depleted Icelandic composition ($^{206}Pb/^{204}Pb$ ~17·9) with a sediment composition through the Öræfajökull field in the uranogenic Pb diagram (Fig. 6b). This reflects the fact that sediments generally have very high Δ7/4Pb for their Δ8/4Pb. Instead, we propose that pelagic sediments of variable composition ($18·5 < {}^{206}Pb/^{204}Pb < 19·3$) mix with a mantle source similar to that feeding the older Öræfajökull volcanics, and that is characterized by $^{206}Pb/^{204}Pb$ ~18·44 (Fig. 6a and b). Assessing the relative proportions of sediment addition is made difficult because of the uncertainty in the Pb concentrations in the proposed mixing endmembers. For example, reported pelagic sediments range widely in Pb concentrations (4–80 ppm; Turekian & Wedepohl, 1961; Hoernle *et al.*, 1991; Plank & Langmuir, 1998), but the lower Pb concentrations generally occur in the less radiogenic compositions. Assuming a relative Pb-poor sediment (e.g. 'MS1': 6 ppm Pb; Fig. 6), which may be justified by preferential Pb loss during the process of subduction, we estimate a maximum sediment source input of ~0·5% to explain the younger Öræfajökull volcanics (Fig. 6a and b). Mixing such minor amounts of marine sediment (Plank & Langmuir, 1998) with an enriched mantle source similar to Primitive Mantle, but about three times more depleted in Pb, and then partially melting it (e.g. by 5% batch melting) can reproduce the trace element variation in the Öræfajökull volcanics (Fig. 11). Some of the Öræfajökull samples with slightly higher $^{206}Pb/^{204}Pb$ ratios would require less input (<0·1%) of a more radiogenic sediment (e.g. 'MS2': 25 ppm Pb; Fig. 6). Thus, the Pb isotopic and the trace element systematics seem to support a model of sediment input in the Öræfajökull source region through subduction and recycling. Considering that we only found this isotopic signature at Öræfajökull, we believe that this is probably a volumetrically minor component. Therefore, in the framework of a recycling origin for the enriched and depleted components, the inferred sediment involvement in the Öræfajökull component is readily provided as recycled pelagic sediments associated with the recycled oceanic slab. The rarity of evidence for recycled sediments and the absence of basalts with $\delta^{18}O$ values greater than the MORB source mantle suggest that the sediment layer and uppermost basaltic ocean crust generally do not survive the recycling process, including subduction and subsequent return to the surface via the Iceland plume. The uppermost portions of the ocean crust may have been accreted instead of subducted, or incompatible elements from this part of the crust may have been primarily lost during subduction.

Role of the ambient upper mantle?

Much of the previous debate about the depleted endmember in Iceland has been polarized in the sense that either it was attributed to depleted ambient MORB source upper mantle or it was an intrinsic depleted plume component. It is, however, not clear why these possibilities should be mutually exclusive. The geochemical and isotopic gradients observed along the Reykjanes Ridge to the SW of Iceland have been interpreted to reflect a diminishing outflow of plume-derived material (e.g. Schilling, 1973; Sun *et al.*, 1975; Taylor *et al.*, 1997; Hilton *et al.*, 2000; Murton *et al.*, 2002). The situation

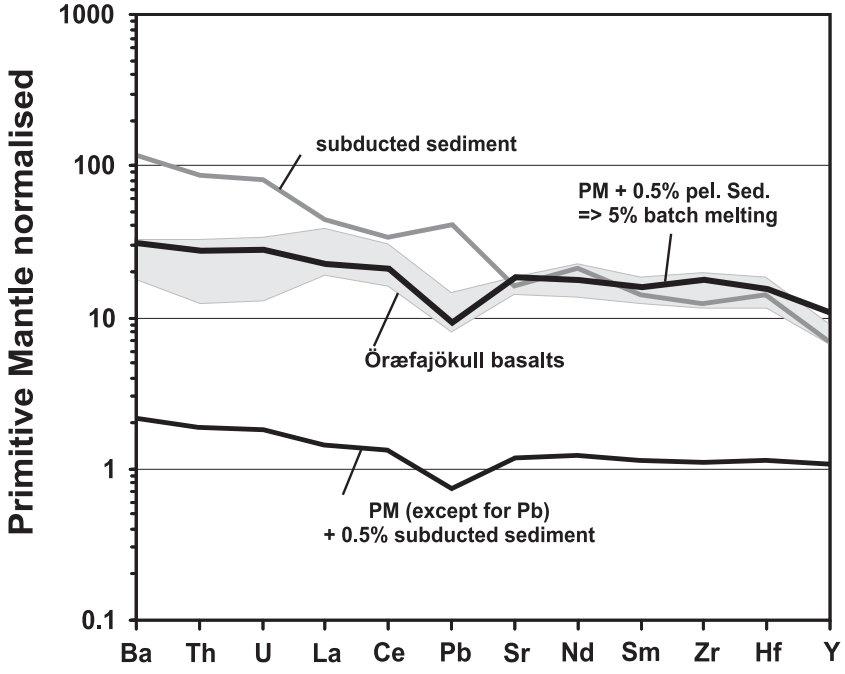

Fig. 11. Primitive mantle-normalized trace element diagram showing mixing and melting calculations for the Öræfajökull basalts. The trace element variation of the Öræfajökull basalts may be explained as 5% partial melting of a source consisting of primitive mantle (except for Pb, which was set to be three times as low) with up to 0·5% (recycled) pelagic sediment addition. There is a reasonably good fit for all elements, except for a slight overestimation of the most incompatible elements (Ba, Th and U). To make a fit for Pb we assumed Pb concentrations in the marine sediments at the lower limits (6 ppm) of the reported range worldwide (4–80 ppm). This may be justified by a plausible Pb-loss during the process of subduction. Data sources: Öræfajökull volcanics: Prestvik *et al.* (2001); primitive mantle: McDonough & Sun (1995); subducted sediment: Plank & Langmuir (1998) (except for Pb).

along the Kolbeinsey Ridge also seems to support plume outflow, based on the isotopic similarities between the NE rift basalts (Theistareykir) and MORB erupted north of the Tjörnes Fracture zone (Schilling *et al.*, 1999). These findings are substantiated by recent Pb isotope data presented for Iceland Neovolcanic and the adjacent ridges (Thirlwall *et al.*, 2004). Their high-precision Pb data show that the Kolbeinsey Ridge and the NE Iceland depleted lavas are very similar in terms of their Pb isotopic characteristics, and differ from global MORB. To the south a mixture of several Icelandic plume components has been identified by Thirlwall *et al.* (2004) at the southern Reykjanes Ridge, whereas a distinct depleted mantle component is sampled at the proximal part of the Reykjanes Ridge.

As already discussed, there is overwhelming evidence that a significant portion of the depleted signature originates from the plume source itself, as an intrinsic recycled component; however, this evidence is mainly based on the distinctive geochemistry (Nb/Y, Zr/Y, Nb/U, Eu/Eu*, Sr/Nd ratios and oxygen isotopes) of the most depleted Icelandic lavas (picrites). The $^{87}Sr/^{86}Sr$ vs $^{143}Nd/^{144}Nd$ and Pb–Pb isotope diagrams require the presence of at least three distinct types of endmember (a depleted, an enriched and the Öræfajökull). The $^{206}Pb/^{204}Pb$ vs $^{87}Sr/^{86}Sr$ and $^{143}Nd/^{144}Nd$ isotope diagrams (Fig. 6), however, show distinct mixing relations for the different rift systems, indicating that the enriched and depleted components can have distinct 'flavours' for each rift system. Apart from the Öræfajökull samples, all lavas may be constrained within a triangular field, defined by the enriched component (EIP) and two distinct depleted components (DIP1 and DIP2). The difference between the two depleted components is regionally related, in that picrites from SW Iceland have higher $^{143}Nd/^{144}Nd$ isotope ratios at a given $^{206}Pb/^{204}Pb$ ratio than those from NE Iceland. It is also clear that within the SW Iceland picrites themselves there is a large isotopic variability, which indicates that heterogeneity occurs locally, even within individual rift systems. Based on this variability, it is unclear whether it is possible to evaluate the importance of the ambient upper mantle in magma generation in the Iceland Neovolcanic zone from the Sr–Nd–Pb isotope variation alone. We note, however, that the picrites and tholeiites from the SW rift zone and Reykjanes Peninsula, as a result of their distinctive trace element signatures (e.g. Ba, Sr, Eu anomalies and high Nb/U) and low $\delta^{18}O$ isotope ratios (Figs 3, 4, 6, 7, 9 and 10), cannot be explained by derivation from a MORB source and therefore require a second depleted (DIP2)

component in the plume (see also discussion of Nb/U below). In conclusion, we recognize at least four distinct plume components (EIP, DIP1, DIP2 and Öræ).

In SW Iceland the RP tholeiites and picrites have Sr–Nd–Pb isotopic similarities to the Reykjanes Ridge basalts, indicating exchange to some extent between the submarine and subaerial parts of the Reykjanes rift systems. Some of the sub-rift systems that are located more marginally to the Iceland plume axis indeed show apparent mixing relations with adjacent MORB source in Sr–Nd–Pb isotope space (Fig. 6c and d). The Theistareykir volcanics from NE Iceland, for which an extensive database exists, show a general overlap with the Kolbeinsey Ridge MORB, apparently indicating a depleted composition similar to Depleted MORB Mantle (DMM; Zindler & Hart, 1986). Stracke *et al.* (2003) interpreted these systematics to reflect mixing between ambient North Atlantic MORB source mantle, ubiquitously present beneath NE Iceland, and shallowly recycled enriched (EMI-like) component, without the requirement of a distinct depleted plume component. Based on the previous discussion about the distinct geochemistry of the Icelandic picrites, however, it is clear that normal MORB source mantle can be ruled out as the major depleted component for these regions. At most, a minor part of the depleted source may be constituted by normal MORB source mantle, consistent with the very restricted range of the Theistareykir mixing array (Fig. 6c and d).

In a $^{206}Pb/^{204}Pb$ vs Nb/U plot (Fig. 6e), lavas from the SW part of Iceland (including SW, RP, Ljósufjöll and Lýsuskarð rifts) have Nb/U ratios considerably higher than the 'normal' mantle range of 47 ± 10 (Hofmann *et al.*, 1986). Importantly, none of the samples with raised Nb/U, including the two samples with extreme ratios (H13: 96; H34: 103) can be explained by alteration processes. All high Nb/U samples have $(^{234}U)/(^{238}U)$ activity ratios at or very close to equilibrium (Kokfelt *et al.*, 2003), arguing against post-eruption U mobility. Furthermore, the trace element concentrations of H13 were successfully reproduced (see Table A3), excluding analytical problems as a viable explanation for the high Nb/U. Figure 6e shows that not only can the ambient mantle be excluded as the depleted source for SW Iceland, but that there are regional differences in the distribution of recycled material, with SW Iceland being characterized by elevated Nb/U ratios. The significance of raised Nb/U ratios is discussed in more detail below.

In conclusion, DMM or North Atlantic N-MORB source probably could occur as a subordinate depleted component beneath the Theistareykir region, as evidenced from the Sr–Nd–Pb systematics. Generally, however, plume–ridge interaction appears to occur along the adjacent ridges, rather than directly beneath Iceland.

SOURCE HETEROGENEITY AND MELTING

Inferences about source lithology

The two main mantle components observed in the post-glacial volcanism on Iceland could represent recycled oceanic crust including a hydrothermally altered basaltic upper crust (enriched component) and gabbroic + ultramafic cumulate lower crust and/or harzburgitic lithospheric mantle (depleted component). This recycled oceanic lithosphere in the Iceland source must be located within the upwelling upper mantle beneath the divergent plate boundary or within a mantle plume. As a result of subduction and deep mantle recycling, oceanic crustal material is transformed into garnet pyroxenite/eclogite. None of the source materials discussed under (5), however, would have the necessary contents of MgO, Ni and Co to generate the primitive magma compositions. Therefore, more refractory peridotite is required in addition to pyroxenite/eclogite. This more refractory material could be recycled ultramafic cumulates from the base of the oceanic crust and/or oceanic lithospheric mantle, which is harzburgitic (Hauff *et al.*, 2000). Alternatively, it could be depleted lower or upper mantle entrained into an upwelling mantle plume. Early experimental studies by Yoder & Tilley (1962) showed that a variety of basaltic compositions might result from melting of eclogite. Those workers showed that exhaustion of either cpx (omphacite) or garnet (almandine–pyrope) during eclogite melting could lead to alkali basalts (garnet) or tholeiitic magmas (cpx). They also showed that changing pressure has an effect on the alkalinity of the resultant melts. More recent melting experiments on homogeneous peridotite–basalt mixtures (KG-1 and KG-2; Kogiso *et al.*, 1998; MIX1; Hirschmann *et al.*, 2003) have confirmed the possibility of producing magmas with chemistry very similar to that of the shield-building lavas at ocean islands, such as basalts with high Fe and Ti. In the experiments of Kogiso *et al.* (1998), the necessary MgO, Ni and Co contents were derived from peridotite. Finally, we note that Sobolev *et al.* (2005) recently suggested that the high Ni and SiO_2 contents in Hawaiian lavas reflect conversion of the source into pyroxenite before it melts. Thus it is argued that Hawaiian lavas form in equilibrium with pyroxenite and not peridotite.

The relationship of FeO* vs SiO_2 in the least evolved lavas appears to support a model in which the picrites and the alkali basalts were generated from recycled oceanic lithosphere at variable depths: greater depths for the alkali basalts (for KG1 source composition: ~2 GPa) than for the picrites (KG1: ~1·5 GPa) (Fig. 2c). Tholeiites could be generated by mixtures of these two end-member melts; these generally have intermediate

FeO* and SiO_2 contents to those of the picrites and alkali basalts. Some of the tholeiites have higher FeO* contents than alkali basalts (Fig. 2c); this could, however, be explained by greater depths of melting as a result of longer melting columns in closer proximity to the hotter Iceland plume.

Partial melting of a heterogeneous source

A way to investigate the nature and scale of the mantle source heterogeneity beneath Iceland is to look at the distribution of the enriched vs depleted volcanism in Iceland today. The enriched (alkalic) volcanism is restricted to the off-rift settings, whereas the more voluminous but also more depleted (tholeiitic and picritic) volcanism takes place along the main rifts (e.g. Hardarson *et al.*, 1997; Fitton *et al.*, 2003). The melting process, rather than geographical differences in the bulk source composition, appears to control the geochemical variations along the Neovolcanic zones in Iceland. If the melting columns in the off-rift regions are shorter, they could erupt lavas formed at greater average depths (with lower SiO_2 and higher FeO*; Fig. 2), as they generally are capped by thicker lithosphere compared with the main rift systems (see also Fitton *et al.*, 2003). In a two-component mantle source, the enriched material (garnet pyroxenite) reaches the solidus and, therefore, starts melting deeper in the melting column than the depleted material (eclogite and ultramafic rocks).

We propose a non-modal dynamic melting model, principally similar to that of Langmuir *et al.* (1977), in which instantaneous melts are extracted from various depths throughout the melting column (calculated in steps of 0·5 km) and aggregated to form a pooled melt that erupts at the surface. Source mineralogy and trace element contents, as well as partition coefficients for the modelled elements (La, Zr, Yb and Hf), change through the column as a function of the pressure-dependent phase changes and the continuous depletion by melting (see Fig. 12 caption for details). We chose the aforementioned moderately incompatible and immobile trace elements, because each Icelandic basalt type has distinct concentrations of these elements. We have modelled partial melting for a series of depleted and enriched sources with different enrichments and bulk source compositions (Table 4). We assume three enriched sources (E1–E3) with identical high trace element contents, but variable cpx to garnet ratios (cpx/gar = 1·7, 5 and 10, respectively). Similarly, we assume three depleted sources (D1–D3), which have the same lower trace element contents, and cpx/gar ratios of 10 and 19 for D1 and D2, respectively (Table 4). The assignment of variable cpx to garnet ratios to both the enriched (off-rift) and depleted (main rift) sources provides a test of source composition that is independent of the melt column morphology. The depleted sources melt over a longer melting column (90–30 km), compared with the enriched sources (80–50 km), simulating the situation at the main and off-rifts, respectively. Hence, the calculated degrees of melting are higher for the main-rift (18·2%) than for the off-rifts (7·8%). For our calculations we applied a standard set of partition coefficients (Table 5).

We present aspects of our melting model on a plot of La/Zr vs Hf/Yb (Fig. 12). In this diagram, the data form an overall positive correlation, with individual rift systems forming relatively distinct positive trends within the larger array. The lavas from SW Iceland (RP, SW and SNP) define the steepest trend with elevated La/Zr. A flatter trend at lower La/Zr is formed by the lavas from the SE rift + MIB. Both these trends overlap completely in Hf/Yb. The NE rift lavas tend to lie in between these two trends. The calculated dynamic melting trajectories for enriched (E1–E3) and depleted (D1–D3) sources show a progressive increase in La/Zr and decrease in Hf/Yb as function of increasing cpx/garnet source ratio (Fig. 12; Table 4). The higher La/Zr ratios in the SNP may be explained by relatively small degrees of partial melting (1–5%) of an enriched source with high proportions of cpx (30%) to garnet (3–6%) (Table 4a). In comparison, the SE rift lavas may be modelled by comparable degrees of melting (3–5%) of an enriched source with lower cpx (10%) but similar garnet (6%) contents, or alternatively, by smaller degrees of partial melting (1–2%) from a depleted source with minor garnet ($\leq$2%) (Fig. 12). The main rift lavas may be generated through high degrees of partial melting ($\leq$18·2%) from a depleted mantle source, or possibly as mixtures of such melts with low-degree enriched melts. Both garnet and cpx fractionate La/Zr (both incorporating Zr over La), but only cpx fractionates this ratio without significantly also fractionating Hf/Yb. Therefore, by applying a standard partition coefficient dataset (Table 5), it is suggested that higher amounts of residual cpx relative to garnet exist in the source region beneath the SNP, compared with other areas of post-glacial volcanism in Iceland. Higher amounts of residual cpx may indicate the presence of appreciable amounts of garnet pyroxenite/eclogite in the source. The preferential sampling of the 'garnet pyroxenite/eclogite' material in SW Iceland does not necessarily indicate a regional difference in the distribution of enriched and depleted source components beneath Iceland. Both types of source components could be present beneath all the Neovolcanic zones. Differences in the depth range of the melting interval and in the proximity to the plume centre of different volcanic areas in Iceland, however, could result in the preferential sampling of either enriched or depleted components.

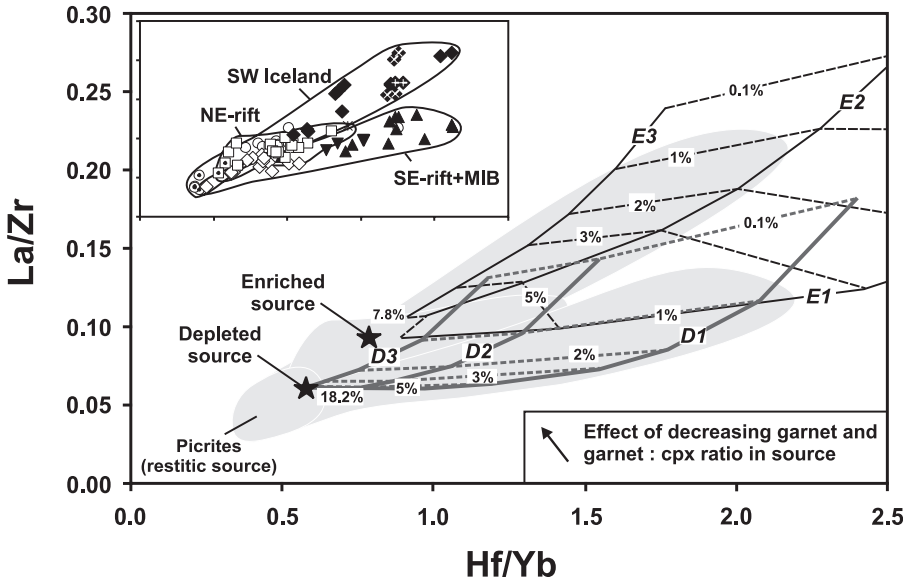

Fig. 12. La/Zr vs Hf/Yb in which Icelandic basalts from distinct geographical locations can be distinguished (see insert). The Iceland data are compared with calculated partial melting curves (continuous lines) that assume incremental batch melting of two distinct sources; a relatively enriched source with Hf/Yb = 0·71 and La/Zr = 0·09, and a depleted source with Hf/Yb = 0·57 and La/Zr = 0·06. Melting trajectories (continuous lines) are calculated for both enriched (E1–E3) and depleted (D1–D3) sources, each of which are characterized by distinct modal proportions (see Table 4). Melting of the enriched source takes place over a relatively short (off-rift) melting column (80–50 km), producing relatively small overall degrees of melting ($F \leq 7{\cdot}8\%$). In contrast, the depleted (on-rift) melting column is deeper and longer (90–30 km), producing higher degrees of melting ($F \leq 18{\cdot}2\%$). The dashed lines indicate similar degrees of partial melting. The higher La/Zr (for their Hf/Yb) in the SW Iceland rocks, relative to SE rift and MIB may be explained as a result of the lower gar/cpx ratio in the former mentioned source. Symbols are as in Fig. 2.

Table 4: Source concentrations and mineralogy used in dynamic melting modelling

	La	Yb	Zr	Hf
'Enriched' source	1	0·38	10·8	0·27
PM-normalized*	1·54	0·86	1·03	0·94
'Depleted' source	0·15	0·35	2·5	0·2
PM-normalized	0·23	0·79	0·24	0·71
Source mineralogy†	ol	opx	cpx	gar
'Enriched' source				
E1	0·64	0·20	0·10	0·06
E2	0·50	0·14	0·30	0·06
E3	0·50	0·17	0·30	0·03
Melting proportions	0·10	0·20	0·30	0·40
'Depleted' source				
D1	0·66	0·23	0·10	0·01
D2	0·66	0·24	0·095	0·005
D3	0·66	0·24	0·10	0·00
Melting proportion	0·10	0·20	0·30	0·40

*Primitive mantle (PM) after McDonough & Sun (1995).
†ol, olivine; opx, orthopyroxene; cpx, clinopyroxene; gar, garnet.

Table 5: Partition coefficients used in dynamic melting modelling

	La[1]	Yb[1]	Zr	Hf[1]
Olivine	3·1E − 05	0·03	0·00068[2]	0·0011
Orthopyroxene	4·4E − 05	0·033	0·0033[3]	0·0044
Clinopyroxene	0·048	0·313	0·1234[4]	0·256
Garnet, (Ca-poor)	0·0016	3·7	0·27[4]	0·24

[1]McKenzie & O'Nions (1991). [2]Kennedy *et al.* (1993). [3]Keleman & Dunn (1992). [4]Johnson (1994).

Is the Iceland plume zoned?

At most hotspots, the long-term chemical structure of the associated mantle plume remains poorly constrained. In a few cases, however, such as the Galápagos (Geist *et al.*, 1988; White *et al.*, 1993; Hoernle *et al.*, 2000) and Hawaii (Stille *et al.*, 1983; Hauri, 1996; Abouchami *et al.*, 2005), spatial variation in the chemical composition of lavas has been proposed to reflect a zonation in the plume and, ultimately, the plume source. At the Galápagos hotspot, enriched plume material has been proposed to

form a horseshoe-shaped region with depleted MORB-like mantle in its inner part (Geist *et al.*, 1988; White *et al.*, 1993), and the enriched region has been subdivided into three distinct geochemical domains that have been preserved over at least the last 15–20 Myr (Hoernle *et al.*, 2000; Geldmacher *et al.*, 2003; Werner *et al.*, 2003).

One of the surprising features of our Iceland dataset is the wide range in incompatible trace element ratios, such as the Nb/U ratio (Fig. 6e), which otherwise has been proposed to stay relatively constant in oceanic basalts (47 ± 10; Hofmann *et al.*, 1986; 50 ± 10; Zou & Zindler, 1996). High Nb/U ratios have been reported for other ocean islands, but generally for those situated on old, thick oceanic lithosphere [e.g. Canary, Madeira and Cape Verde Islands (Gerlach *et al.*, 1988; Geldmacher & Hoernle, 2000; Lundstrom *et al.*, 2003)]. For most of these OIBs the lithosphere has been proposed to play an important role in generating the geochemical anomalies; for example, as a buffer and reaction zone containing plume-derived ultramafic veins (e.g. Lundstrom *et al.*, 2003). In Iceland, however, the lithosphere is comparatively young and thin, and so any potential role in imprinting a geochemical signature is diminished. Therefore, the most obvious origin for the anomalous Nb/U ratios in Iceland basalts is within the plume source itself. As discussed above, the Nb/U ratio in the oceanic crust can be modified while the crust is near the mid-ocean ridge, at which it was created; here low-temperature alteration can cause an increase of U. Subsequent subduction partially removes U from the slab to the overlying mantle wedge. For example, Geldmacher & Hoernle (2000) proposed that recycled oceanic crust could have high Nb/U, K/U and Ba/Th, resulting from the subduction process. Because Nb is unaffected by this process, the net Nb/U ratio in the material being subducted (and hence future OIB source material) will reflect the balance of the sea-floor alteration and subduction processes, which work in opposite directions. This cancelling effect may explain why similar Nb/U ratios are found in many, but not all, OIB.

On $^{206}Pb/^{204}Pb$ vs $^{87}Sr/^{86}Sr$ and $^{143}Nd/^{144}Nd$ diagrams (in particular the Pb vs Nd isotope diagrams, Fig. 6c and d), the Neovolcanic rift systems (i.e. SW, SE/E and NE rift systems, the Snæfellsjökull Peninsula and Öræfajökull) form five distinct fields, which could reflect an unsystematic and rather complex geographical (spatial) zonation of the Iceland plume. In the absence of data showing that these five geochemical zones were present in a similar configuration in the past, it is difficult to rule out a complexly zoned plume. Nevertheless, we feel that there is a simpler explanation for the geochemical variations in Iceland, as discussed below.

Using contoured plots of parameters characterizing the source region, e.g. $^{87}Sr/^{86}Sr$, $^{143}Nd/^{144}Nd$, $^{206}Pb/^{204}Pb$ and Sr/Nd (Fig. 13), we can investigate the geographical distribution of the different enriched and depleted components on a regional scale in Iceland. Such plots may serve to clarify tendencies and trends existing in a larger dataset, which may not be readily identified by plotting the data in normal *x–y* scatter plots. The contours were generated through a smoothening function of the *x–y–z* dataset, using the PC program SigmaPlot®. It should be noted that the contours extending outside the Neovolcanic zones are not based on real data, but represent an artefact of the smoothing function of the program (through extrapolation). The contoured representation of the Sr–Nd–Pb isotope dataset (Fig. 13a–c) reveals a distribution pattern of maxima in isotopic enrichment (highest $^{87}Sr/^{86}Sr$ and $^{206}Pb/^{204}Pb$, lowest $^{143}Nd/^{144}Nd$) towards the NW and SE, and enrichment minima towards the SW and NE along the RP and NE rift, respectively. Sr/Nd ratios generally mimic the contours for the Sr, Nd and Pb isotope compositions with low Sr/Nd ratios in SE Iceland and in the SNP, increasing towards the SW and NE along the RP and NE rift, respectively. This distribution suggests that the enriched component (recycled basaltic upper oceanic crust) is predominantly tapped beneath the SNP and the SE propagating rift, whereas the depleted component (recycled gabbroic ± ultramafic cumulates from the lower crust) dominates the melt compositions along the main rift systems in Iceland.

To explain the observed distribution of enriched and depleted components as reflected in the lavas at the surface, we propose that the Iceland plume is heterogeneous on a small scale (<1 km), consisting of enriched streaks or blobs of more fusible pyroxenite in a more refractory matrix, which comprises a mixture of eclogite and ultramafic rocks (e.g. harzburgite) (Fitton *et al.*, 2003; Kokfelt *et al.*, 2003). Melting columns beneath different regions of Iceland have different lengths, reflecting differences in the temperature of the upwelling mantle and differences in lithosphere thickness. In Fig. 14, we show a model profile through the melting region beneath SW Iceland (see profile A–A' in Fig. 1). Two off-rift systems are represented in the profile: Snæfellsjökull Peninsula (SNP; a recently abandoned rift system) and Vestmannaeyjar (VM; an actively propagating rift system), whereas the Reykjanes Peninsula (RP) represents the main rift system as the prolongation of the MAR. Because the cross-section runs at an oblique angle to the proposed plume centre (see Fig. 1), the upwelling mantle will become progressively cooler going from VM to RP to SNP. As a result, the solidus (bottom of the melting column) will be reached at progressively shallower depths from VM to SNP (Fig. 14). The primary difference in the melting column geometry (depth interval of melting) between the main rifts and the off-rifts is that the tops of the off-rift melting columns are deeper than for the main rifts, reflecting thicker lithosphere above the off-rift

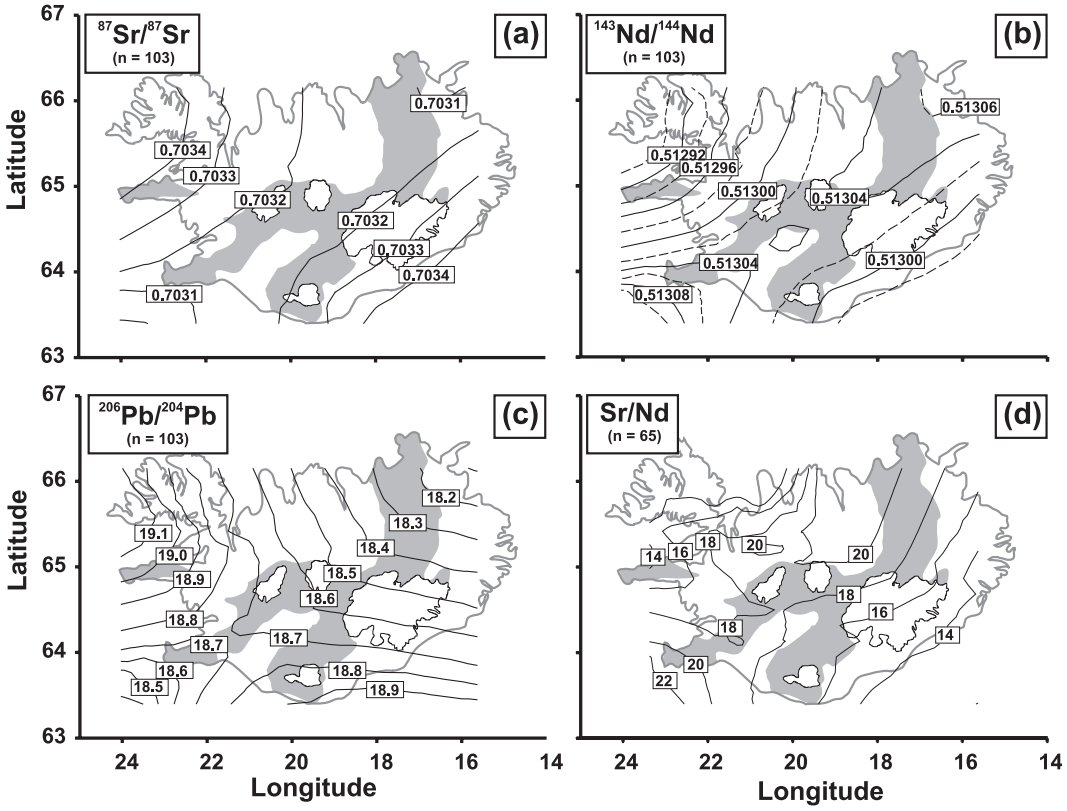

Fig. 13. Contoured maps of Iceland showing the distribution of $^{87}Sr/^{86}Sr$ (a), $^{143}Nd/^{144}Nd$ (b), $^{206}Pb/^{204}Pb$ (c) and Sr/Nd (d) as tracers of various recycled crustal components in the source of the basaltic lavas. (a)–(c) are based on the present dataset (total of 83) plus that of Thirlwall *et al.* (2004); (d) is based on lavas from our dataset with MgO > 6 wt % to reduce the effects of differentiation.

areas. As a direct consequence of the melting column geometry, only limited amounts of melting occur above the solidus for the ultramafic component in the off-rift areas, whereas in the main rifts, melting proceeds to shallower levels, considerably exceeding the solidus of the depleted component. In the context of this melting model, the progressively diminishing influence of the Iceland plume on the adjacent ridges (discussed above) may simply reflect a shallowing of the lower boundary of the plume material in relation to the absolute position of the melting column. Therefore, the acquired bulk melt composition will mainly differ according to the lithospheric lid thickness and mantle potential temperature, providing an explanation for why the more enriched melts dominate along the off-rift systems, even though the bulk source composition throughout all the rift systems is roughly equally depleted or enriched. In conclusion, although we cannot rule out a plume with a complex spatial zonation, we believe that the melting model proposed above best explains the relationship between tectonic setting and major element, trace element and isotopic geochemistry of the post-glacial lavas on Iceland. If the Iceland plume is spatially zoned, then this relationship appears to be fortuitous.

CONCLUSIONS

The following conclusions may be drawn from this regional geochemical study in Iceland.

(1) The combined major and trace element geochemistry and Sr–Nd–Pb–O isotopic composition of post-glacial volcanism indicate the presence of two major intrinsic plume components beneath Iceland: (a) an enriched HIMU-like component, giving rise to the alkalic basalts; (b) a depleted plume component that produced the picritic rocks. The preferred explanation for the origin of these components is the recycling of upper hydrothermally altered basaltic crust and lower gabbroic + ultramafic cumulates and/or harzburgitic lithospheric mantle, respectively, consistent with the conclusions reached by Chauvel & Hémond (2000), Skovgaard *et al.* (2001) and Breddam (2002).

(2) It is suggested that the range in oxygen isotopic composition ($\delta\delta^{18}O_{olivine}$ = 4·45–5·35‰) in the lavas reflects ancient hydrothermal alteration processes at a mid-oceanic ridge and that the O isotopic compositions survived the subduction and subsequent recycling processes. In the picrites, low $\delta^{18}O$ values are correlated with high ratios of Sr/Nd, Ba/Th, and Eu/Eu*, high

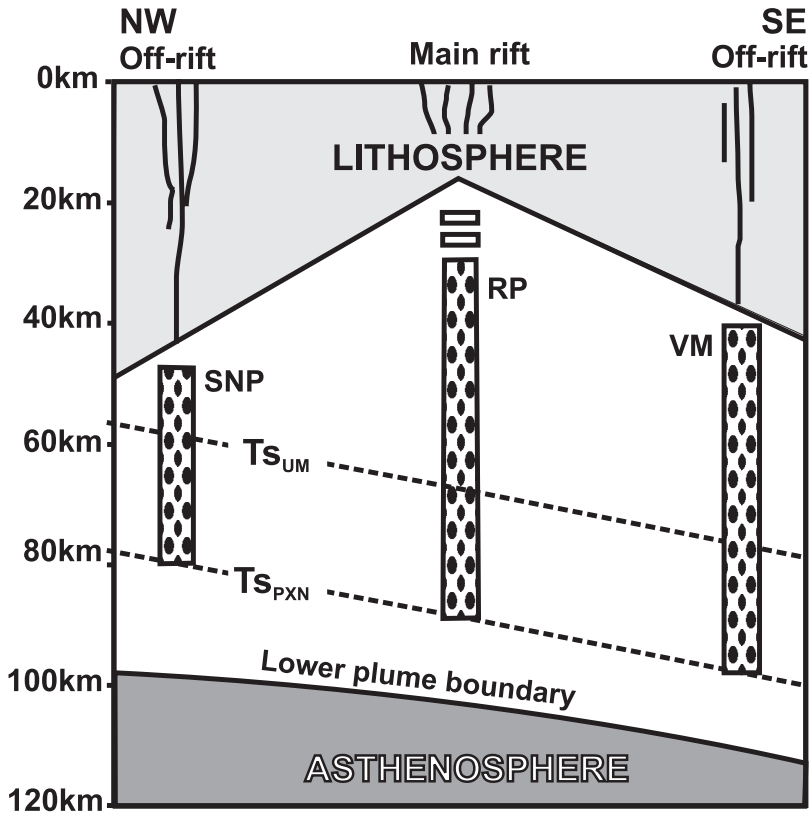

Fig. 14. Sketched cross-section of the melting region at semi-radial distance from the plume (see Fig. 1), illustrating the differences in melting conditions between main rift (RP) and off-rift regions (SNP and VM). The solidus curves for (enriched) pyroxenite (Ts_{PXN}) and (depleted) eclogite and ultramafic mixture (Ts_{UM}) are indicated schematically. (See text for discussion.) The closer proximity of the Vestmannaeyjar Islands (VM) to the hot Iceland plume, compared with the Snæfellsjökull Peninsula (SNP), is reflected in a deeper initiation of melting in the column beneath VM, as reflected by the diagonal (versus horizontal) outline of the lower plume boundary.

$^{143}Nd/^{144}Nd$, and low $^{87}Sr/^{86}Sr$ and $^{206}Pb/^{204}Pb$, indicating that all these features were inherited from a mantle source consisting of ancient hydrothermally altered lower gabbroic (+ ultramafic cumulate) crust. Higher $\delta^{18}O$ values in the alkali basalts may reflect less intense hydrothermal alteration in the upper basaltic part of the oceanic crust.

(3) Each rift system (SW, SE/E, NE and the Snæfellsjökull Peninsula) has distinct isotopic compositions in Sr–Nd–Pb isotope space. Although the SW rift zone lavas have Sr–Nd–Pb isotopic compositions similar to MORB, their distinct trace element characteristics (e.g. higher Nb/U ratios, ~68) indicate that this is a plume component and not MORB. Excluding Öræfajökull [see point (4) below], at least three additional plume components are required: two depleted and one enriched. The distinct composition of each Neovolcanic zone suggests that they sample different packages of recycled oceanic lithosphere or that lavas from each Neovolcanic zone represent a different mixture of the same depleted (DIP1, DIP2) and enriched (EIP) components in the plume.

(4) The Öræfajökull component found in SE Iceland is interpreted to be a local enriched component, reflecting the addition of small amounts (≤0·5%) of pelagic sediments to the recycled package of oceanic crust.

(5) Modelling of the partial melting systematics indicates that the alkalic lavas from the SNP could be explained by partial melting over a relatively shallow depth interval (~80–50 km) from a cpx-rich lithology with ~3–6% garnet. The more depleted tholeiitic lavas from the main rift systems can be modelled by partial melting of a depleted mantle source with up to ~2% garnet. In accordance with conclusions of previous workers (Elliott *et al.*, 1991; Fitton *et al.*, 2003), we propose that the picrites may be derived from continuous melting at shallow levels in the restitic and virtually garnet-free part of the melting column, with the more enriched melts having been previously exhausted from the column or diluted by the more voluminous shallow melts.

(6) Using $^{206}Pb/^{204}Pb$, $^{87}Sr/^{86}Sr$, $^{143}Nd/^{144}Nd$ and Sr/Nd ratios as a tracers for recycled upper and lower oceanic crustal components, a contoured representation of the regional dataset suggests that recycled upper oceanic crust predominates in the melts on the Snæfellsnes

Peninsula and the SE-propagating rift, whereas the main rift systems (Mid-Iceland Belt, SW and NE rifts) appear to sample more of the depleted components.

(7) The distribution of enriched and depleted components along the Neovolcanic rifts is proposed to reflect differences in the geometry of the melting region, with the off-rift columns being truncated deeper (as a result of a thicker lithospheric cap), compared with the main rift systems. Deeper average melting in the off-rifts leads to the preferential melting of the more fusible (recycled upper crustal) parts of the source region, whereas the solidus for the more refractory mantle (recycled lower crust/mantle lithosphere) material is only significantly exceeded in the main rifts, where the melting continues to shallower levels. This model does not require the existence of a complex spatial zonation in the bulk composition of the source beneath Iceland and thus the lavas erupted at the surface do not necessarily reflect the actual bulk composition of the underlying mantle. In accordance with the model proposed here, the Iceland plume is heterogeneous on a small ($\leq$1 km) scale.

ACKNOWLEDGEMENTS

Christel van den Bogaard, Shane Cronin and Paul van den Bogaard are warmly thanked for their extensive help in collecting the samples. The Geological Museum in Iceland is acknowledged for kind co-operation in allowing us access to sampling in Iceland. Tore Prestvik is thanked for donating sample powder from the Öræfajökull volcano (OR58), and Dagmar Rau (IFM-GEOMAR) for analysing major and trace elements by XRF. Members of Research Division 4 'Dynamics of the Ocean Floor' at IFM-GEOMAR and the Institute for Geosciences at the Kiel University are acknowledged for many stimulating discussions on Iceland and related topics during seminars and elsewhere. This manuscript benefited from constructive reviews by Geoffrey Fitton, Christophe Hémond and Colin Devey. We thank the German Research Foundation for funding this project (HO1833/4) within the specialty program SSP 1055 'Formation, transport and differentiation of silicate melts'.

REFERENCES

Abelson, M. & Agnon, A. (2001). Hotspot activity and plume pulses recorded by geometry of spreading ridges. *Earth and Planetary Science Letters* **189**, 31–47.

Abouchami, W. H., Hofmann, A. W., Galer, S. J. G., Frey, F. A., Eisel, J. & Feigenson, M. (2005). Lead isotopes reveal bilateral asymmetry and vertical continuity in the Hawaiian mantle plume. *Nature* **434**, 851–856.

Allègre, C. J. & Minster, J. F. (1978). Quantitative models of trace element behavior in magmatic processes. *Earth and Planetary Science Letters* **38**, 1–25.

Ben Othman, D., White, W. M. & Pratchett, J. (1989). The geochemistry of marine sediments, island arc genesis, and crust–mantle recycling. *Earth and Planetary Science Letters* **94**, 1–21.

Bijwaard, H. & Spakman, W. (1999). Tomographic evidence for a narrow whole mantle plume below Iceland. *Earth and Planetary Science Letters* **166**, 121–126.

Blundy, J. D. & Green, T. (2000). A partitioning origin for strontium anomalies in mantle-derived melts. *Journal of Conference Abstracts* **5**, 219.

Breddam, K. (2002). Kistufell: primitive melt from the Iceland mantle plume. *Journal of Petrology* **43**, 345–373.

Breddam, K., Kurz, M. & Storey, M. (2000). Mapping out the conduit of the Iceland mantle plume with helium isotopes. *Earth and Planetary Science Letters* **176**, 45–55.

Chaffey, D. J., Cliff, R. A. & Wilson, B. M. (1989) Characterization of the St Helena magma source. In: Saunders, A. D. & Norry, M. J. (eds) *Magmatism in the Ocean Basins. Geological Society, London, Special Publications* **42**, 257–276.

Chauvel, C. & Hémond, C. (2000). Melting of a complete section of recycled oceanic crust: trace element and Pb isotopic evidence from Iceland. *Geochemistry, Geophysics, Geosystems* **1**, 1999GC000002.

Chauvel, C., Hofmann, A. W. & Vidal, P. (1992). HIMU-EM: the French Polynesian connection. *Earth and Planetary Science Letters* **110**, 99–119.

Condomines, M., Grönvold, K., Hooker, P. J., Muehlenbachs, K., O'Nions, R. K., Òskarsson, N. & Oxburgh, E. R. (1983). Helium, oxygen, strontium and neodymium isotopic relationships in Icelandic volcanics. *Earth and Planetary Science Letters* **66**, 125–136.

Darbyshire, F. A., White, R. S. & Priestley, K. F. (2000). Structure of the crust and uppermost mantle of Iceland from a combined seismic and gravity study. *Earth and Planetary Science Letters* **181**, 409–428.

Dixon, E. T. (2003). Interpretation of helium and neon isotopic heterogeneity in Icelandic basalts. *Earth and Planetary Science Letters* **206**, 83–99.

Dixon, E. T., Honda, M., McDougall, I., Campbell, I. H. & Sigurdsson, I. (2000). Preservation of near-solar neon isotopic ratios in Icelandic basalts. *Earth and Planetary Science Letters* **180**, 309–324.

Eiler, J. M., Grönvold, K. & Kitchen, N. (2000). Oxygen isotope evidence for the origin of chemical variations in lavas from Theistareykir volcano in Iceland's northern volcanic zone. *Earth and Planetary Science Letters* **184**, 269–286.

Elliott, T., Hawkesworth, C. J. & Grönvold, K. (1991). Dynamic melting of the Iceland plume. *Nature* **351**, 201–206.

Elliott, T., Jeffcoate, A. & Bouman, C. (2004). The terrestrial Li isotope cycle: light-weight constraints on mantle convection. *Earth and Planetary Science Letters* **220**, 231–245.

Fitton, J. G., Saunders, A. D., Norry, M. J., Hardason, B. S. & Taylor, R. N. (1997). Thermal and chemical structure of the Iceland plume. *Earth and Planetary Science Letters* **153**, 197–208.

Fitton, J. G., Saunders, A. D., Kempton, P. D. & Hardason, B. S. (2003). Does depleted mantle form an intrinsic part of the Iceland plume? *Geochemistry, Geophysics, Geosystems* **4**, 2002GC000424.

Foulger, G. R. & Natland, J. H. (2003). Is 'hotspot' volcanism a consequence of plate tectonics? *Science* **300**, 921–922.

Furman, T., Frey, F. & Park, K.-H. (1991). Chemical constraints on the petrogenesis of mildly alkaline lavas from Vestmannaeyjar, Iceland: the Eldfell (1973) and Surtsey (1963–1967) eruptions. *Contributions to Mineralogy and Petrology* **109**, 19–37.

Garbe-Schönberg, D. (1993). Simultaneous determination of thirty-seven trace elements in twenty-eight international rock standards by ICP-MS. *Geostandards Newsletter* **17**, 81–97.

Gautason, B. & Muehlenbachs, K. (1998). Oxygen isotopic fluxes associated with high-temperature processes in the rift zones of Iceland. *Chemical Geology* **145**, 275–286.

Gee, M. A. M., Thirlwall, M. F., Taylor, R. N., Lowry, D. & Murton, B. J. (1998). Crustal processes: major controls on Reykjanes Peninsula lava chemistry, SW Iceland. *Journal of Petrology* **39**, 819–839.

Geist, D. J., White, W. M. & McBirney, A. R. (1988). Plume–asthenosphere mixing beneath the Galápagos archipelago. *Nature* **333**, 657–660.

Geldmacher, J. & Hoernle, K. (2000). The 72 Ma geochemical evolution of the Madeira Hotspot (eastern North Atlantic); recycling of Paleozoic (≤500 Ma) oceanic lithosphere. *Earth and Planetary Science Letters* **183**, 73–92.

Geldmacher, J., Hanan, B. B., Blichert-Toft, J., Harpp, K., Hoernle, K. A., Hauff, F., Werner, R. & Kerr, A. C. (2003). Hafnium isotopic variations in volcanic rocks from the Carribean Large Igneous Province and Galápagos hot spot tracks. *Geochemistry, Geophysics, Geosystems* **4**, 2002GC000477.

Gerlach, D. C., Cliff, R. A., Davies, G. D., Norry, M. & Hodgson, N. (1988). Magma sources of the Cape Verdes archipelago: isotopic and trace element constraints. *Geochimica et Cosmochimica Acta* **52**, 2979–2992.

Govindaraju, K. (1994). Compilation of working values and sample descriptions for 383 geostandards. *Geostandards Newsletter* **18**, Special Issue, 1-158.

Gurenko, A. A. & Chaussidon, M. (1995). Enriched and depleted primitive melts included in olivine from Icelandic tholeiites—origin by continuous melting of a single mantle column. *Geochimica et Cosmochimica Acta* **59**, 2905–2917.

Hanan, B. B. & Schilling, J.-G. (1997). The dynamic evolution of Iceland mantle plume: the lead isotope perspective. *Earth and Planetary Science Letters* **151**, 43–60.

Hanan, B. B., Blichert-Toft, J., Kingsley, R. & Schilling, J.-G. (2000). Depleted Iceland mantle plume geochemical signature: artifact or multicomponent mixing? *Geochemistry, Geophysics, Geosystems* **1**, 1999GC000009.

Hardarson, B. S., Fitton, J. G., Ellam, R. M. & Pringle, M. S. (1997). Rift relocation—a geochemical and geochronological investigation of a paleo-rift in northwest Iceland. *Earth and Planetary Science Letters* **153**, 181–196.

Harmon, R. S. & Hoefs, J. (1995). Oxygen isotope heterogeneity of the mantle deduced from global ^{18}O systematics of basalts from different geotectonic settings. *Contributions to Mineralogy and Petrology* **120**, 95–114.

Harrison, D., Burnard, P. & Turner, G. (1999). Noble gas behaviour and composition in the mantle; constraints from the Iceland plume. *Earth and Planetary Science Letters* **171**, 199–207.

Hart, S. R. (1984). A large-scale isotope anomaly in the southern hemisphere mantle. *Nature* **309**, 753–757.

Hart, S. R., Schilling, J.-G. & Powell, J. L. (1973). Basalts from Iceland and along the Reykjanes Ridge: Sr isotope geochemistry. *Nature* **246**, 104–107.

Hart, S. R., Blusztajn, J., Dick, H. J. B., Meyer, P. S. & Muehlenbachs, K. (1999). The fingerprint of seawater circulation in a 500-meter section of ocean crust gabbros. *Geochimica et Cosmochimica Acta* **63**, 4059–4080.

Hattori, K. & Muehlenbachs, K. (1982). Oxygen isotope ratios of the Icelandic crust. *Journal of Geophysical Research* **87**, 6559–6565.

Hauff, F., Hoernle, K., Tilton, G., Graham, D. W. & Kerr, A. C. (2000). Large volume recycling of oceanic lithosphere over short time scales: geochemical constraints from the Caribbean Large Igneous Province. *Earth and Planetary Science Letters* **174**, 247–263.

Hauri, E. H. (1996). Major-element variability in the Hawaiian mantle plume. *Nature* **382**, 415–419.

Helmberger, D. V., Wen, L. & Ding, X. (1998). Seismic evidence that the source of the Iceland hotspot lies at the core–mantle boundary. *Nature* **396**, 251–255.

Hémond, C., Condomines, M., Fourcade, S., Allègre, C. J., Óskarsson, N. & Javoy, M. (1988). Thorium, strontium and oxygen isotopic geochemistry in recent tholeiites from Iceland: crustal influence on mantle-derived magmas. *Earth and Planetary Science Letters* **87**, 273–285.

Hémond, C., Arndt, N. T., Lichtenstein, U. & Hofmann, A. W. (1993). The heterogeneous Iceland plume: Nd–Sr–O isotopes and trace element constraints. *Journal of Geophysical Research* **98**, 15833–15850.

Hieronymus, C. & Baker, J. A. (2004). Deep subduction of the mantle wedge and the origin of OIB. Abstract at the 14th Annual Goldschmidt Meeting, Copenhagen, Geochimica Cosmochimica Acta 68, A560.

Hilton, D., Grönvold, K., Macpherson, C. G. & Castillo, P. R. (1999). Extreme $^{3}He/^{4}He$ ratios in northwest Iceland: constraining the common component in mantle plumes. *Earth and Planetary Science Letters* **173**, 53–60.

Hilton, D., Thirlwall, M. F., Taylor, R. N., Murton, B. J. & Nichols, A. (2000). Controls on magmatic degassing along the Reykjanes Ridge with implications for the helium paradox. *Earth and Planetary Science Letters* **183**, 43–50.

Hirschmann, M. M., Kogiso, T., Baker, M. B. & Stolper, E. M. (2003). Alkalic magmas generated by partial melting of garnet pyroxenite. *Geology* **31**, 481–484.

Hirose, K. & Kushiro, I. (1993). Partial melting of dry peridotites at high pressures; determination of compositions of melts segregated from peridotite using aggregates of diamond. *Earth and Planetary Science Letters* **114**, 477–489.

Hoernle, K. (1998). Geochemistry of Jurassic oceanic crust beneath Gran Canaria (Canary islands): implications for crustal recycling and assimilation. *Journal of Petrology* **39**, 859–880.

Hoernle, K. A. & Tilton, G.R. (1991). Sr–Nd–Pb isotope data for Fuerteventura (Canary islands) basal complex and subaerial volcanics: application to magma genesis and evolution. *Schweizerisches Mineralogiche und Petrographische Mitteilungen* **71**, 3–18.

Hoernle, K., Tilton, G. & Schmincke, H.-U. (1991). Sr–Nd–Pb isotopic evolution of Gran Canaria; evidence for shallow enriched mantle beneath the Canary Islands. *Earth and Planetary Science Letters* **106**, 44–63.

Hoernle, K., Werner, R., Phipps-Morgan, J., Garbe-Schoenberg, D., Bryce, J. & Mrazek, J. (2000). Existence of complex spatial zonation in the Galápagos Plume for at least 14 m.y. *Geology* **28**, 435–438.

Hofmann, A. W. (1997). Mantle geochemistry: the message from oceanic volcanism. *Nature* **385**, 219–229.

Hofmann, A. W. & White, W. M. (1982). Mantle plumes from ancient oceanic crust. *Earth and Planetary Science Letters* **57**, 421–436.

Hofmann, A. W., Jochum, K. P., Seufert, M. & White, W. M. (1986). Nb and Pb in oceanic basalts; new constraints on mantle evolution. *Earth and Planetary Science Letters* **79**, 33–45.

Ito, G. (2001). Reykjanes 'V'-shaped ridges originating from a pulsing and dehydrating mantle plume. *Nature* **411**, 681–684.

Jochum, K.-P., Seufert, H. M. & Thirlwall, M. F. (1990). Multi-element analyses of 15 international standard rocks by isotope dilution spark source mass spectrometry. *Geostandards Newsletter* **14**, 469–473.

Johnson, K. T. M. (1994). Experimental cpx/ and garnet/melt partitioning of REE and other trace elements at high pressures; petrogenetic implications. *Mineralogical Magazine* **58**, 454–455.

Kamenetsky, V. S., Eggins, S. M., Crawford, A. J., Green, D. H., Gasparon, M. & Falloon, T. J. (1998). Calcic melt inclusions in

primitive olivine at 43°N MAR: evidence for melt-rock reaction/melting involving clinopyroxene-rich lithologies during MORB generation. *Earth and Planetary Science Letters* **160**, 115–132.

Keleman, P. B. & Dunn, J.T. (1992). Depletion of Nb relative to other highly incompatible elements by melt/rock reaction in the upper mantle. *EOS, AGU Transactions,* **73**, 656–657.

Kempton, P. D., Fitton, J. G., Saunders, A. D., Nowell, G. M., Taylor, R. N., Hardason, B. S. & Pearson, G. (2000). The Iceland plume in space and time: a Sr–Nd–Pb-Hf study of the North Atlantic rifted margin. *Earth and Planetary Science Letters* **177**, 255–271.

Kennedy, A.K., Lofgren, G. E. & Wasserburg, G. J. (1993). An experimental study of trace element partitioning between olivine, orthopyroxene and melt in chondrules; equilibrium values and kinetic effects. *Earth and Planetary Science Letters* **115**, 177–195.

Kerr, A. C., Saunders, A. D., Tarney, J. & Berry, N. H. (1995). Depleted mantle-plume geochemical signatures: no paradox for plume theories. *Geology* **23**, 843–846.

Kogiso, T. & Hirschmann, M. A. (2001). Experimental study of clinopyroxenite partial melting and the origin of ultra-calcic melt inclusions. *Contributions to Mineralogy and Petrology* **142**, 347–360.

Kogiso, T., Tatsumi, Y. & Nakano, S. (1997). Trace element transport during dehydration processes in the subducted oceanic crust: 1. Experiments and implications for the origin of ocean island basalts. *Earth and Planetary Science Letters* **148**, 193–205.

Kogiso, T., Hirose, K. & Takahashi, E. (1998). Melting experiments on homogeneous mixtures of peridotite and basalt; application to the genesis of ocean island basalts. *Earth and Planetary Science Letters* **162**, 45–61.

Kogiso, T., Hirschmann, M. A. & Frost, D. J. (2003). High-pressure partial melting of garnet pyroxenite: possible mafic lithologies in the source of ocean island basalts. *Earth and Planetary Science Letters* **216**, 603–617.

Kokfelt, T. F., Hoernle, K. & Hauff, F. (2003). Upwelling and melting of the Iceland plume from radial variation of ^{238}U–^{230}Th disequilibria in postglacial volcanic rocks. *Earth and Planetary Science Letters* **213**, 167–186.

Kokfelt, T. F., Lundstrom, C. Hoernle, K., Hauff, F. & Werner, R. (2005). Plume–ridge interaction studied at the Galápagos Spreading Center: evidence from ^{226}Ra–^{230}Th–^{238}U and ^{231}Pa–^{235}U isotopic disequilibria. *Earth and Planetary Science Letters* **234**, 165–187.

Krolikowska-Ciaglo, S., Hauff, F. & Hoernle, K. (2005). Sr–Nd isotope systematics in 14–28 Ma low-temperature altered mid-ocean ridge basalt from the Australian Antarctic Discordance, Ocean Drilling Program Leg 187. *Geochemistry, Geophysics, Geosystems* **6**, doi:10.1029/2004GC000802.

Kurz, M. D., Meyer, P. S. & Sigurdsson, H. (1985). Helium isotopic systematics within the neovolcanic zones of Iceland. *Earth and Planetary Science Letters* **74**, 291–305.

Kyser, T. K., O'Neil, J. R. & Carmichael, I. S. E. (1982). Genetic relations among basic lavas and ultramafic nodules: evidence from oxygen isotope compositions. *Contributions to Mineralogy and Petrology* **81**, 88–102.

Langmuir, C. H., Bender, J. F., Bence, A. E. & Hanson, G. N. (1977). Petrogenesis of basalts from the Famous area: Mid-Atlantic ridge. *Earth and Planetary Science Letters* **36**, 133–156.

Le Bas, M. J., Le Maitre, R. W., Streckeisen, A. & Zanettin, B. (1986). A chemical classification of volcanic rocks based on total alkali–silica diagram. *Journal of Petrology* **27,** 745–750.

Lundstrom, C., Hoernle, K. & Gill, J. (2003). U-series disequilibria in volcanic rocks from the Canary islands: plume versus lithospheric melting. *Geochimica et Cosmochimica Acta* **67**, 4153–4177.

Mattey, D., Lowry, D. & Macpherson, C. (1994). Oxygen isotope composition of mantle peridotite. *Earth and Planetary Science Letters* **128**, 231–241.

McDonough, W. F. & Sun, S.-s. (1995). The composition of the Earth. *Chemical Geology* **120**, 223–253.

McKenzie, D. & O'Nions, R. K. (1991). Partial melt distributions from inversion rare earth element concentration. *Journal of Petrology* **32,** 1021–1091.

Mertz, D. & Haase, K. (1997). The radiogenic isotope composition of the high-latitude North Atlantic mantle. *Geology* **25**, 411–414.

Mertz, D., Devey, C. W., Todt, W., Stoffers, P. & Hofmann, A. W. (1991). Sr–Nd–Pb isotope evidence against plume–asthenosphere mixing north of Iceland. *Earth and Planetary Science Letters* **107**, 243–255.

Montelli, R., Nolet, G., Dahlen, F. A., Masters, G., Engdahl, E. R. & Hung, S.-H. (2004). Finite-frequency tomography reveals a variety of plumes in the mantle. *Science* **303**, 338–343.

Moreira, M. & Kurz, M. D. (2002). Subducted oceanic lithosphere and the origin of the 'high-μ' basalt helium isotopic signature. *Earth and Planetary Science Letters* **189**, 49–57.

Moreira, M., Breddam, K., Curtice, J. & Kurz, M. D. (2001). Solar neon in the Icelandic mantle: new evidence for an undegassed lower mantle. *Earth and Planetary Science Letters* **185**, 15–23.

Muehlenbachs, K., Anderson, A. T. & Sigvaldason, G. E. (1974). Low-O^{18} basalts from Iceland. *Geochimica et Cosmochimica Acta* **38**, 577–588.

Murton, B. J., Taylor, R. N. & Thirlwall, M. F. (2002). Plume–ridge interaction; a geochemical perspective from the Reykjanes Ridge. *Journal of Petrology* **43**, 1987–2012.

Nicholson, H., Condomines, M., Fitton, J. G., Fallick, A. E., Grönvold, K. & Rogers, G. (1991). Geochemical and isotopic evidence for crustal assimilation beneath Krafla, Iceland. *Journal of Petrology* **32**, 1005–1020.

Niu, Y. & O'Hara, M. J. (2003). Origin of ocean island basalts: a new perspective from petrology, geochemistry, and mineral physics considerations. *Journal of Geophysical Research* **108**, 2002JB002048.

O'Nions, R. K. & Pankhurst, R. J. (1973). Secular variation in the Sr-isotope composition of Icelandic volcanic rocks. *Earth and Planetary Science Letters* **21**, 13–21.

O'Nions, R. K., Pankhurst, R. J. & Grönvold, K. (1976). Nature and development of basalt magma sources beneath Iceland and the Reykjanes Ridge. *Journal of Petrology* **17**, 315–338.

O'Nions, R. K., Hamilton, P. J. & Evensen, N. M. (1977). Variations in $^{143}Nd/^{144}Nd$ and $^{87}Sr/^{86}Sr$ ratios in oceanic basalts. *Earth and Planetary Science Letters* **34**, 13–22.

Óskarsson, N., Sigvaldason, G. E. & Steinthórsson, S. (1982). A dynamic model of rift zone petrogenesis and the regional petrology of Iceland. *Journal of Petrology* **23**, 28–74.

Plank, T. & Langmuir, C. H. (1998). The chemical composition of subducting sediment and its consequences for the crust and mantle. *Chemical Geology* **145**, 325–394.

Poreda, R., Schilling, J.-G. & Craig, H. (1986). Helium and hydrogen isotopes in ocean-ridge basalts north and south of Iceland. *Earth and Planetary Science Letters* **78**, 1–17.

Prestvik, T. (1985). *Petrology of Quaternary volcanic rocks from Öraefi, southest Iceland. Reports of the Department of Geology, University of Trondheim* **21,** 81 pp.

Prestvik, T., Goldberg, S., Karlsson, H. & Grönvold, K. (2001). Anomalous strontium and lead isotope signatures in the off-rift Öræfajökull central volcano in south-east Iceland evidence for enriched endmember(s) of the Iceland mantle plume? *Earth and Planetary Science Letters* **190**, 211–220.

Rampone, E., Piccardo, G. B., Vannucci, R., Bottazzi, P. & Ottolini, L. (1993). Subsolidus reactions monitored by trace elements partitioning: the spinel- to plagioclase-facies transition in mantle peridotites. *Contributions to Mineralogy and Petrology* **115**, 1–17.

Saemundsson, K., (1979). Outline of the geology of Iceland. *Jökull* **29,** 7–28.

Schilling, J.-G. (1973). Iceland mantle plume geochemical study of the Reykjanes Ridge. *Nature* **242**, 565–571.

Schilling, J.-G. & Noe-Nygaard, A. (1974). Faeroe–Iceland plume; rare-earth evidence. *Earth and Planetary Science Letters* **24**, 1–14.

Schilling, J.-G., Kingsley, R., Fontignie, D., Poreda, R. & Xue, S. (1999). Dispersion of the Jan Mayen and Iceland mantle plumes in the Arctic; a He–Pb–Nd–Sr isotope tracer study of basalt from the Kolbeinsey, Mohns, and Knipovich ridges. *Journal of Geophysical Research* **104**, 10543–10569.

Schmincke, H.-U., Klügel, A., Hansteen, T.H., and Hoernle, K. (1998). Samples from the Jurassic ocean crust beneath Gran Canaria, La Palma and Lanzarote (Canary Islands). *Earth Planetary Science Letters* **163**, 343–360.

Sharp, Z. D. (1990). A laser-based microanalytical method for the in-situ determination of oxygen isotope ratios of silicates and oxides. Geochimica et Cosmochimica Acta **54**, 1353–1357.

Shen, Y., Solomon, S. C., Bjarnason, I. T. & Wolfe, C. J. (1998). Seismic evidence for a lower-mantle origin of the Iceland plume. *Nature* **395**, 62–65.

Shimizu, N. & Kushiro, I. (1975). Partitioning of rare-earth elements between garnet and liquid at high-pressures—preliminary experiments. *Geophysical Research Letters* **2**, 413–416.

Sigmarsson, O. (1991). Extreme magma homogeneity in the 1783–84 Lakagigar eruption; origin of a large volume of evolved basalt in Iceland. *Geophysical Research Letters* **18**, 2229–2232.

Sigmarsson, O., Condomines, M. & Fourcades, S. (1992a). A detailed Th, Sr, O isotope study of Hekla; differentiation processes in an Icelandic volcano. *Contributions to Mineralogy and Petrology* **112**, 20–34.

Sigmarsson, O., Condomines, M. & Fourcades, S. (1992b). Mantle and crustal contribution in the genesis of recent basalts from off-ridge zones in Iceland: constraints from Th, Sr and O isotopes. *Earth and Planetary Science Letters* **110**, 149–162.

Skovgaard, A. C., Storey, M., Baker, J., Blusztajn, J. & Hart, S. R. (2001). Osmium–oxygen isotopic evidence for a recycled and strongly depleted component in the Iceland mantle plume. *Earth and Planetary Science Letters* **194**, 259–275.

Sobolev, A. V., Hofmann, A. W., Sobolev, S. V. & Nikogosian, I. K. (2005). An olivine-free mantle source of Hawaiian shield basalts. *Nature* **434**, 590–597.

Staudigel, H., Hart, S. R. & Richardson, S. H. (1981). Alteration of the oceanic crust: processes and timing. *Earth and Planetary Science Letters* **52**, 311–327.

Stecher, O., Carlson, R. W. & Gunnarsson, B. (1999). Torfajökull; a radiogenic end-member of the Iceland Pb-isotopic array. *Earth and Planetary Science Letters* **165**, 117–127.

Stille, P., Unruh, D. M. & Tatsumoto, M. (1983). Pb, Sr, Nd and Hf isotopic evidence of multiple sources for Oahu, Hawaii basalts. *Nature* **304**, 25–29.

Stracke, A., Zindler, A., Salters, V. J. M., McKenzie, D., Blichert-Toft. J., Albarède, F. & Grönvold, K. (2003). Theistareykir revisited. *Geochemistry, Geophysics, Geosystems* **4**, 2001GC000201.

Sun, S.-S. (1980). Lead isotopic study of young volcanic rocks from mid-ocean ridges, ocean islands and island arcs. *Philosophical Transactions of the Royal Society of London, Series A* **297**, 409–445.

Sun, S.-S. & Jahn, B. M. (1975). Lead and strontium isotopes in post-glacial basalts from Iceland. *Nature* **255**, 527–530.

Sun, S.-S., Tatsumoto, M. & Schilling, J.-G. (1975). Mantle plume mixing along the Reykjanes Ridge axis: lead isotopic evidence. *Science* **190**, 143–147.

Taylor, R. N., Thirlwall, M. F., Murton, B. J., Hilton, D. R. & Gee, M. A. M. (1997). Isotopic constraints on the influence of the Icelandic plume. *Earth and Planetary Science Letters* **148**, E1–E8.

Thirlwall, M. (1997). Pb isotopic and elemental evidence for OIB derivation from young HIMU mantle. *Chemical Geology* **139**, 51–74.

Thirlwall, M., Taylor, R., Mattaey, D., Gee, M. & Murton, B. (1999) The origin of Iceland plume mantle: constraints from high-precision oxygen and Pb isotope analyses of Reykjanes Ridge lavas. EUG X. Strasbourg. *Terra Abstracts* 340.

Thirlwall, M., Gee, M. A. M., Taylor, R. N. & Murton, B. J. (2004). Mantle components in Iceland and adjacent ridges investigated using double-spike Pb isotope ratios. *Geochimica et Cosmochimica Acta* **68**, 361–386.

Turekian, K. K. & Wedepohl, K. H. (1961). Distribution of the elements in some major units of the Earth's crust. *Geological Society of America Bulletin* **72,** 175–192.

Valley, J. W., Kitchen, N., Kohn, M. J., Niendorff, C. R. & Spicuzza, M. J. (1995). UWG-2, a garnet standard for oxygen isotope ratios: strategies for high-precision oxygen isotope analyses by laser fluorination. *Geochimica et Cosmochimica Acta* **59**, 5223–5231.

Vidal, P. (1992). More HIMU mantle in the future? *Geochimica et Cosmochimica Acta* **56**, 4295–4299.

Weir, N. R. W., White, R. S., Brandsdóttir, B., Einarsson, P., Shimamura, H., Shiobara, H. & the RISE Fieldwork Team (2001). Crustal structure of the northern Reykjanes Ridge and Reykjanes Peninsula, southwest Iceland. *Journal of Geophysical Research* **106**, 6347–6368.

Werner, R., Hoernle, K., Barckhausen, U. & Hauff, F. (2003). The geodynamic evolution of the Galápagos System (Central East Pacific) over the past 20 m.y.: constraints from morphology, geochemistry, and magnetic anomalies. *Geochemistry, Geophysics, Geosystems* **4**, 2003GC000576.

White, R. S., Bown, J. W. & Smallwood, J. R. (1995). The temperature of the Iceland plume and origin of outward-propagating V-shaped ridges. *Journal of the Geological Society, London* **152**, 1039–1045.

White, W. M., McBirney, A. R. & Duncan, R. A. (1993). Petrology and geochemistry of the Galápagos islands: portrait of a pathological mantle plume. *Journal of Geophysical Research* **98**, 19533–19563.

Wolfe, C., Bjarnason, I. T., VanDecar, J. C. & Solomon, S. C. (1997). Seismic structure of the Iceland mantle plume. *Nature* **385**, 245–247.

Wood, D. A. (1978). Major and trace element variations in the Tertiary lavas of eastern Iceland and their significance with respect to the Iceland geochemical anomaly. *Journal of Petrology* **19**, 393–436.

Wood, D. A. (1979). Dynamic partial melting: its application to the petrogeneses of basalts erupted in Iceland, the Faeroe Islands, the Isle of Skye (Scotland) and the Troodos Massif (Cyprus). *Geochimica et Cosmochimica Acta* **43**, 1031–1046.

Wood, D. A., Joron, J. L., Treuil, M., Norry, M. & Tarney, J. (1979). Elemental and Sr isotope variations in basic lavas from Iceland and the surrounding ocean floor; the nature of mantle source inhomogeneities. *Contributions to Mineralogy and Petrology* **70**, 319–339.

Yoder, H. S. J. & Tilley, C. E. (1962). Origin of basalt magmas: an experimental study of natural and synthetic rock systems. *Journal of Petrology* **3**, 342–529.

Zindler, A. & Hart, S. R. (1986). Chemical geodynamics. *Annual Review in Earth and Planetary Sciences* **14**, 493–571.

Zindler, A., Hart, S. R., Frey, F. A. & Jakobsson, S. P. (1979). Nd and Sr isotope ratios and rare earth element abundances in Reykjanes

Table A1: Reproducibility and accuracy of ICP-MS trace element data evaluated from BIR-1

Element	No. 1	No. 2	No. 3	No. 4	No. 5	No. 6	Av.	±1σ	(%)	Ref. value*	Rel. dev. (%)
Rb	0·202	0·191	0·292	0·239	0·236	0·212	0·216	0·021	9·7	0·24	−10·0
Sr	108	107	117	112	116	112	112	4	3·5	110	2·0
Y	15·7	15·7	14·6	15·5	15·9	16·2	15·6	0·5	3·4	15·5	0·5
Zr	13·4	13·5	14·2	13·4	13·7	14·8	13·8	0·6	4·1	14·0	−1·1
Nb	0·634	0·819	0·534	0·534	0·541	0·528	0·554	0·045	8·1	0·55	0·8
Cs	0·0061	0·0058	0·0058	0·0043	0·0049	0·0068	0·0059	0·0007	11·8	0·004	46·7
Ba	6·54	6·64	6·91	6·68	7·27	7·06	6·85	0·28	4·1	7·1	−3·5
La	0·598	0·585	0·616	0·652	0·650	0·600	0·617	0·028	4·6	0·61	1·1
Ce	1·88	1·86	1·96	1·95	2·01	1·91	1·93	0·06	2·9	1·95	−1·2
Pr	0·366	0·356	0·387	0·388	0·400	0·377	0·379	0·016	4·2	0·38	−0·2
Nd	2·31	2·32	2·41	2·48	2·51	2·41	2·41	0·08	3·4	2·34	2·8
Sm	1·08	1·06	1·13	1·16	1·16	1·15	1·13	0·04	3·8	1·1	2·5
Eu	0·502	0·498	0·529	0·536	0·547	0·535	0·524	0·020	3·8	0·52	0·8
Gd	1·77	1·75	1·80	1·91	1·92	1·81	1·83	0·07	3·9	1·84	−0·6
Tb	0·356	0·350	0·369	0·379	0·382	0·376	0·369	0·013	3·4	0·36	2·4
Dy	2·55	2·53	2·63	2·74	2·75	2·70	2·65	0·09	3·5	2·51	5·7
Ho	0·568	0·563	0·584	0·610	0·612	0·598	0·589	0·021	3·5	0·56	5·2
Er	1·74	1·70	1·71	1·78	1·80	1·73	1·74	0·04	2·2	1·66	5·1
Tm	0·247	0·241	0·254	0·263	0·266	0·260	0·255	0·010	3·8	0·25	2·1
Yb	1·65	1·64	1·70	1·75	1·74	1·74	1·70	0·05	2·8	1·63	4·5
Lu	0·248	0·243	0·251	0·263	0·265	0·261	0·255	0·009	3·5	0·25	2·1
Hf	0·582	0·588	0·610	0·590	0·566	0·616	0·592	0·019	3·1	0·581	1·9
Ta	0·046	0·056	0·043	0·038	0·036	0·043	0·041	0·004	10·3	0·038	7·6
Pb	2·89	3·04	3·20	3·22	3·20	3·03	3·10	0·13	4·3	2·94	5·3
Th	0·034	0·035	0·034	0·037	0·034	0·030	0·034	0·002	6·3	0·031	9·4
U	0·010	0·011	0·010	0·011	0·011	0·010	0·011	0·0005	5·0	0·0097	8·5

*Concentrations given for Zr, Nb, Ta and Hf in BIR-1 are from Carsten Münckeer (formerly at the University of Münster), as these values are considered the most reliable.

Peninsula basalts; evidence for mantle heterogeneity beneath Iceland. *Earth and Planetary Science Letters* **45**, 249–262.

Zou, H. & Zindler, A. (1996). Constraints on the degree of dynamic partial melting and source composition using concentration ratios in magmas. *Geochimica et Cosmochimica Acta* **60**, 711–717.

APPENDIX

Major elements (SiO_2, Al_2O_3, MgO, Fe_2O_3, CaO, Na_2O, K_2O, TiO_2, MnO and P_2O_5) and some trace elements (Co, Cr, Ni, V, Zn) were determined on fused beads using a Philips X'Unique PW1480 XRF spectrometer equipped with a Rh-tube at IFM-GEOMAR. The H_2O and CO_2 contents were determined on a Rosemount CWA 5003. Approximately 0·2 g sample powder was heated at 980°C for ∼5 min during which all H_2O and CO_2 was released through thermic dissociation; thereafter it was led to the statothermic BINOS^R Infrared Gas Analyser using N_2 as carrier gas. The precision of the method is about ±1·0% relative (2 SD). Additional trace elements (Rb, Sr, Y, Zr, Nb, Cs, Ba, REE, Hf, Ta, Pb, Th, U) were determined by ICP-MS on a VG Plasmaquad PQ1 ICP-MS system at the Geological Institute of the University of Kiel following the methods of Garbe-Schönberg (1993). The accuracy of reference material BIR-1 and BHVO-1, measured along with the samples, is within 10% of the suggested working values (Jochum *et al.*, 1990; Govindaraju, 1994), but generally better than 5% for REE (see Tables A1 and A2). Replicate analyses of individual digestions of samples are on average within 3% (Table A3).

Sr–Nd–Pb isotope analyses were carried out by Folkmar Hauff on unleached powders and leached

Table A2: Reproducibility and accuracy of ICP-MS trace element data evaluated from BHVO-1

Element	No. 1	No. 2	No. 3	No. 4	Av.	±1σ	(%)	Ref. value*	(%)
Rb	9·81	8·22	10·7	9·62	9·58	1·022	10·7	11·00	−12·9
Sr	424	374	405	396	400	21	5·2	403	−0·8
Y	25·0	21·7	25·9	27·1	24·9	2·3	9·3	28·0	−11·0
Zr	171	149	174	185	170	15	8·9	179	−5·1
Nb	18·3	16·8	18·2	18·3	17·9	0·7	4·0	19	−5·8
Cs	0·098	0·088	0·096	0·101	0·096	0·005	5·7	0·13	−26·5
Ba	139	131	139	137	136	4	2·9	139	−1·9
La	15·9	14·8	16·3	15·4	15·6	0·6	4·0	16	−2·5
Ce	38·8	37·0	39·5	38·2	38·4	1·1	2·8	39	−1·6
Pr	5·51	5·18	5·63	5·49	5·45	0·19	3·5	5·7	−4·4
Nd	24·7	23·2	25·8	25·1	24·7	1·1	4·5	25	−1·2
Sm	6·22	5·84	6·49	6·37	6·23	0·28	4·5	6·2	0·5
Eu	2·05	2·00	2·15	2·12	2·08	0·07	3·3	2·06	0·9
Gd	6·33	5·96	6·62	6·34	6·31	0·27	4·3	6·4	−1·3
Tb	0·952	0·882	0·986	0·998	0·955	0·052	5·4	0·96	−0·6
Dy	5·34	4·98	5·68	5·61	5·40	0·32	5·9	5·2	3·9
Ho	0·985	0·912	1·05	1·03	0·994	0·062	6·2	0·99	0·4
Er	2·50	2·29	2·64	2·59	2·51	0·15	6·1	2·42	3·5
Tm	0·332	0·311	0·351	0·342	0·334	0·017	5·2	0·33	1·1
Yb	2·05	1·89	2·12	2·09	2·04	0·10	5·0	2·0	1·8
Lu	0·281	0·256	0·293	0·292	0·280	0·017	6·2	0·29	−3·3
Hf	4·47	4·18	4·37	4·63	4·41	0·19	4·2	4·4	0·3
Ta	1·10	1·17	1·10	1·15	1·13	0·03	3·1	1·2	−5·8
Pb	2·13	1·99	2·12	2·22	2·11	0·10	4·5	2·6	−18·7
Th	1·23	1·21	1·32	1·23	1·25	0·05	4·0	1·1	13·5
U	0·409	0·409	0·449	0·428	0·424	0·019	4·4	0·42	0·9

*Concentrations are from Govindaraju (1994) and US Geological Survey (at http://minerals.cr.usgs.gov/geo_chem_stand/basaltbhvo1.html), except Pr and U concentrations, which are from University of California, Davis (at: http//icpms.geology.ucdavis.edu/).

1–2 mm sized chips (Table 2). Samples were dissolved in a hot HF–HNO_3 mixture; ion exchange procedures followed those described by Hoernle & Tilton (1991). Sr–Nd–Pb isotopic ratios were measured by thermal ionization mass spectrometry on a Finnigan MAT262 RPQ^{2+} system at the Leibniz Institute of Marine Sciences (IFM-GEOMAR), operating in static mode for Sr and Pb and in multidynamic mode for Nd. Sr and Nd isotopic ratios are normalized within run to $^{86}Sr/^{88}Sr = 0{\cdot}1194$ and $^{146}Nd/^{144}Nd = 0{\cdot}7219$, respectively. All errors are reported as 2σ. A systematic, temporal decline in $^{87}Sr/^{86}Sr$ for NBS987 from the year 2000 until cup replacement in 2003 caused relatively high external errors of $^{87}Sr/^{86}Sr = 0{\cdot}710216 \pm 0{\cdot}000025$ ($n = 125$). Therefore NBS 987 measured along with the samples ($n = 29$) is normalized to $^{87}Sr/^{86}Sr = 0{\cdot}710250$ and the normalization factors are applied to the sample data. This measure improves the reproducibility of the NBS 987 data to ±0·000009. La Jolla measured along with the samples gave $^{143}Nd/^{144}Nd = 0{\cdot}511848 \pm 0{\cdot}000009$ ($n = 22$). NBS 981 ($n = 93$) resulted in $^{206}Pb/^{204}Pb = 16{\cdot}898 \pm 0{\cdot}006$, $^{207}Pb/^{204}Pb = 15{\cdot}436 \pm 0{\cdot}007$, $^{208}Pb/^{204}Pb = 36{\cdot}526 \pm 0{\cdot}022$, corresponding to an external 2σ precision of 0·016%/a.m.u. The NBS 981 data were corrected for mass bias to the double-spike NBS 981 values given by Thirlwall *et al.* (2004) to facilitate comparison between the datasets. Total chemistry blanks were <100 pg for Sr and Nd, <30 pg for Pb, and thus considered negligible. Twelve out of 18 Sr replicates are within the external precision of the normalized NBS987 data, and the other replicates are within ±0·000025 or better, except for H2. Nd replicates ($n = 23$) are within the external precision of La Jolla, except H4 and H125. Pb replicates ($n = 19$) were reproduced within 0·018%/a.m.u. except H83 (0·027%/a.m.u.) and H125 (0·028%/a.m.u.).

Table A3: Reproducibility of ICP-MS trace element data evaluated from five individually digested samples

Element	H10(1)	H10(2)	Rel. dev.* (%)	H127(1)	H127(2)	Rel. dev. (%)	H131(1)	H131(2)	Rel. dev. (%)	H24(1)	H24(2)	Rel. dev. (%)	H13(1)	H13(2)	Rel. dev. (%)	Max. dev.† (%)	Av. dev. (%)
Rb	4·43	5·03	6·4	0·956	0·940	0·8	7·23	6·14	8·1	7·02	7·09	0·5	2·54	2·42	2·4	8·1	3·6
Sr	244	276	6·0	102	101	0·5	172	150	6·6	233	257	4·9	193	199	1·5	6·6	3·9
Y	17·1	15·2	5·8	15·6	15·4	0·6	34·3	28·9	8·6	20·6	18·6	5·0	26·1	22·0	8·4	8·6	5·7
Zr	86·5	89·8	1·9	30·2	29·8	0·7	119	101	7·9	91·0	89·6	0·8	90·8	85·3	3·1	7·9	2·9
Nb	11·1	13·1	8·2	1·7	1·6	1·2	11·6	10·9	3·4	11·1	11·5	1·8	12·2	12·3	0·5	8·2	3·0
Cs	0·053	0·057	3·3	0·014	0·013	2·3	0·086	0·078	4·7	0·079	0·078	0·9	0·029	0·029	0·1	4·7	2·3
Ba	78·4	83·6	3·2	15·8	15·6	0·7	89·1	88·6	0·3	95·2	102	3·5	50·8	54·5	3·5	3·5	2·2
La	9·69	10·1	2·2	1·67	1·65	0·6	9·73	9·64	0·4	9·16	9·77	3·2	8·10	8·29	1·1	3·2	1·5
Ce	23·6	25·3	3·4	4·57	4·50	0·7	23·8	24·3	0·9	21·7	23·9	4·9	20·4	21·3	2·2	4·9	2·4
Pr	3·24	3·43	2·7	0·749	0·743	0·4	3·39	3·46	1·1	3·01	3·25	3·9	2·98	3·04	1·1	3·9	1·8
Nd	14·6	15·1	1·6	3·93	3·89	0·5	15·7	16·4	2·3	13·5	15·0	5·4	14·1	13·9	0·7	5·4	2·1
Sm	3·75	3·80	0·7	1·46	1·45	0·5	4·55	4·79	2·6	3·55	3·94	5·2	3·90	3·87	0·5	5·2	1·9
Eu	1·29	1·31	0·8	0·600	0·596	0·3	1·55	1·61	2·0	1·26	1·32	2·3	1·41	1·46	1·8	2·3	1·5
Tb	0·615	0·583	2·6	0·393	0·391	0·2	0·963	0·946	0·8	0·639	0·648	0·7	0·766	0·720	3·1	3·1	1·5
Gd	3·85	3·82	0·4	2·05	2·07	0·5	5·52	5·52	0·1	3·87	4·03	2·0	4·54	4·40	1·6	2·0	0·9
Dy	3·61	3·45	2·2	2·71	2·69	0·4	6·14	6·21	0·5	3·93	4·13	2·4	4·81	4·50	3·4	3·4	1·8
Ho	0·689	0·659	2·2	0·586	0·586	0·0	1·30	1·31	0·6	0·812	0·842	1·8	0·992	0·910	4·3	4·3	1·8
Er	1·82	1·71	2·9	1·71	1·68	0·9	3·72	3·77	0·7	2·19	2·33	3·1	2·74	2·48	5·0	5·0	2·5
Tm	0·247	0·226	4·5	0·258	0·252	1·1	0·542	0·529	1·2	0·311	0·295	2·7	0·394	0·370	3·1	4·5	2·5
Yb	1·53	1·46	2·5	1·72	1·71	0·3	3·64	3·60	0·6	2·05	2·01	1·0	2·56	2·44	2·4	2·5	1·3
Lu	0·217	0·198	4·7	0·257	0·257	0·0	0·542	0·521	2·0	0·297	0·293	0·8	0·377	0·343	4·7	4·7	2·4
Hf	2·79	2·56	4·4	0·930	0·902	1·5	3·22	3·18	0·5	2·55	2·61	1·2	2·62	2·42	4·0	4·4	2·3
Ta	0·823	0·875	3·1	0·106	0·102	2·1	0·693	0·793	6·7	0·689	0·826	9·0	0·775	0·779	0·3	9·0	4·2
Pb	0·722	0·700	1·5	0·244	0·246	0·4	0·821	0·783	2·4	0·825	0·747	5·0	0·605	0·683	6·0	6·0	3·1
Th	0·876	0·810	3·9	0·097	0·094	1·6	0·741	0·745	0·3	0·797	0·796	0·1	0·408	0·393	1·9	3·9	1·5
U	0·265	0·272	1·3	0·032	0·030	2·5	0·220	0·251	6·7	0·232	0·276	8·6	0·129	0·126	1·0	8·6	4·0

*Calculated as the relative deviation from the arithmetic mean.
†Conservative estimate of the analytical reproducibility at 1σ confidence level.